ELUCIDATING THE MECHANISMS OF INFECTION AND PROLIFERATION IN CNIDARIAN-SYMBIODINIACEAE SYMBIOSIS

by

Andrea Lashae Kirk

A dissertation submitted to the faculty of
The University of North Carolina at Charlotte
in partial fulfillment of the requirements
for the degree of Doctor of Philosophy in
Biology

Charlotte

2024

Approved by:

_____
Dr. Adam M. Reitzel

_____
Dr. Tingting Xiang

_____
Dr. Paola Lopez-Duarte

_____
Dr. Richard Chi

_____
Dr. Rebekah Rogers

ABSTRACT

ANDREA LASHAE KIRK, Elucidating the Mechanisms of Infection and Proliferation in Cnidarian-Symbiodiniaceae Symbiosis
(Under the direction of DR. ADAM REITZEL)

Coral reef ecosystems are supported by diverse mutualisms formed between cnidarians such as corals, sea anemones, and jellyfish, and dinoflagellate algae in the family Symbiodiniaceae. These dynamic symbiotic relationships rely on the successful establishment of algal endosymbionts, often from the surrounding seawater, within cnidarian host tissues. Due to the current limitations in cellular and molecular tools in the field of cnidarian-Symbiodiniaceae symbiosis, the mechanisms of symbiosis establishment including infection, proliferation, and maintenance are poorly understood. The aim of this thesis is to uncover the cellular processes essential to cnidarian-algal symbiosis by developing *in vitro* and *in hospite* assays across Symbiodiniaceae and cnidarian species. In chapter two, the trophic flexibility of Symbiodiniaceae was explored. Symbiodiniaceae *Breviolum minutum* grown *in vitro* with organic nutrients showed stable growth and photosynthetic function when compared to limited nutrient conditions; this suggests that the oligotrophic waters of coral reef ecosystems may drive free-living Symbiodiniaceae into symbiosis with cnidarians. Next in chapter three, a new protocol for single-cell dissociation of cnidarian hosts is introduced and used to determine the localization of the first Symbiodiniaceae photosynthesis mutant *ora1*. Here, *ora1* was found to retain its ability to form symbiosis in cnidarians, indicating that photosynthesis is not required for symbiosis establishment. Finally, the newly generated Symbiodiniaceae green mutant, *gr02*, is introduced and co-inoculated with the brown wild type *B. minutum* in the sea anemone Aiptasia to uncover the cellular events contributing to symbiont proliferation. For the first time, two algal genotypes (*gr02* and wild type

B. minutum) were observed co-localized in a single host cell via dissociation and microscopy but were rare in frequency. These results suggest that algal cell division and primary infections drive the proliferation of symbionts *in hospite*. Furthermore, the co-inoculation of *gr02* with other species of Symbiodiniaceae in three cnidarian hosts (coral, sea anemone, and jellyfish) reveals intracellular localization and possible interaction between symbionts in host tissues. Together, this work lays the foundation for future cellular biological research using Symbiodiniaceae mutants to answer pressing questions surrounding cnidarian-Symbiodiniaceae symbiosis.

DEDICATION

This dissertation is dedicated to my parents Judy and Kyle Kirk, my sister Monica Kirk, and my partner in crime Nicholas Nolan. Thank you for your love and words of encouragement during this journey.

ACKNOWLEDGEMENTS

I am immensely grateful for my mentors and Ph.D. supervisors Dr. Tingting Xiang and Dr. Adam Reitzel for their unwavering support throughout my Ph.D. journey. Both Dr. Xiang and Dr. Reitzel have given me irreplaceable encouragement and guidance through both the challenging and joyous moments of my Ph.D. The knowledge I have gained by working under Dr. Xiang has made me a better scientist, and I will continue to value the skills and lessons she has taught me. I am also appreciative of Dr. Reitzel for lending his guidance and mentorship so that I could achieve my goals. I would also like to thank my other committee members Dr. Paola Lopez-Duarte, Dr. Richard Chi, and Dr. Rebekah Rogers for their critical questions and discussions that guided my research.

Additional acknowledgement goes to the Department of Biological Sciences at UNC Charlotte, and I extend thanks to the friends, graduate students, post-doctoral fellows, and faculty that I have had the pleasure of meeting and working with at UNC Charlotte. Special thanks goes to Anne McMahon for her dedicated friendship. I am also appreciative of the helpful discussions and advice provided by the Reitzel lab members on my research.

I am thankful for the thoughtful discussions and experimental help provided by the past and present lab members of the Xiang and Jinkerson laboratories at The University of California at Riverside. I extend my appreciation to Dr. Robert Jinkerson for his collaboration during my dissertation. I am also extremely grateful to Joseph Russo for his emotional and scientific support during our collaborative research endeavors.

Finally, I am thankful to my family, companions, and partner for their continued love and support as I pursue my dreams. Most notably, without the encouragement from Nicholas Nolan, this dissertation would not have been possible.

TABLE OF CONTENTS

LIST OF TABLES

LIST OF FIGURES

CHAPTER 1: INTRODUCTION

1.1 Overview

Photosynthetic organisms sustain diverse ecosystems by harnessing the sun's light energy and converting it into chemical energy for the production of organic nutrients (Falkowski et al., 1984; Kautza et al., 2016; Muscatine et al., 1984). In the oligotrophic waters of tropical coral reef ecosystems, the trophic foundation is formed from the mutualistic symbiosis between cnidarians (coral, sea anemones, and jellyfish) and photosynthetic dinoflagellate algae (family Symbiodiniaceae). Cnidarian hosts supply algal symbionts with primarily inorganic nutrients from the seawater while the symbionts provide up to 100% of the hosts energetic needs from photosynthates (Davy et al., 2012). The co-evolution of cnidarians and Symbiodiniaceae has resulted in some hosts resembling terrestrial plants, providing symbionts with preferential access to light while forming a structural habitat for diverse marine species (Falkowski et al., 1984; Foo et al., 2020; Venn et al., 2008). Cnidarian-Symbiodiniaceae symbiosis is threatened by global climate change (Hoegh-Guldberg et al., 2017) that is increasing sea surface temperatures and resulting in the expulsion of symbionts from host tissue referred to as *bleaching* (Davy et al., 2012). If prolonged, bleaching results in host death, reef decimation, and a loss of economic and cultural significance for coastal communities (Hoegh-Guldberg, 2011). Understanding the mechanisms of a healthy symbiosis is essential for protecting and predicting how corals will respond to future climate perturbations (Weis, 2008; Weis et al., 2008).

1.2 Establishment of cnidarian-Symbiodiniaceae symbiosis

The establishment of symbiosis between cnidarians and Symbiodiniaceae algae proceeds through three primary stages: infection, proliferation, and maintenance (Figure 1.1). During

infection, algal symbionts are recognized and engulfed into the host gastrodermal cells. This recognition and engulfment may be impacted by host-symbiont species specificity (Jinkerson et al., 2022; LaJeunesse et al., 2018). Some studies suggest this may be modulated by Microbe-associated Molecular Pattern and Pattern Recognition Receptor (MAMP-PRR) interactions that trigger symbiont recognition and subsequent suppression of host immune responses for beneficial symbiont entry (Jacobovitz et al., 2021; Tortorelli, Rautengarten, et al., 2022). Once acquired, symbionts are enclosed in a host-derived symbiosome membrane, across which nutrients are translocated between host and symbiont (Figure 1.1). As observed in the infection of the sea anemone *Exaiptasia diaphana* (Figure 1.2) few algal symbionts initially occupy host tissue (day 4), but then proliferate or spread throughout the host gastrodermal tissue layer (day 18). The exact mechanism of symbiont proliferation in cnidarian host tissue is not well understood, but some studies suggest proliferation may depend on host-symbiont cell cycle coordination and nutrient cycling (Cui et al., 2022; Tivey et al., 2020; Xiang et al., 2020). Proliferation of symbionts in host tissue continues until maintenance densities are achieved (Davy et al., 2012). Maintenance of optimal symbiont density *in hospite* is accomplished through the control of nitrogen, specifically ammonium, from the host to the symbiont (Rädecker et al., 2021; Xiang et al., 2020). Rising temperatures or pollution can trigger cellular stress that destabilizes this nutrient cycling and results in symbiosis breakdown or bleaching (Figure 1.1) (Hoegh-Guldberg et al., 2017; Rädecker et al., 2021; Weis et al., 2008; Xiang et al., 2020). Despite the importance of these symbiotic interactions, the cellular mechanisms governing cnidarian-Symbiodiniaceae symbiosis establishment and breakdown have not been fully elucidated.

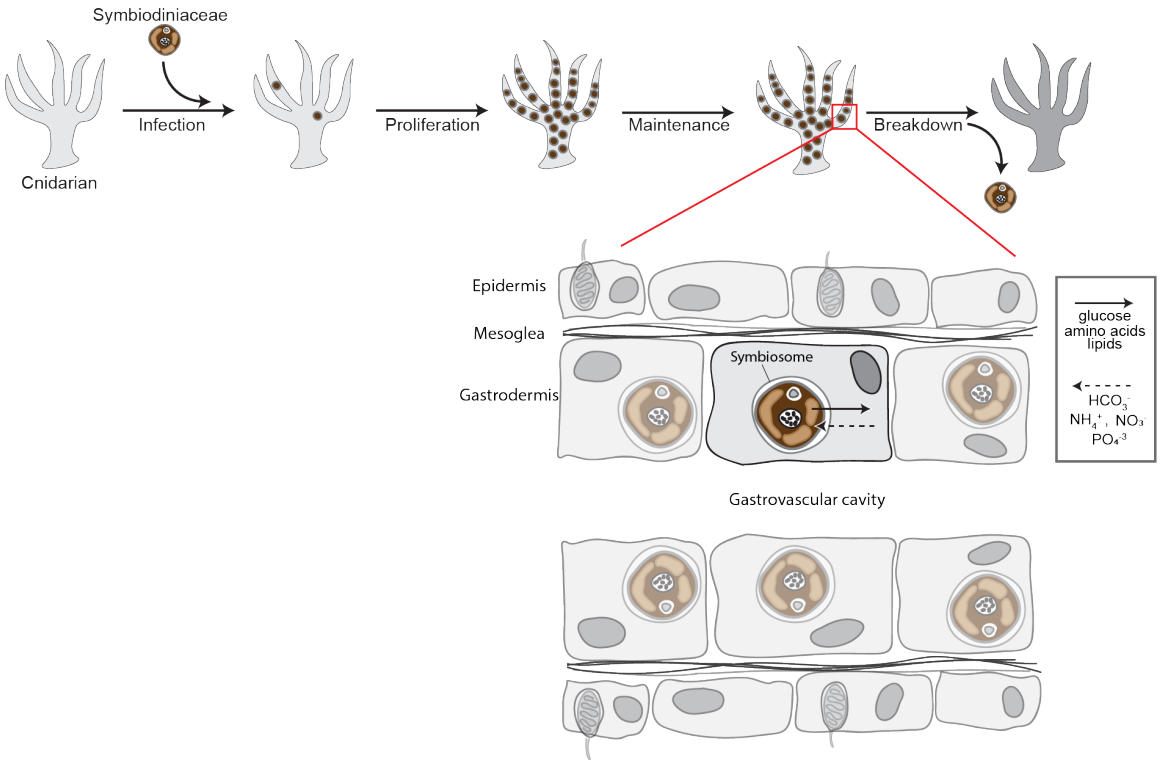

Figure 1.1 Cnidarian-Symbiodiniaceae symbiosis establishment occurs on a cellular-level. Symbiosis establishment involves the infection or engulfment of Symbiodiniaceae algae into host gastrodermal cells where algae are enclosed in a host-derived symbiosome membrane. Symbionts proliferate throughout the host tissue and are maintained at a steady-state density. Inorganic nutrients are supplied from the host to the algal symbionts, and the symbionts photosynthesize and translocate fixed carbon and other photosynthates back to the host. Symbiosis breakdown results in the loss of algal symbionts from host tissues (coral bleaching).

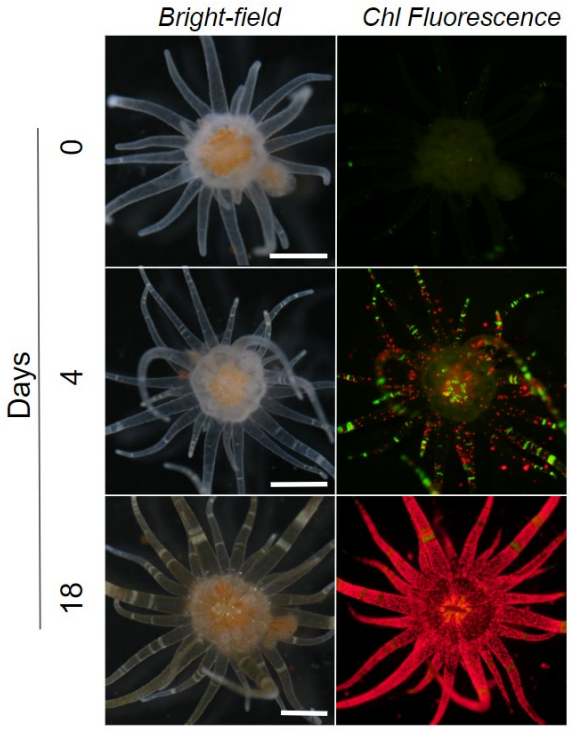

Figure 1.2 Symbiodiniaceae infects, proliferates, and is maintained in Aiptasia host tissue. Representative microscopic images of aposymbiotic sea anemones Aiptasia (*Exaiptasia diaphana*, CC7) inoculated with *Breviolum minutum* (clonal, axenic strain SSB01 (Xiang et al., 2013). Animals were then kept in 12 h light / 12 h dark. A top-down view of animals in bright-field and fluorescence is shown. Chlorophyll autofluorescence from algal cells is in red. Scale bars represent 1 mm.

1.3 Symbiodiniaceae diversity

Symbiodiniaceae algal family is morphologically and physiologically diverse, containing species that can survive in contrasting environmental conditions and have varying abilities to form symbiosis (LaJeunesse et al., 2018). Some Symbiodiniaceae species are found solely free-living in the water column, while others can shift between symbiotic and free-living lifestyles by adjusting metabolic strategies (Maor-Landaw et al., 2020; Xiang et al., 2018). Of the species that form symbiosis, the relationships can be flexible with a wide range of hosts including protists and ciliates (J. J. Lee, 1995; Leutenegger, 1984; Lobban et al., 2005), or limited due to some level of

host-symbiont specificity (Baker, 2003; Keshavmurthy et al., 2020; Xiang et al., 2013). For instance, Symbiodiniaceae *Symbiodinium pilosum*, fails to form symbiosis in the sea anemone *Exaiptasia diaphana* (Xiang et al., 2013) and jellyfish *Cassiopea xamachana* (LaJeunesse, 2001), while species in the genus *Cladocopium* are widely distributed geographically and found in a variety of host organisms (LaJeunesse et al., 2018; Zamora-Jordán et al., 2022). These sometimes species-specific associations may impact stability of cnidarian-Symbiodiniaceae symbiosis in warming sea waters (Cunning & Baker, 2020). For example *Durusdinium trenchii* is a thermotolerant Symbiodiniaceae species that resists bleaching and dominates host tissues following prolonged heat exposure (Silverstein et al., 2015), and association with thermotolerant Symbiodiniaceae species may increase the resilience of cnidarian-Symbiodiniaceae symbiosis to future heat stress events (Qin et al., 2019). However, researchers suggest that host specificity may limit the acquisition of thermally tolerant Symbiodiniaceae species (Gabay et al., 2019). Despite the importance of Symbiodiniaceae diversity in cnidarian-algal associations, it is still unclear what drives Symbiodiniaceae algae into symbiosis and how some species can resist thermal bleaching.

1.4 Cnidarian-Symbiodiniaceae model systems

Decoupling the interactions of host and symbiont at each stage of symbiosis requires laboratory strains for host and symbiont that are amenable to cellular biological studies (Davy et al., 2012; Weis et al., 2008). Classically the freshwater *Hydra viridis* (*Hydra*) and its symbiosis with *Chlorella* (Kovacević et al., 2010) has been instrumental in studying fundamentals of symbiosis biology (Davy et al., 2012). More recently, *Exaiptasia diaphana* (Aiptasia) sea anemone has emerged as a versatile model host in the study of cnidarian-Symbiodiniaceae symbiosis (Baumgarten et al., 2015; Rosset et al., 2021; Xiang et al., 2020). Clonal Aiptasia strains (Thornhill

et al., 2013) are able to form symbiosis similar to corals with a wide range of Symbiodiniaceae species (LaJeunesse et al., 2018), be propagated to large numbers rapidly (Presnell et al., 2022), and are easily maintained in a laboratory environment. With translucent tissues and absence of a calcium carbonate skeleton common of reef building corals, Aiptasia are ideal for cellular biological studies of host-symbiont interactions.

Clonal, axenic strains of Symbiodiniaceae algal species (Xiang et al., 2013) allow for orthogonal culturing of algal symbionts. Nutrient rich media can now be supplied to these axenic algal strains, increasing culturing densities and allowing for *in vitro* observations of morphological, physiological, and transcriptomic responses (Maor-Landaw et al., 2020; Xiang et al., 2018). For example, under glucose supplementation, the surface composition of the Symbiodiniaceae species *Breviolum minutum* (clonal, axenic strain SSB01 (Xiang et al., 2013) was found to significantly change when compared to cells grown in minimal media (Xiang et al., 2018). These physiological and metabolic shifts give insight into the lifestyles of both host and symbiont when free-living and in symbiosis. However, the genetic intractability of Symbiodiniaceae algae makes CRISPR-cas9 manipulation (Chen et al., 2019) difficult and has stymied the identification of algal genes essential for symbiosis. Recent development of Symbiodiniaceae mutants using classical UV mutagenesis (Russo et al., 2023) makes functional screens for mutants with deficient or distinct phenotypes possible. Using these unique phenotypes in the study of cnidarian-Symbiodiniaceae symbiosis may help answer fundamental questions about host-symbiont interactions.

1.5 Research aims: Cellular biological study of cnidarian-Symbiodiniaceae symbiosis

In this collection of works, the cellular interactions between cnidarian hosts and Symbiodiniaceae algal symbionts are investigated through a series of *in vitro* and *in hospite* analyses. The overall aims are to (1) understand the trophic transitions of Symbiodiniaceae algae underpinning symbiotic associations, and (2) assess the cellular events contributing to symbiosis establishment using newly generated Symbiodiniaceae mutants.

In chapter two, the physiological and molecular responses of Symbiodiniaceae algae are investigated *in vitro*. Here, the algae *Breviolum minutum* clonal, axenic strain SSB01 was used as a model and demonstrates the physiological and transcriptome reprogramming of Symbiodiniaceae in response to organic nutrients in comparison to inorganic nutrient supplementation. Symbiodiniaceae may experience a similar shift when transitioning from free-living lifestyles in nutrient-poor waters into symbiotic associations with cnidarian hosts. Therefore, understanding the *in vitro* trophic transitions in Symbiodiniaceae can serve as an orthogonal platform to further understand the factors that impact the Symbiodiniaceae life strategies.

In chapter three and four, the mechanisms essential for symbiosis establishment are investigated. In these chapters, cellular biological methods are optimized for the study of cnidarian-Symbiodiniaceae symbiosis. The first protocol for producing a single-cell suspension of symbiont-containing and symbiont-free adult Aiptasia cells is presented. This protocol is then used to understand the localization of the first Symbiodiniaceae photosynthesis mutant in host tissue. The photosynthesis mutant is found to establish symbiosis in cnidarians hosts, indicating that other mechanisms separate from photosynthesis are important for symbiosis establishment. Expanding on these methods, a visually distinct Symbiodiniaceae green mutant is generated and used with the brown wild type to better understand symbiont proliferation in Aiptasia. While observing

proliferation patterns, interesting co-localization of Symbiodiniaceae species across cnidarian hosts is discovered.

These studies provide invaluable tools for the investigation of cellular biological processes in cnidarian-Symbiodiniaceae symbiosis and uncover the primary mechanisms by which algae occupy and proliferate within host tissues. The methodologies described in this dissertation will make possible future studies utilizing molecular and cellular analysis such as fluorescent microscopy, flow cytometry, and single-cell transcriptomics to reveal cellular interactions essential in cnidarian-Symbiodiniaceae symbiosis. This knowledge provides a framework for biotechnological discoveries to protect coral reef ecosystems from future stressors.

CHAPTER 2: TRANSCRIPTOME REPROGRAMMING OF SYMBIODINIACEAE *BREVIOLUM MINUTUM* IN RESPONSE TO CASEIN AMINO ACIDS SUPPLEMENTATION

This chapter is reprinted from the following publication with permission from all authors:

Kirk, A. L., Clowez, S., Lin, F., Grossman, A. R., & Xiang, T. (2020). Transcriptome reprogramming of Symbiodiniaceae Breviolum minutum in response to organic nutrients casein amino acids supplementation. *Frontiers in Physiology*, *11*, 1301.

2.1 Introduction

Endosymbiotic dinoflagellates from the family Symbiodiniaceae enter symbiosis with cnidarians, which include corals, sea anemones, and jellyfish (Bucher et al., 2016; Davy et al., 2012; Fransolet et al., 2012); this association is fundamental to the survival of coral-reef ecosystems. Cnidarian hosts benefit from the photosynthetically fixed carbon received from the alga (Burriesci et al., 2012; Muscatine & Porter, 1977), utilizing it to meet its energy requirements and enhance calcification rates (Pearse & Muscatine, 1971). The endosymbiotic alga gains access to inorganic nutrients from the host, establishes a stable location in the water column, and is protected from grazers (Davy et al., 2012). The breakdown of the symbiotic relationship between corals and its endosymbiotic alga, or "coral bleaching," occurs under stress conditions, including elevated temperature and pollution of reef habitats (Hoegh-Guldberg, 1999; Weis & Allemand, 2009). Coral bleaching plays a major role in the global decline of reef communities (Hughes et al.,

2017), and yet we still know little about the molecular mechanisms that govern the establishment, maintenance and breakdown of the symbiotic association (Davy et al., 2012).

Symbiodiniaceae and corals often must acclimate to diverse environments with different availabilities of nutrients (Conti-Jerpe et al., 2020; Fox et al., 2019; Leal et al., 2015; Morris et al., 2019). The trophic flexibility of the Symbiodiniaceae algae is essential for survival during both free-living and intracellular growth, especially when environmental conditions challenge growth and physiological processes in both the animal and alga (Morris et al., 2019; Xiang et al., 2018). Free-living Symbiodiniaceae in the ocean have been shown to directly take up nutrients from their surroundings (Brading et al., 2013; D'Elia et al., 1983), although the waters around coral reefs are typically oligotrophic (low-nutrient) (Cook & D'elia, 1987). Recent work has shown that some Symbiodiniaceae algae can thrive under different trophic conditions; autotrophy, heterotrophy, and mixotrophy (Xiang et al., 2013, 2018). For instance, two Symbiodiniaceae algae, both formerly considered clade E (classifications have recently been updated), that were cultured from environmental samples and from the tissues of the coral *Alveopora japonica*, were able to survive through the acquisition of fixed carbon by heterotrophic feeding (Jeong et al., 2012). Low levels of nutrients, such as nitrogen (N), arrest cell division and elicit transcriptional and physiological responses that help the organism cope with the limited nutrient availability (Dagenais-Bellefeuille & Morse, 2013; Jiang et al., 2014; T. Li et al., 2021; Xiang et al., 2020), while excess inorganic N could impair processes in the alga and host and weaken the symbiotic association (Morris et al., 2019).

We previously reported that the Symbiodiniaceae alga *Breviolum minutum* strain SSB01 (designated SSB01 throughout), formerly placed in clade B (Lajeunesse et al., 2012; LaJeunesse et al., 2018; Xiang et al., 2013), grew rapidly under mixotrophic conditions (minimal medium

supplemented with organic nutrients in the light), with slower growth in the absence of organic nutrients (Xiang et al., 2013). SSB01 is one of the well-studied species with available genome and transcriptome resources (Parkinson et al., 2016; Shoguchi et al., 2013; Xiang et al., 2015). It readily forms symbiosis with cnidarian hosts (Hambleton et al., 2014; Maor-Landaw et al., 2020; Xiang et al., 2013) and has been shown to grow under various trophic conditions (Xiang et al., 2013, 2018). This ability to accommodate different nutrient resources (organic and inorganic) affords the alga trophic flexibility within its host where nutrient conditions may fluctuate (Xiang et al., 2013); for example, the dynamic changes in nutrient availability may reflect both the level of various nutrients in the environment and changes in the density of the algal population within the host tissue (Xiang et al., 2020). The cnidarian host may also feed and transport ingested organic nutrients, such as amino acids, lipids and fatty acids to the endosymbiont, potentially creating a mixotrophic interaction for the algae (Imbs et al., 2014; Steen, 1986; Wang & Douglas, 1999). However, the physiological responses and molecular mechanisms that guide metabolic acclimation to changes in the types and levels of available nutrients are not well understood.

In this study, to explore the physiological and molecular mechanisms that underlie trophic shifts in the Symbiodiniaceae, we analyzed the physiology and transcriptome profiles of axenic SSB01 cultured under various nutrient conditions: Artificial Sea Water (ASW), ASW supplemented with inorganic nutrients (IMK), and IMK supplemented with casein amino acids (CAS), which contains a variety of organic nutrients. Inclusion of CAS in IMK improved growth, allowed sustained photosynthetic function, and caused extensive transcriptome changes relative to cells maintained in either ASW or IMK media. Furthermore, there were only minor changes in the transcriptome of the algae grown in IMK compared to ASW. An understanding of the physiological and molecular features that underlie trophic transitions in the Symbiodiniaceae can

provide insights into trophic changes associated with the growth of Symbiodiniaceae algae within their cnidarian hosts and help establish more general “rules" that govern symbiotic associations.

2.2 Materials and Methods

2.2.1 Strain and Growth Conditions

The clonal, axenic Symbiodiniaceae *B. minutum* (formerly Symbiodinium minutum) strain SSB01 (Xiang et al., 2013) was used throughout this study. Liquid cultures of SSB01 were grown either in ASW, ASW supplemented with 0.252 g L^{-1} of Daigo’s IMK medium for marine microalgae (Wako Pure Chemicals, Osaka, Japan) as recommended in the manufacturer’s instructions (IMK medium), or in IMK medium supplemented with 4 gL^{-1} casein hydrolysate (CAS; Affymetrix USB) (Xiang et al., 2013). Cultures were maintained at 27°C on a 12 h-light/12 h-dark cycle with an irradiance of ∼10 μmol photons m^{-2} s^{-1} provided by Philips ALTO II 25-W bulbs. To assess the effects of different nutrients on SSB01, approximately 2×10^7 SSB01 cells from an IMK culture in log growth were collected by centrifugation at 100 *g* for 5 min in an Eppendorf 5810R centrifuge at room temperature. Cells were washed once with 50 mL autoclave-sterilized ASW and resuspended in 50 mL of either ASW medium, IMK medium or IMK + CAS medium in 250-mL flasks. For the recovery experiments, SSB01 cells were grown in ASW for 20 days. On day 20, the cells were pelleted by centrifugation at 100 *g* for 5 min at room temperature (RT) in an Eppendorf 5810R centrifuge and then resuspended in IMK + CAS and allowed to grow for an additional 20 days.

2.2.2 Analysis of Photosynthetic Function

The cultures were prepared as described in (Xiang et al., 2018, 2020) for measuring photosynthetic function. Maximum quantum yields of photosystem II (PSII) (calculated as F_v/F_m

= (F_m–F_0)/F_m) were determined for cell cultures using a JTS-10 spectrophotometer (Bio-Logic) (Joliot & Delosme, 1974) after ∼10 min of dark adaptation.

2.2.3 Growth Studies

SSB01 stock cultures were grown in IMK medium at 27°C on a 12 h-light/12 h-dark cycle with an irradiance of ∼10 μmol photons m^{-2} s^{-1}. Approximately 6×10^6 cells in log phase growth were pelleted by centrifugation at 100 g for 5 min at RT. Cells were washed twice with 20 mL sterile ASW medium, and resuspended in 30 mL of liquid ASW, IMK, or IMK + CAS media. SSB01 cells were quantified using a CountessTM II Automated Cell Counter following the manufacturer's instructions. Three biological replicates were performed for the growth experiments; they all yielded similar results.

2.2.4 RNA-Seq Analyses

Cultured SSB01 cells grown in different nutrient conditions were prepared as described in "growth studies" (above). Approximately 5×10^7 mid-log phase SSB01 cells grown in ASW, IMK, and IMK + CAS were collected by centrifugation and extracted with phenol/chloroform to prepare total RNA (Xiang et al., 2015, 2018). RNA was prepared from three biological replicates for cells grown in IMK and IMK + CAS, and two biological replicates for cells grown in ASW. ASW cultures were transferred from IMK precultures and allowed to grow for 2 weeks before proceeding to RNA extraction. Approximately 1 μg of total RNA from each sample was used to construct libraries with the TruSeq RNA Sample Prep Kit (Illumina FC-122–1001) following the manufacturer's instructions. The resulting libraries were sequenced on an Illumina HiSeq 2000 sequencer (2×10^1 bp) at the Stanford Center for Genomics and Personalized Medicine. All raw sequencing reads are available in the Sequence Read Archive1 with SRA accession numbers SRS5754975 (CAS samples) in the BioProject PRJNA591730 (Xiang et al., 2020), and

SRS6837549 (IMK samples) and SRS6837550 (ASW samples) in the BioProject PRJNA639352. RNA-seq reads for populating symbiotic SSB01 samples (that were populating Aiptasia for 12 days and 30 days) were obtained from SRA, Project PRJNA261862 (Baumgarten et al., 2015). Differential expression analysis was performed as previously described (Xiang et al., 2020). Briefly, RNA-seq raw reads of each SSB01 sample grown in ASW, IMK, or CAS were aligned to the SSB01 transcriptome assembly Symb6 that we established previously (Xiang et al., 2015) [deposited at SRA, Project PRJNA5910702 using BWA (H. Li & Durbin, 2009)]. The number of reads aligned to transcripts with a cutoff mapping quality score of 30 was counted using SAMtools. Differential expression from different nutrient conditions was further analyzed using the DESeq2 Bioconductor package (Love et al., 2014), with the transcripts comparing IMK vs. ASW, and IMK + CAS vs. ASW. Expression levels were analyzed as transcripts per kilobase million (TPM) (Wagner et al., 2012). Differential expression of transcripts was called based on the cutoff of a false-discovery rate (Benjamini-Hochberg method) adjusted p-value of ≤0.001. GO-term enrichment was analyzed using the BiNGO plugin for Cytoscape (Maere et al., 2005).

2.2.5 Amino Acid-Sequence Alignment

Amino acid sequence alignments for topoisomerases in SSB01 was conducted using MUSCLE (Edgar, 2004). 11 topoisomerase protein sequences predicted in symb6 and a total of 17 topoisomerase protein sequences from Arabidopsis (*Arabidopsis thaliana*; TOP1A, TOP1B, TOP2, TOP3A, TOP3B, TOP6A, TOP6B, TOP6BL, and GYRA), yeast (*Saccharomyces cerevisiae*, TOP1, TOP2, and TOP3), and human (*Homo sapiens*, TOP1, TOP2A, TOP2B, TOP3A, and TOP3B) were aligned. Protein sequences from the model systems were retrieved from the UniProt database with identifier IDs shown in Supplementary Table 2.1. The

phylogenetic tree was constructed using the neighbor-joining method of Geneious tree builder in Geneious 9.13.

2.3 Results and Discussion

2.3.1 IMK + CAS Medium Allows Faster Growth and Sustains Photosynthetic Function

To assess the impacts of inorganic and organic nutrients on the physiology of SSB01, we grew the cells in three different media with different nutrient compositions: (1) ASW; (2) IMK, which includes nitrate and ammonium; and (3) IMK + CAS. SSB01 cells were transferred from IMK medium to ASW, IMK, and IMK + CAS, respectively, and the growth characteristics and measurements of maximum quantum efficiency of PSII (F_v/F_m) were monitored.

Growth of SSB01 was significantly more rapid in IMK + CAS (*p*-value is 3.05E-05 based on two-sided t-test) and cells were able to reach much higher densities compared to ASW (during the 20 days of growth), while the difference between growth rates in IMK and ASW was small (p-value is 0.06 based on two-sided t-test) (Figure 2.1). The F_v/F_m remained stable over a growth period of 30 days in IMK + CAS but exhibited a significant decrease when the cells were grown in ASW (*p*-value = 0.004, two-sided t-test) or IMK (p-value = 0.006, two-sided t-test) for the same period of time (Figure 2.2). Interestingly, the decline in F_v/F_m was fully reversed in 2 days following supplementation of ASW-grown SSB01 cells with CAS; it remained stable for the additional 20 days of the experiment (Figure 2.3).

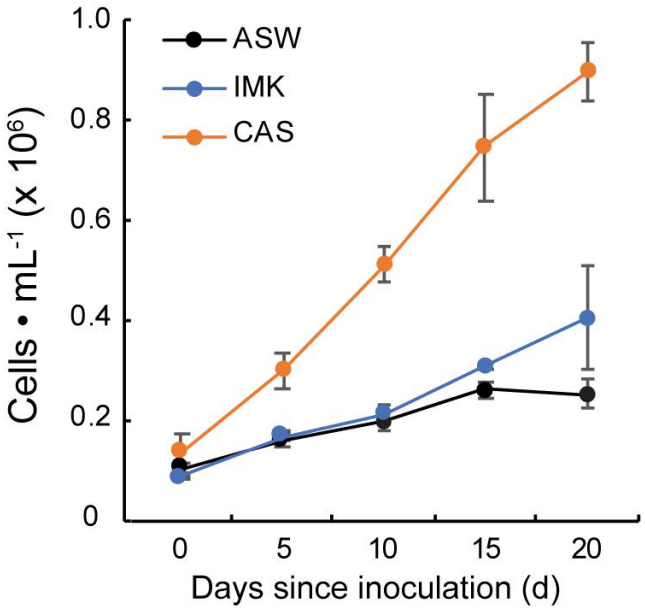

Figure 2.1 Growth of SSB01 cells in ASW, IMK, and IMK + CAS.
Growth of SSB01 was assessed in ASW (black line), IMK (blue line), and IMK + CAS (CAS, orange line) medium for 20 days. Error bars show standard errors derived from three replicate experiments.

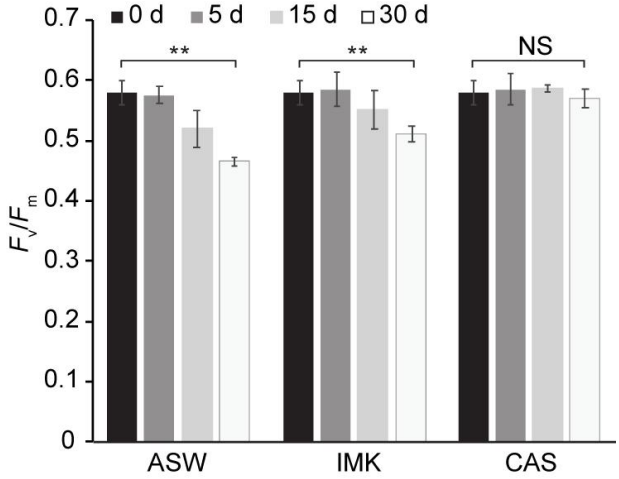

Figure 2.2 Stability of PSII efficiency for SSB01 cells grown in ASW, IMK, and IMK + CAS (CAS).
The F_v/F_m was measured (see "Materials and Methods") at 0, 5, 15, and 30 days when SSB01 cells were grown in ASW, IMK, and IMK + CAS, respectively. p-values (two sided t-test) for the significance of the 0 vs. 30 days differences are indicated (**p-value < 0.01, NS, not significant).

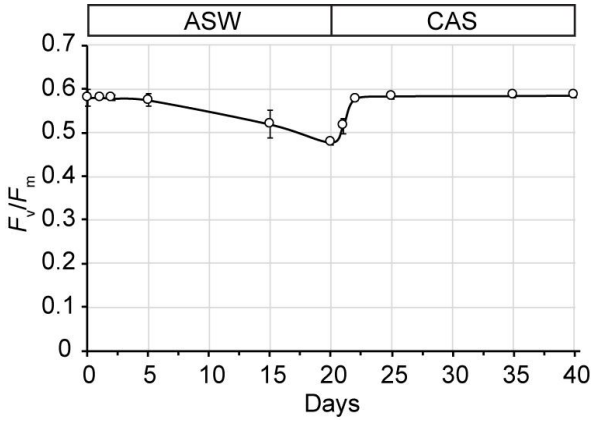

Figure 2.3 Recovery of F_v/F_m after transfer of ASW-grown SSB01 cells to IMK + CAS medium (CAS).
Cells were grown in seawater for 20 days and then transferred to IMK + CAS medium; the F_v/F_m was measured for cells before and after the transfer. Error bars show standard errors derived from three replicate experiments.

2.3.2 Extensive Transcriptome Changes in Response to IMK + CAS

To determine the changes in gene expression potentially associated with the physiological observations and to gain new insights into the acclimation of the cells to different trophic conditions, RNA-Seq was conducted for SSB01 grown in ASW, IMK, and IMK + CAS, with comparisons of transcript abundances of IMK + CAS relative to ASW, and IMK relative to ASW. Based on a cutoff of adjusted p-values (based on Benjamini-Hochberg correction) ≤0.001, we identified 20,549 transcripts (approximately 34.4%) that were differentially expressed when comparing cells grown in IMK + CAS relative to ASW (Figure 2.4). In contrast, only 141 transcripts (approximately 0.2%) were scored as differentially expressed when comparing SSB01 cells grown in IMK relative to ASW (Figure 2.4).

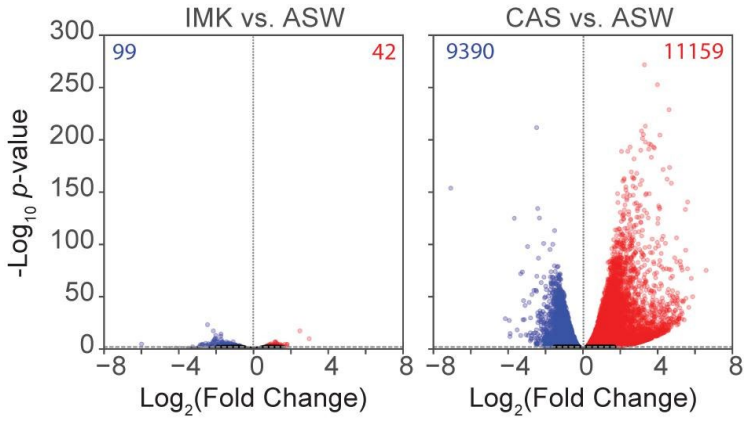

Figure 2.4 Expression in SSB01 in IMK + CAS or IMK compared to ASW.
Volcano plot of relative abundances of individual transcripts in IMK vs. ASW and IMK + CAS vs. ASW. x-axis, fold-changes; y-axis, adjusted p-values based on Benjamini-Hochberg correction; red dots indicate transcripts more abundant in IMK (left) or in IMK + CAS (right). Blue dots indicate transcripts more abundant in ASW. Both axes use log scales. The horizontal line indicates adjusted p-values = 0.001, the cutoff used for considering differences to be significant.

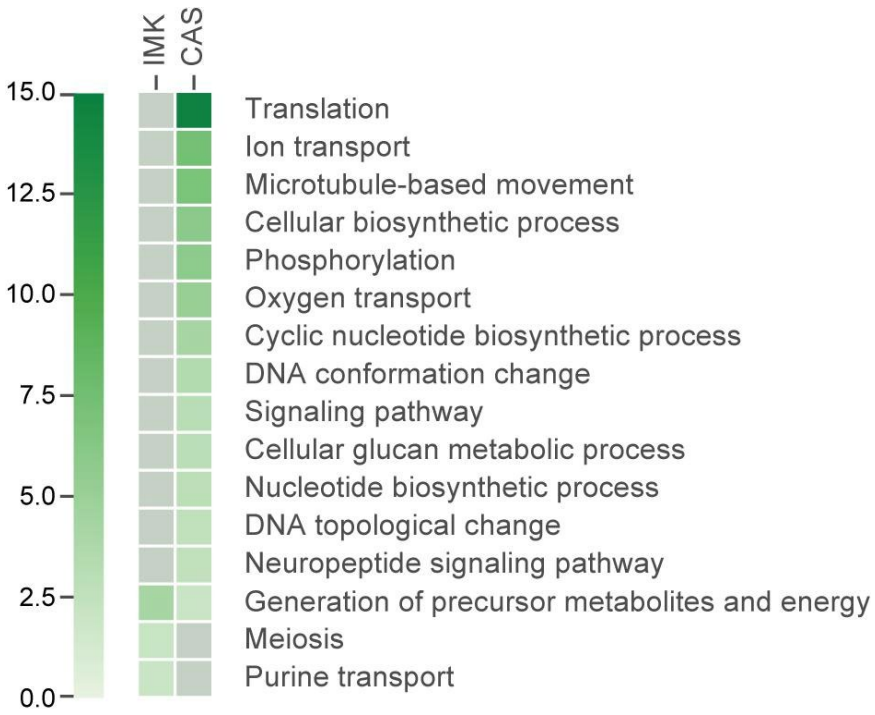

Figure 2.5 The GO categories enriched (based on adjusted hypergeometric p-value < 0.1) in the transcripts showing significant differential expression.
Heatmap showing the p-value for the enrichment of each category. Gray colored boxes indicate not significant.

We applied a Gene Ontology (GO) enrichment analysis and further analyzed the functional categories of the differentially expressed genes. GO terms for the proteins encoded by the transcripts enriched in IMK + CAS relative to ASW were represented by a wide variety of processes including “translation,” “DNA conformation change” (“DNA topological change” in particular), “ion transport,” cytoskeleton such as “microtubule-based movement,” “phosphorylation” (mostly “protein amino acid phosphorylation”), “oxygen transport” which is fundamental to aerobic respiration, “nucleotide biosynthetic process,” “cyclic nucleotide biosynthetic process,” “signaling pathway,” “neuropeptide signaling pathway,” and “cellular glucan metabolic process.” By contrast, few GO terms were enriched for the proteins encoded by transcripts expressed in IMK relative to ASW, but those terms that were slightly enriched include “generation of precursor metabolites and energy,” “purine transport,” and “meiosis” (Figure 2.5).

2.3.3 CAS May Modulate Translation and Protein Synthesis

The greatest number of genes that showed differential regulation in IMK + CAS relative to ASW medium encode proteins associated with translation. The transcript (s6_33548) encoding the General Control Non-derepressible 2 (GCN2) exhibited an ~18-fold increase in IMK + CAS. GCN2 is a serine/threonine-protein kinase that acts as an amino acid sensor in S. cerevisiae and can affect expression of genes encoding enzymes involved in amino acid synthesis (Castilho et al., 2014). Symbiodiniaceae GCN2 may perform similar functions in amino-acid sensing. Interestingly, the expression levels of GCN2 in symbiotic SSB01 increased gradually when the algal symbiont population increased (Supplementary Figure 2.1). This data suggests that sensing and controlling the biosynthesis of amino acids in the symbiont may be integral to host-symbiont interactions as the symbiont populates the host.

Elongation factor thermo unstable (EF-Tu) is an essential component of translation that places the aminoacyl-tRNA complex at the A-site of the ribosome (Rodnina et al., 2005). The transcript encoding EF-Tu (s6_1943) increased in abundance by more than 3-fold in IMK + CAS. The transcript encoding valine tRNA ligase also showed a >2-fold change in abundance. In addition, expression of 15 transcripts involved in translation initiation were significantly changed in IMK + CAS. For example, the abundance of the transcript (s6_51857) encoding the eukaryotic translation initiation factor 3 subunit B protein (eIF-3B) increased by almost 3-fold in IMK + CAS. This translation initiation factor is an RNA-binding component of the eukaryotic translation initiation factor 3 (eIF-3) complex, which specifically initiates translation of a subset of mRNAs involved in cell proliferation (A. S. Y. Lee et al., 2015). In contrast, the level of the transcript (s6_38195) encoding translation initiation factor 5A decreased by almost 3 fold in IMK + CAS (Supplementary Table 2.3). This translation initiation factor was recently reported to be involved

in polypeptide elongation rather than initiation (Gregio et al., 2009; Saini et al., 2009) and was shown to stimulate protein synthesis in *S. cerevisiae* (Henderson & Hershey, 2011). The precise meaning of these results is unclear, although measuring the intracellular levels of amino acids in both ASW and IMK + CAS grown cells may provide insights into potential feedback signals that might be involved in modulating protein homeostasis through the controlled expression of genes related to translation and protein synthesis.

2.3.4 Changes in Transcripts Encoding Transporters Associated With Limiting Nutrient Availability

Many changes in expression were observed for transcripts related to ion transporters, with 402 transcripts differentially expressed when SSB01 cells were grown in IMK + CAS (Supplementary Table 2.6). Of those differentially expressed in IMK + CAS, 279 showed elevated transcript accumulation while 123 showed reduced transcript levels (Supplementary Table 2.6). Transcripts encoding voltage-gated sodium channel and voltage-gated ion channel superfamily proteins were some of the most highly expressed in IMK + CAS. For example, the level of the transcript (s6_2946) encoding a voltage-gated sodium channel increased by more than 7-fold. Additionally, four transcripts (s6_9034, s6_3890, s6_2386, s6_1118) encoding chloride channel proteins increased in abundances by more than 2-fold. Voltage-gated ion channels are transmembrane proteins that function in action potential generation in animal, plant, and algal cells (Ward et al., 2009). Levels of transcripts encoding calcium channels were also elevated in IMK + CAS, with 15 of these transcripts exhibiting ~2-fold increase in abundance relative to ASW (Supplementary Table 2.6). Calcium is an essential micronutrients and calcium signaling is critical for the cells to decode internal and external stimuli, and transduce them into changes in gene expression that modulates physiological processes (Demidchik et al., 2018). In addition, many

transcripts involved in nitrogen transport including ammonium transporters and nitrate transporters were significantly changed in IMK + CAS. 20 transcripts encoding ammonium transporters were preferentially expressed in ASW while three were elevated (s6_7783, s6_5492, s6_32551) in IMK + CAS. However, only one transcript encoding an ammonium transporter (s6_51578), and one transcript involved in purine transport (s6_1521) were differentially expressed in IMK relative to ASW. The abundance of the transcript s6_51578 decreased >4-fold in both IMK and IMK + CAS relative to ASW. Similarly, we found seven transcripts encoding nitrate transporters that were expressed at higher levels in ASW (Supplementary Table 2.6). Symbiodiniaceae increases the level of transcripts encoding most transporters associated with the uptake of nitrogen compounds when the cells become limited for nitrogen (T. Li et al., 2021; Xiang et al., 2020). Previous studies have also shown that members of the former clade B Symbiodiniaceae displayed decreased growth rates under nitrogen-deprivation (Jiang et al., 2014). The elevation of transcripts encoding ammonium and nitrate transporters observed for cells maintained on ASW medium suggests that SSB01 is experiencing nitrogen limitation, which is consistent with its slow growth (Figure 2.1) and the decreased maximum efficiency of photosystem II (Figure 2.2) in ASW medium. The presence of organic nutrients along with appropriate amounts of ammonium and nitrate were suggested to increase the health of the holobiont (Morris et al., 2019). The transcriptome responses observed for SSB01 cells grown in IMK + CAS compared to ASW medium also suggests that ASW-grown cells are experiencing nitrogen deprivation and that the amino acids of CAS may provide the alga with a sufficient supply of nitrogen; this also suggests that when necessary, organic nutrients, including amino acids, may be provided by the host to the symbiont (Imbs et al., 2014; Steen, 1986; Wang & Douglas, 1999).

2.3.5 IMK + CAS May Elevate the Synthesis of Cyclic Nucleotides

The cyclic nucleotides cAMP and cGMP are important second messengers that modulate many fundamental cellular processes including metabolism, development and differentiation, cell proliferation, and cell survival under adverse conditions (Scheib et al., 2018). Transcripts encoding adenylyl cyclase and guanylate cyclases, enzymes that synthesize cAMP and cGMP (Potter, 2011; Steer, 1975), respectively, were differentially expressed in SSB01 cells grown in IMK + CAS relative to ASW and IMK (Supplementary Table 2.4). Of the 21 transcripts encoding adenylyl and guanylate cyclases, 19 increased while only two decreased in IMK + CAS relative to ASW or IMK. The potential increase in the synthesis of adenylyl and guanylate cyclases in IMK + CAS raises the possibility that organic nutrients/amino acids may trigger the production of second messengers such as cGMP and cAMP (Carucci et al., 2000), which in turn might regulate aspects of Symbiodiniaceae cell growth, proliferation and/or might enable the cells to better cope with suboptimal environmental conditions. Two decades ago cAMP was shown to regulate cell cycle progression and growth of the dinoflagellate *Crypthecodinium cohnii (Lam et al., 2001)*.

2.3.6 Massive Changes in Abundances of Transcripts for Enzymes Involved in Protein Phosphorylation

Dinoflagellates appear to have permanently condensed chromosomes and transcriptional control may be limited (e.g., transcript levels rarely become very high during acclimation processes), suggesting that post-translational modifications play important roles in dinoflagellates responses to environmental change (Gierz et al., 2016; Krueger et al., 2015; Leggat et al., 2007; Rosic et al., 2015; Xiang et al., 2015). Quantification of transcripts encoding enzymes involved in protein phosphorylation strongly suggest that phosphorylation may be modulating many cellular processes in response to different nutrient conditions. There are 64 transcripts encoding calcium-

dependent protein kinases that are differentially expression in IMK + CAS relative to IMK (and ASW) (Supplementary Table 2.5); 50 of these differentially expressed transcripts were elevated while 14 were diminished in IMK + CAS. For example, a transcript encoding a calcium dependent protein kinase (s6_33927) increased by almost 10-fold in IMK + CAS relative to ASW. Furthermore, 17 transcripts related to cGMP-dependent protein kinases increased in IMK + CAS while only one decreased. The largest change in abundance for cGMP-dependent kinases was for cGMP-dependent protein kinase isozyme 1 (s6_7176), which exhibited a greater than 16-fold elevation in IMK + CAS relative to ASW (Supplementary Table 2.5). The increase observed for transcripts related to cGMP-dependent protein kinases is congruent with changes in the levels of transcripts associated with cyclic nucleotide metabolism. Overall, our results indicate that growth of SSB01 in a source of organic nitrogen elicits an increase in the synthesis of adenylyl and guanylate cyclases and cyclic nucleotide dependent kinases, which likely promotes signal transductions through cGMP and cAMP second messengers.

2.3.7 Changes in the Levels of Transcripts for DNA Topoisomerases and Histones Suggest That the Chromosomes Experience Nutrient Driven Changes in DNA Conformation

Some notable differences in cells maintained in IMK + CAS relative to IMK or ASW involves transcripts encoding proteins associated with DNA topography. Dinoflagellate chromosomes are permanently condensed and maintain a liquid crystalline state that does not appear to rely on histones (Wisecaver & Hackett, 2011). Differences in mechanisms controlling DNA replication and transcription in dinoflagellates may occur as a consequence of their permanently condensed chromosomes and the absence of nucleosomes or the presence of divergent nucleosomes. It has been suggested that extrachromosomal loops protruding from the condensed chromatin structure may allow access of the DNA to the cell's transcriptional

machinery (Wisecaver & Hackett, 2011). However, analysis of the 3-dimensional organization of the *B. minutum* genome revealed large topological domains demarcated by convergent gene array boundaries ["dinoTADs," topologically associating domains (TADs) in dinoflagellates], possibly formed as a consequence of transcription-induced supercoiling (Marinov et al., 2020).

Many transcripts encoding DNA topoisomerases were elevated in IMK + CAS relative to ASW medium. We identified 22 transcripts encoding topoisomerases I, II, and III in SSB01. These enzymes change the topology of DNA by overwinding or underwinding the polynucleotide strands and have been implicated in critical cellular functions including DNA replication, DNA repair, and transcription (Champoux, 2001; Levin et al., 1993). Topoisomerase I functions in DNA replication and transcription by creating a single-strand break that allows relief of strain caused by DNA supercoiling (Champoux, 2001). Type II topoisomerases, which can form dimers with Type III topoisomerases, similarly relieve supercoiling strain through the generation of double-stranded DNA breaks (Ahmad et al., 2016; Hartung et al., 2008). The atypical type II topoisomerase, DNA gyrase, is essential for negative supercoiling during replication and transcription (Kampranis & Maxwell, 1996).

The transcripts for 11 topoisomerases, marked with an asterisk in Supplementary Table 2.2, had significantly increased mRNA abundances in IMK + CAS relative to ASW (Supplementary Table 2.2). Of the 11 topoisomerase transcripts, one was type I, five were type II, and five were type III (Figure 2.6). The transcript for the DNA gyrase (s6_445) increased by more than 3-fold in IMK + CAS and also showed increased levels when symbiotic SSB01 algae populate the Aiptasia host (Supplementary Figure 2.1). Elevated transcripts for five Type II topoisomerases in *B. minutum* suggest that they may form a complex and participate in unwinding of DNA that relieves topological stresses and allows access of the genome to transcription factors.

Topoisomerases have been detected in various dinoflagellates (Mak et al., 2005; Mínguez et al., 1994) and it was suggested that *C. cohnii* type II topoisomerase unwinds condensed chromosomes of the G1 phase of the cell cycle for transcription (Mak et al., 2005). Our results also raise the possibility that these topoisomerases may be important for exposing regions of the chromosomal DNA during replication and transcription in the Symbiodiniaceae.

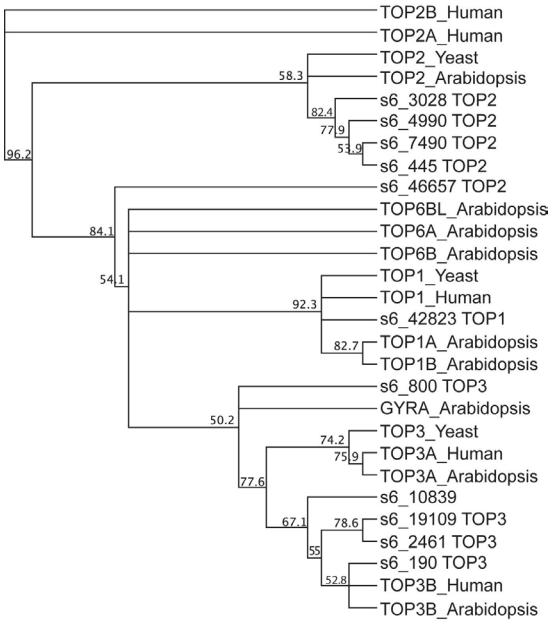

Figure 2.6 Phylogenetic analysis of DNA topoisomerase sequences in SSB01.
Protein polypeptide sequences of 11 DNA topoisomerases in SSB01, 9 in Arabidopsis (Arabidopsis thaliana; TOP1A, TOP1B, TOP2, TOP3A, TOP3B, TOP6A, TOP6B, TOP6BL, and GYRA), 3 in yeast (S. cerevisiae, TOP1, TOP2, and TOP3), and 5 in human (Homo sapiens, TOP1, TOP2A, TOP2B, TOP3A, and TOP3B) were aligned using the MUSCLE program. The phylogenetic tree was built using the neighbor-joining method by Geneious tree builder. The numbers on the nodes indicate the percentage of bootstrap p-values obtained from 1,000 replicates.

Previously it was thought that dinoflagellate histones play limited roles in DNA packaging, supercoiling and transcriptional changes, even though both conserved and divergent histones and the histone code were found in these organisms, including in B. minutum, through genomics

analysis (Marinov & Lynch, 2015). Symbiodiniaceae possess transcripts for all core histones, but these histones do not appear to play major roles in the organization and packaging of nuclear DNA (Gornik et al., 2012; Wisecaver & Hackett, 2011). We identified several transcripts encoding core histones and histone protein variants that were differentially expressed when SSB01 was grown on IMK + CAS. Interestingly, the level of the transcript encoding a protein similar to the H3-like centromeric protein A (CENP-A, s6_36342) increased by more than 3-fold. Transcripts encoding Histone H3 (s6_4125 and s6_16949) and Histone H2A (s6_34360) were modestly downregulated. In addition, the expression levels of the transcript for CENP-A increased when SSB01 algae were populating the Aiptasia host (Supplementary Figure S1). CENP-A, a histone H3 variant, confers epigenetic identity to centromeres and promotes the assembly of kinetochores, chromosome segregation, and cell division (Black et al., 2007; McKinley & Cheeseman, 2016). Tight regulation of CENP-A is critical for proper centromere assembly. It is possible that histones and histone variants could play similar roles in Symbiodiniaceae in modulating chromatin structures and accessibility during cell proliferation. CENP-A has also been shown to prevent the binding of H1 and modify the wrapping of DNA in the nucleosome (Roulland et al., 2016). The elevation of the CENP-A transcripts and the decline of the H3 transcripts in SSB01 cells grown in IMK + CAS may allow for DNA to become more accessible for replication and transcription. These changes may reprogram cell metabolism with respect to its nutrient status.

We also observed massive changes in the levels of transcripts encoding motor proteins. Kinesins are microtubule-bound molecular motors that hydrolyze ATP to perform a range of functions, including the transport of organelles, modulation of cellular organization, mitosis, and signal transduction (Hirokawa et al., 2009; Marx et al., 2009). Many transcripts (53) encoding kinesin family proteins were differentially expressed in SSB01 cells grown in IMK + CAS

(Supplementary Table 2.7). The most significantly upregulated transcript encoding a chromosome-associated kinesin (s6_51770) showed more than 6-fold elevation in IMK + CAS relative to ASW. These results suggest that the nutrient status of the medium could significantly impact the levels and functions of microtubule bound motors which may play essential roles in cell division and cellular organization and would be a critical point for control during growth *in hospite*.

Interestingly, the level of the transcript for nucleosome assembly protein-1 (NAP1, s6_2729) is also elevated in IMK + CAS. NAP1 functions in shuttling histones into the nucleus, assembling nucleosomes, and promoting chromatin fluidity, thereby regulating transcription. The loss of NAP1 in yeast resulted in prolonged delays in mitosis, and it is hypothesized that the stimulation of transcription factor binding by NAP1 could result in greater DNA accessibility (Park & Luger, 2006).

Structural maintenance of chromosomes (SMC) proteins are part of a large family of ATPases that form dimers at the core of the condensin complexes (Hirano, 2002; Löwe et al., 2001). As key organizers of chromosome architecture, SMC proteins play major roles in higher-order chromosome organization and dynamics, including chromosome condensation, cohesion of sister chromatids, DNA repair, and gene expression (Harvey et al., 2002). The levels of transcripts encoding SMC1-like protein (s6_5945) and SMC2 (s6_3357) increased in IMK + CAS, whereas another transcript encoding SMC1 (s6_638) decreased in abundance (Supplementary Table 2.2). In addition, the transcript encoding condensin complex subunit 1 (s6_5055), which is a regulatory subunit of the condensin complex, increased in abundance by almost 3-fold in IMK + CAS. Together, our results raise the possibility that the supplementation of IMK medium with CAS impacts Symbiodiniaceae chromosome architecture through the core histone proteins, histone chaperones, topoisomerases, and SMC ATPases.

2.4 Conclusion

The study presented here provides insights into the responses of Symbiodiniaceae to organic and inorganic nutrients. When IMK medium is supplemented with CAS, a mixture of organic nitrogen containing compounds (mostly amino acids), SSB01 cells grow faster and maintain their photosynthetic apparatus; maximum quantum yield of photosystem II was diminished in cells cultivated for long periods in IMK or ASW. Analysis of differentially expressed transcripts showed that SSB01 grown in ASW and IMK showed few differences in transcript accumulation. In contrast, SSB01 cells grown in IMK + CAS exhibited significant differences in the abundances of transcripts that encode proteins associated with ion transport, translation, cyclic nucleotide biosynthesis, phosphorylation, and DNA conformation. Many of the changes appear to be related to rapid growth and cell division which may be coupled to the nutrient status of the cells. ASW is not conducive to rapid algal growth and may not provide the cells with adequate nutrients, as indicated by activation of nutrient scavenging pathways. Experiencing a scarcity of nutrients may also drive Symbiodiniaceae into establishing a symbiotic association with a cnidarian host, where nutrients may be more readily available and also play a major role in regulating host-symbiont interactions. More detailed physiological and molecular analyses of Symbiodiniaceae algae exposed to various conditions in culture may define the impact of light, temperature and nutrients (e.g., nitrogen, fixed carbon, phosphate) on growth and photosynthesis, suggest metabolic pathways associated with stress conditions and the different trophic life-styles (e.g., autotrophic, mixotrophic, heterotrophic), and provide a detailed picture of the ways in which these algae accommodate environmental change. Ultimately, by comparing transcriptional responses observed in culture with those associated with algae growing in hospite may help

elucidate the in hospite conditions experienced by the endosymbiotic alga and identify key genes that are specifically involved in symbiosis. One important example of this is the elevation in levels of transcripts encoding GCN2 protein kinases, which may act as an amino acid/organic nitrogen sensor in SSB01, similar to its function in *S. cerevisiae* (Castilho et al., 2014).

2.5 Chapter 2 Supplementary Tables and Figures

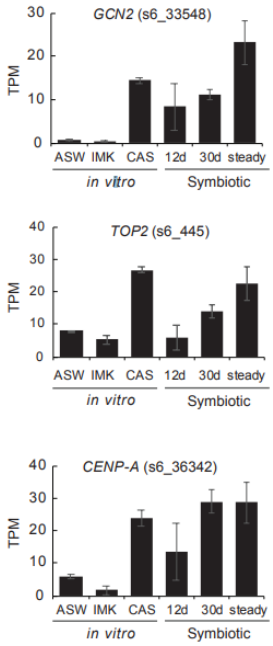

Supplementary Figure 2.1 SSB01 transcripts for GCN2, TOP2, and CENP-A under different culturing and symbiotic conditions.
Transcript levels for General Control Nonderepressible 2 (GCN2, s6_33548), topoisomerase II (TOP2, s6_445) and histone h3-like centromeric protein a-like (CENP-A, s6_36342) expressed as transcripts per kilobase million(TPM) from in vitro cultures (ASW, IMK and CAS) and populating symbiotic SSB01 (12 d, 30 d, and steady state) in the Aiptasia host. Results of symbiotic SSB01 were obtained by analyzing the data from (Baumgarten et al., 2015; Xiang et al., 2020). Shown are means ± SDs from at least three biological replicates.

Supplementary Table 2.1 UniProt IDs of protein sequences used for amino acid-sequence alignment and phylogenetic tree.

ID	Description
s6_445	dna gyrase topoisomerase a subunit family protein (type II)
s6_4990	dna topoisomerase 2
s6_7490	dna topoisomerase 2
s6_800	dna topoisomerase 3-alpha
s6_2461	dna topoisomerase 3-beta-1
s6_190	dna topoisomerase III beta
s6_10839	dna topoisomerase family protein
s6_3028	dna topoisomerase II
s6_42823	dna topoisomerase I
s6_19109	topoisomerase III beta
s6_46657	mca1_debha (has a dna topoisomerase 2-like protein domain)
P30181	TOP1A_ARATH
Q9FJ79	TOP1B_ARATH
P30182	TOP2_ARATH
Q9LVP1	TOP3A_ARATH
F4ISQ7	TOP3B_ARATH
Q9LZ03	TOP6A_ARATH
P11387	TOP1_HUMAN
P04786	TOP1_YEAST
P06786	TOP2_YEAST
P13099	TOP3_YEAST
P11388	TOP2A_HUMAN
Q02880	TOP2B_HUMAN
Q13472	TOP3A_HUMAN
O95985	TOP3B_HUMAN
Q5Q0E6	TO6BL_ARATH
Q9CAF6	GYRA_ARATH
Q9C5V6	TOP6B_ARATH

Supplementary Table 2.2 Annotations and expression levels of transcripts involved in DNA conformation change in IMK and IMK + CAS relative to ASW.

ID	Annotation	Log2(Fold Change)	
		IMK	CAS
s6_36342	histone h3-like centromeric protein a-like	NS	1.840309839
s6_445	dna gyrase topoisomerase a subunit family protein (type II)	NS	1.605050216
s6_4990	dna topoisomerase 2	NS	1.475542553
s6_5055	condensin complex subunit 1	NS	1.437911577
s6_7490	dna topoisomerase 2	NS	1.217750319
s6_800	dna topoisomerase 3-alpha	NS	1.089148206
s6_2461	dna topoisomerase 3-beta-1	NS	1.087360945
s6_190	dna topoisomerase III beta	NS	1.08305918
s6_3357	structural maintenance of chromosomes 2 (SMC2)	NS	1.005647138
s6_10839	dna topoisomerase family protein	NS	0.886451327
s6_5945	structural maintenance of chromosomes protein 1 (SMC1) like protein	NS	0.82016822
s6_2729	nucleosome assembly protein 1,1	NS	0.777967651
s6_3028	dna topoisomerase II	NS	0.666457278
s6_42823	dna topoisomerase I	NS	0.485587077
s6_19109	topoisomerase III beta	NS	0.479841491
s6_46657	mca1_debha (has a dna topoisomerase 2-like protein domain)	NS	0.288942868
s6_4125	h3	NS	-0.390963094
s6_34360	histone h2a	NS	-0.661519768
s6_16949	histone h3	NS	-0.74061421
s6_638	structural maintenance of chromosomes 1 (SMC1)	NS	-0.86264299

NS = Not significant

Supplementary Table 2.3 Annotations and expression levels of transcripts involved in translation in IMK and IMK + CAS relative to ASW.

ID	Annotation	Log2(Fold Change)	
		IMK	CAS
s6_33548	eif2 alpha kinase gcn2	NS	4.242509
s6_1943	elongation factor tu	NS	1.84401
s6_1025	valine--trna ligase	NS	1.704732
s6_51857	eukaryotic translation initiation factor 3 subunit	NS	1.425556
s6_21694	seryl-trna synthetase	NS	1.218633
s6_6586	lysyl-trna synthetase	NS	1.193531
s6_877	eukaryotic translation initiation factor 4a	NS	1.117279
s6_15298	translation initiation factor if-2	NS	1.07941
s6_34150	hypothetical protein Pmar_PMAR005139	NS	1.003872
s6_9800	seryl-trna serine--trna	NS	0.947004
s6_3865	achain crystal structure of engineered northeast structural genomics consortium target	NS	0.878087
s6_40474	poly binding cytoplasmic isoform cra_c	NS	0.838509
s6_7607	alanyl-trna synthetase	NS	0.767272
s6_28691	elongation factor	NS	0.717606
s6_52019	hypothetical protein Pmar_PMAR028699	NS	0.640479
s6_6433	isoleucine trna	NS	0.618561
s6_3694	glutamate--trna ligase	NS	0.614944
s6_69	asparaginyl-trna synthetase	NS	0.613084
s6_10329	leucyl-trna cytoplasmic-like	NS	0.604945
s6_24243	prolyl-trna synthetase	NS	0.593424
s6_8934	chloroplast translation factor ts	NS	0.592851
s6_13292	histidyl-trna	NS	0.587008
s6_40676	50s ribosomal protein	NS	0.571693
s6_14811	ribosome recycling factor	NS	0.540693
s6_31340	rna helicase-1	NS	0.534643
s6_5496	ribosomal protein n-terminal domain containing protein	NS	0.530623
s6_51362	eukaryotic translation initiation	NS	0.507587

s6_245	lysyl-trna synthetase	NS	0.493046
s6_3048	glycyl-trna synthetase	NS	0.467294
s6_6170	riken cdna 2610011n19 gen	NS	0.460501
s6_34673	leucine--trna cytoplasmic	NS	0.445342
s6_12216	tryptophanyl-trna synthetase	NS	0.440592
s6_10417	elongation factor tu	NS	0.410769
s6_25344	aspartyl-trna synthetase	NS	0.38872
s6_23169	non-discriminatory gln-glu-trna synthetase	NS	0.370669
s6_33760	valyl trna synthetase	NS	0.359458
s6_33966	60s ribosomal protein	NS	-0.28204
s6_16477	glycyl-trna synthetase	NS	-0.31597
s6_984	eukaryotic translation initiation	NS	-0.33233
s6_34333	50s ribosomal protein l13	NS	-0.3402
s6_34952	lsu ribosomal protein l24p	NS	-0.34854
s6_5949	ribosomal protein mitochondrial	NS	-0.37972
s6_10622	phenylalanyl-trna synthetase beta chain	NS	-0.38861
s6_34927	eukaryotic peptide chain release	NS	-0.39972
s6_3187	ribosomal protein	NS	-0.40724
s6_32631	eukaryotic translation initiation	NS	-0.40935
s6_40633	glycyl-trna synthetase	NS	-0.41492
s6_9625	ribosomal protein l15	NS	-0.41835
s6_46745	60s ribosomal protein	NS	-0.41918
s6_53712	40s ribosomal protein	NS	-0.42157
s6_11490	Ribosomal protein L36	NS	-0.42526
s6_51269	30s ribosomal protein s13	NS	-0.42597
s6_32439	eukaryotic translation initiation factor 4e-like	NS	-0.43424
s6_51036	60s ribosomal protein	NS	-0.44817
s6_33483	60s ribosomal protein l29	NS	-0.458
s6_31435	60s ribosomal protein	NS	-0.46612
s6_31133	60s acidic ribosomal protein lp2	NS	-0.47092
s6_39736	50s ribosomal protein l14	NS	-0.47795
s6_15407	60s ribosomal protein l23a	NS	-0.49093

s6_26280	60s ribosomal protein	NS	-0.49229
s6_3805	seryl-trna	NS	-0.49294
s6_25684	translation initiation factor eif-1a	NS	-0.50022
s6_39167	ribosomal protein s21	NS	-0.50303
s6_28183	ribosomal protein s27a	NS	-0.5118
s6_40185	elongation factor	NS	-0.512
s6_24162	ribosomal protein l29	NS	-0.51635
s6_31416	50s ribosomal subunit l24	NS	-0.52363
s6_17156	hypothetical protein THAOC_31095	NS	-0.52536
s6_48138	60s ribosomal protein	NS	-0.52625
s6_36630	60s ribosomal protein	NS	-0.52861
s6_29281	ribosomal protein	NS	-0.53121
s6_36116	40s ribosomal protein	NS	-0.53771
s6_31751	40s ribosomal protein	NS	-0.54103
s6_38180	ribosomal protein	NS	-0.55223
s6_34592	ribosomal protein l18a	NS	-0.55451
s6_48933	40s ribosomal protein s16	NS	-0.55603
s6_1531	50s ribosomal protein l2	NS	-0.55794
s6_14372	50s ribosomal protein l11	NS	-0.56475
s6_40921	ribosomal protein l44	NS	-0.57265
s6_26347	ribosomal protein	NS	-0.57908
s6_27741	60s ribosomal protein	NS	-0.5791
s6_34411	translation initiation factor if-1	NS	-0.59041
s6_40242	eukaryotic translation initiation factor 3	NS	-0.59327
s6_21497	eukaryotic translation initiation factor 3 subunit	NS	-0.59631
s6_25721	mitochondrial ribosomal protein s8	NS	-0.59983
s6_34382	eukaryotic translation initiation	NS	-0.60095
s6_23858	50s ribosomal protein l17	NS	-0.6049
s6_35193	eukaryotic translation initiation factor 3 subunit k	NS	-0.61211
s6_41281	50s ribosomal protein l24	NS	-0.61664
s6_32906	60s ribosomal protein l43	NS	-0.62846
s6_183	eukaryotic translation initiation factor 4a	NS	-0.62998

s6_4671	ribosomal protein s27a	NS	-0.6369
s6_2973	40s ribosomal protein	NS	-0.64549
s6_30966	predicted protein	NS	-0.66081
s6_42717	60s ribosomal protein l39-like 5-like	NS	-0.6699
s6_26371	60s ribosomal protein l6	NS	-0.68172
s6_32071	60s ribosomal protein l38	NS	-0.686
s6_33393	60s ribosomal protein	NS	-0.69213
s6_31405	phenylalanyl-trna synthetase alpha	NS	-0.69798
s6_10921	40s ribosomal protein s19	NS	-0.71299
s6_32202	30s ribosomal protein s17	NS	-0.71709
s6_1945	40s ribosomal protein	NS	-0.71768
s6_37353	small subunit ribosomal protein 14	NS	-0.72653
s6_6001	30s ribosomal protein	NS	-0.72888
s6_39569	ribosomal protein s11	NS	-0.73265
s6_28386	40s ribosomal protein	NS	-0.73601
s6_25546	60s ribosomal protein	NS	-0.74147
s6_27737	40s ribosomal protein s8	NS	-0.75551
s6_29989	hypothetical protein Pmar_PMAR024716	NS	-0.7576
s6_39096	60s ribosomal protein l12	NS	-0.76454
s6_38166	ribosomal protein	NS	-0.77151
s6_26370	60S ribosomal protein L6E	NS	-0.77812
s6_3715	ubiquitin a-52 residue ribosomal protein fusion product 1	NS	-0.77938
s6_38901	60s ribosomal protein l13a	NS	-0.78213
s6_41050	ribosomal protein	NS	-0.78956
s6_40418	40s ribosomal protein s8	NS	-0.79182
s6_40914	40s ribosomal s14	NS	-0.79504
s6_32963	ribosomal protein component of cytosolic 80s ribosome and 60s large subunit	NS	-0.79689
s6_27641	50s ribosomal protein l23	NS	-0.79887
s6_39165	ribosomal protein l35	NS	-0.80028
s6_28154	60s ribosomal protein l22	NS	-0.80457
s6_53694	60s ribosomal subunit protein	NS	-0.80579
s6_38667	60s ribosomal protein	NS	-0.80789

s6_38673	40s ribosomal protein	NS	-0.81064
s6_27665	60s ribosomal protein l10a-	NS	-0.81074
s6_8479	60s ribosomal protein	NS	-0.81148
s6_5641	60s ribosomal protein	NS	-0.81369
s6_37881	60s ribosomal protein l38	NS	-0.81436
s6_4321	60s acidic ribosomal protein lp2	NS	-0.83937
s6_46766	ribosomal protein l22	NS	-0.84117
s6_2792	60s ribosomal protein	NS	-0.85442
s6_28121	40s ribosomal protein	NS	-0.8687
s6_12026	ribosomal protein l16	NS	-0.86983
s6_40774	ribosomal protein s27a	NS	-0.87122
s6_7050	60s ribosomal protein l33-	NS	-0.8734
s6_25911	ribosomal protein l22	NS	-0.87836
s6_29376	60s ribosomal protein l43	NS	-0.87856
s6_16140	ribosomal protein	NS	-0.88276
s6_16595	mitochondrial large subunit ribosomal protein	NS	-0.88852
s6_31770	60s ribosomal protein l10a-	NS	-0.89039
s6_3265	ribosomal protein l2	NS	-0.8972
s6_10600	ribosomal protein l18	NS	-0.90013
s6_39100	40s ribosomal protein	NS	-0.90019
s6_38452	40s ribosomal protein s27-	NS	-0.90134
s6_14822	60s ribosomal protein l26	NS	-0.90262
s6_48149	40s ribosomal protein x	NS	-0.90776
s6_31664	ribosomal protein l22	NS	-0.91792
s6_48126	ribosomal protein	NS	-0.92022
s6_38964	ribosomal protein l35	NS	-0.93954
s6_1599	60s ribosomal protein	NS	-0.94402
s6_28838	probable rpl43b-60s large subunit ribosomal protein	NS	-0.94944
s6_52510	60s ribosomal protein l34	NS	-0.94954
s6_11592	50s ribosomal protein l28	NS	-0.95415
s6_53684	ribosomal protein l21	NS	-0.9597
s6_758	40s ribosomal protein	NS	-0.961

s6_53742	60s ribosomal protein l12	NS	-0.97236
s6_51480	ribosomal protein component of cytosolic 80s ribosome and 60s large subunit	NS	-0.9729
s6_39751	60s ribosomal protein l12	NS	-0.97295
s6_22560	Ribosomal protein S14, conserved site	NS	-0.97986
s6_46793	ribosomal protein l13a	NS	-0.98261
s6_36110	60s ribosomal protein	NS	-0.98936
s6_36853	ribosomal protein	NS	-0.99281
s6_27740	40s ribosomal protein	NS	-0.99518
s6_38201	60s ribosomal protein l37	NS	-0.99656
s6_28989	40s ribosomal protein s0-	NS	-0.99811
s6_51344	60s ribosomal protein l34	NS	-1.00337
s6_50944	40s ribosomal protein	NS	-1.00549
s6_48125	ribosomal protein	NS	-1.009
s6_12874	40s ribosomal protein	NS	-1.01049
s6_30746	60s ribosomal protein l13a	NS	-1.01265
s6_37413	ribosomal protein s27a	NS	-1.0143
s6_35012	60s ribosomal protein l33-	NS	-1.01942
s6_28643	40s ribosomal protein	NS	-1.02194
s6_39087	ubiquitin-60s ribosomal protein l40-like isoform 2	NS	-1.02213
s6_4453	60s ribosomal protein l33-	NS	-1.0275
s6_36442	60s ribosomal protein	NS	-1.02831
s6_6061	60s ribosomal protein l37	NS	-1.02929
s6_34387	60s ribosomal protein	NS	-1.03058
s6_36998	60s ribosomal protein	NS	-1.032
s6_6232	40s ribosomal protein	NS	-1.03204
s6_26708	60s ribosomal protein	NS	-1.03355
s6_55679	60s ribosomal protein	NS	-1.03801
s6_55304	40s ribosomal protein	NS	-1.04057
s6_5609	ribosomal protein 29 40s small ribosomal subunit	NS	-1.05065
s6_23082	40s ribosomal protein	NS	-1.05377
s6_42704	40s ribosomal protein s15	NS	-1.05457
s6_24709	50s ribosomal protein	NS	-1.05562

s6_28010	40s ribosomal protein	NS	-1.05586
s6_9191	elongation factor	NS	-1.05905
s6_35857	60s ribosomal protein	NS	-1.05935
s6_52684	60s ribosomal protein l23a	NS	-1.06293
s6_25598	ribosomal protein s21	NS	-1.0647
s6_366	40s ribosomal protein s26-	NS	-1.06577
s6_35420	40s ribosomal protein	NS	-1.06984
s6_40704	40s ribosomal protein	NS	-1.07465
s6_53687	40s ribosomal protein	NS	-1.08281
s6_48169	ribosomal protein l18	NS	-1.08358
s6_46964	40s ribosomal protein	NS	-1.09781
s6_11408	ribosomal protein component of cytosolic 80s ribosome and 40s small subunit	NS	-1.10138
s6_51116	60s ribosomal protein	NS	-1.10504
s6_42399	40s ribosomal protein	NS	-1.11416
s6_39608	40s ribosomal protein s26-	NS	-1.11522
s6_23390	40s ribosomal protein	NS	-1.1235
s6_32094	60s ribosomal protein	NS	-1.12385
s6_51103	40s ribosomal protein	NS	-1.13124
s6_55206	40s ribosomal protein x	NS	-1.13508
s6_2390	60s ribosomal protein	NS	-1.13678
s6_31392	40s ribosomal protein s19	NS	-1.14349
s6_24298	ribosomal protein l21	NS	-1.15059
s6_2361	60s ribosomal protein l18a-	NS	-1.15273
s6_13942	40s ribosomal protein s15	NS	-1.16253
s6_53828	40s ribosomal protein s0-	NS	-1.16271
s6_30900	40s ribosomal protein s26-	NS	-1.17383
s6_36911	40s ribosomal protein s27-	NS	-1.19011
s6_31367	ribosomal protein component of cytosolic 80s ribosome and 40s small subunit	NS	-1.19074
s6_35077	40s ribosomal protein	NS	-1.19885
s6_51184	60s ribosomal protein	NS	-1.20238
s6_31753	60s ribosomal protein l37	NS	-1.20277

s6_40285	60s ribosomal protein	NS	-1.21391
s6_30773	40s ribosomal protein s0-	NS	-1.22109
s6_38264	60s ribosomal protein l10a-	NS	-1.22736
s6_53807	40s ribosomal protein	NS	-1.2286
s6_33719	ribosomal protein l18	NS	-1.22927
s6_27864	peptide chain release factor 1	NS	-1.23151
s6_31891	ubiquitin a-52 residue ribosomal protein fusion product 1	NS	-1.2405
s6_39224	component of cytosolic 80s ribosome and 60s large subunit	NS	-1.25943
s6_29130	60s ribosomal protein	NS	-1.28668
s6_39729	40s ribosomal protein	NS	-1.29733
s6_41657	ribosomal protein component of cytosolic 80s ribosome and 40s small subunit	NS	-1.32699
s6_703	60s ribosomal protein	NS	-1.3276
s6_5395	40s ribosomal protein s29-like	NS	-1.34213
s6_53743	60s ribosomal protein l34	NS	-1.35737
s6_15286	60s ribosomal protein	NS	-1.36654
s6_36617	60s ribosomal protein	NS	-1.38249
s6_39219	40s ribosomal protein s15	NS	-1.45956
s6_51072	ribosomal phosphoprotein	NS	-1.61353
s6_38195	translation initiation factor 5a	NS	-1.61924

NS = Not significant

Supplementary Table 2.4 Annotations and expression levels of transcripts involved in cyclic nucleotide metabolic process in IMK and IMK + CAS relative to ASW.

ID	Annotation	Log2(Fold Change)	
		IMK	CAS
s6_40118	adenylate guanylate cyclase with integral membrane sensor	NS	2.78401944
s6_22656	adenylate guanylate cyclase with gaf sensor and fha related	NS	2.6666916
s6_40135	adenylate guanylate cyclase with integral membrane sensor	NS	1.92327721
s6_12083	Adenylyl cyclase class-3/4/guanylyl cyclase	NS	1.62641752
s6_7850	adenylate cyclase	NS	1.35867394
s6_9878	p25-alpha family protein	NS	1.33787639
s6_9596	adenylate cyclase 1	NS	1.32518058
s6_6330	adenylyl cyclase	NS	1.2656074
s6_4484	adenylate guanylate cyclase	NS	1.22227468
s6_28434	guanylate cyclase beta 1	NS	1.14067638
s6_7394	guanylate cyclase soluble subunit beta-2	NS	1.11808505
s6_15693	guanlylate cyclase	NS	0.94279261
s6_29427	signal transduction histidine kinase	NS	0.93207999
s6_8711	hypothetical protein	NS	0.89682325
s6_8273	adenylyl cyclase	NS	0.8583253
s6_40171	adenylyl cyclase	NS	0.82129304
s6_7007	adenylyl cyclase	NS	0.81293912
s6_7433	adenylate guanylate cyclase with integral membrane sensor	NS	0.76804944
s6_11617	chase2 domain protein	NS	0.75453081
s6_4274	guanylyl cyclase	NS	0.71035587
s6_2141	adenylyl cyclase	NS	0.5434649
s6_5101	adenylyl cyclase	NS	0.47922861
s6_10501	adenylate cyclase	NS	0.42236834
s6_27791	serine threonine rgc	NS	0.33239402
s6_9597	adenylate cyclase	NS	-0.7546788

s6_51552	adenylate guanylate cyclase with integral membrane sensor	NS	-1.4107271

NS = Not significant

Supplementary Table 2.5 Annotations and expression levels of transcripts involved in phosphorylation in IMK and IMK + CAS relative to ASW.

ID	Annotation	Log2(Fold Change)	
		IMK	CAS
s6_29014	3-phosphoinositide-dependent protein kinase-1	NS	-0.2970172
s6_9528	achain crystal structure of kinase domain of calcium-dependent protein kinase cgd3_920 from cryptosporidium parvum	NS	0.45160336
s6_14659	agc family protein kinase	NS	-0.4529622
s6_42278	alpha kinase	NS	-1.7820837
s6_19353	alpha-glucan water dikinase	NS	1.29858263
s6_5312	alpha-glucan water dikinase	NS	0.87687741
s6_2517	alpha-glucan water dikinase 2	NS	1.2174411
s6_5935	ankyrin unc44	NS	1.56502548
s6_27927	atp synthase alpha	NS	0.43317488
s6_52041	atp synthase delta subunit	NS	0.52289262
s6_16600	atp synthase subunit b	NS	-0.4189052
s6_19485	aur protein kinase	NS	-0.7438986
s6_9157	aurora-like serine threonine protein kinase	NS	-0.6369279
s6_2516	br serine threonine-protein kinase	NS	0.68203421
s6_10751	ca2+ calmodulin-dependent protein kinase i-like protein	NS	0.66483463
s6_13002	calcium calmodulin-dependent protein	NS	0.73119046
s6_17142	calcium calmodulin-dependent protein kinase	NS	1.9088002
s6_12210	calcium calmodulin-dependent protein kinase	NS	-0.8852656
s6_34043	calcium calmodulin-dependent protein kinase type	NS	2.06792567
s6_34534	calcium calmodulin-dependent protein kinase type	NS	1.03082566
s6_2960	calcium calmodulin-dependent protein kinase type	NS	0.7759898
s6_48302	calcium calmodulin-dependent protein kinase type	NS	0.68081322

s6_35513	calcium calmodulin-dependent protein kinase type	NS	-0.5228451
s6_14521	calcium calmodulin-dependent protein kinase type	NS	-0.576285
s6_4161	calcium calmodulin-dependent protein kinase type iv-like	NS	-0.560907
s6_33927	calcium dependent protein kinase	NS	3.34446722
s6_34663	calcium dependent protein kinase	NS	0.50018488
s6_23097	calcium dependent protein kinase 16	NS	-0.3308253
s6_29537	calcium-dependent protein	NS	3.02191675
s6_9931	calcium-dependent protein	NS	2.43027933
s6_13375	calcium-dependent protein	NS	2.41586879
s6_3854	calcium-dependent protein	NS	1.67555829
s6_2437	calcium-dependent protein	NS	1.64293709
s6_35045	calcium-dependent protein	NS	1.5552293
s6_1775	calcium-dependent protein	NS	1.5330225
s6_12850	calcium-dependent protein	NS	1.40396187
s6_33864	calcium-dependent protein	NS	1.3783706
s6_33623	calcium-dependent protein	NS	1.34367269
s6_3678	calcium-dependent protein	NS	1.3143613
s6_32754	calcium-dependent protein	NS	1.12885393
s6_6131	calcium-dependent protein	NS	1.11985275
s6_27792	calcium-dependent protein	NS	1.06504227
s6_32695	calcium-dependent protein	NS	1.06290068
s6_28331	calcium-dependent protein	NS	0.81124585
s6_3703	calcium-dependent protein	NS	0.80027077
s6_266	calcium-dependent protein	NS	0.7917278
s6_6874	calcium-dependent protein	NS	0.78527557
s6_13295	calcium-dependent protein	NS	0.77023468
s6_13355	calcium-dependent protein	NS	0.66690404
s6_29481	calcium-dependent protein	NS	0.66319956
s6_28973	calcium-dependent protein	NS	0.65282405
s6_34005	calcium-dependent protein	NS	0.64651064

s6_14731	calcium-dependent protein	NS	0.64089167
s6_16157	calcium-dependent protein	NS	0.61913442
s6_13624	calcium-dependent protein	NS	0.61273346
s6_1312	calcium-dependent protein	NS	0.58961873
s6_3000	calcium-dependent protein	NS	0.58904588
s6_31935	calcium-dependent protein	NS	0.53075361
s6_15599	calcium-dependent protein	NS	0.50973011
s6_797	calcium-dependent protein	NS	0.50242322
s6_7042	calcium-dependent protein	NS	0.4983566
s6_40503	calcium-dependent protein	NS	0.49151925
s6_604	calcium-dependent protein	NS	0.4775329
s6_13436	calcium-dependent protein	NS	0.42948172
s6_621	calcium-dependent protein	NS	0.40198055
s6_33726	calcium-dependent protein	NS	0.36409148
s6_1992	calcium-dependent protein	NS	-0.5116787
s6_1314	calcium-dependent protein	NS	-0.5156398
s6_6584	calcium-dependent protein	NS	-0.5535508
s6_24327	calcium-dependent protein	NS	-0.5771301
s6_8954	calcium-dependent protein	NS	-0.6120375
s6_32589	calcium-dependent protein kinase	NS	1.73812731
s6_51276	calcium-dependent protein kinase	NS	1.294519
s6_1525	calcium-dependent protein kinase	NS	0.89831989
s6_19358	calcium-dependent protein kinase	NS	-0.3926256
s6_30991	calcium-dependent protein kinase	NS	-0.53885
s6_40713	calcium-dependent protein kinase 7	NS	-0.6119753
s6_26556	calcium-dependent protein related	NS	-0.4830769
s6_5035	calmodulin-domain protein	NS	2.09873721
s6_32530	calmodulin-domain protein	NS	1.91265011
s6_23228	calmodulin-domain protein	NS	1.8908936
s6_33644	calmodulin-domain protein	NS	1.67055
s6_5407	calmodulin-domain protein	NS	1.59914707
s6_728	calmodulin-domain protein	NS	1.54835661

s6_1432	calmodulin-domain protein	NS	1.35699117
s6_33884	calmodulin-domain protein	NS	1.10372692
s6_10397	calmodulin-domain protein	NS	0.86537792
s6_8460	calmodulin-domain protein	NS	0.81958919
s6_23315	calmodulin-domain protein	NS	0.78058605
s6_23947	calmodulin-domain protein	NS	0.72044164
s6_30827	calmodulin-domain protein	NS	0.6334984
s6_52407	calmodulin-domain protein	NS	0.47365575
s6_34574	calmodulin-domain protein kinase	NS	0.81087301
s6_38119	calmodulin-domain protein kinase	NS	-0.6068509
s6_19742	calmodulin-domain protein kinase 1	NS	1.48976275
s6_8018	calmodulin-domain protein kinase 1	NS	1.1808073
s6_43243	camk family protein kinase	NS	1.46442331
s6_12254	camk family protein kinase	NS	1.02054439
s6_30001	camk family protein kinase	NS	0.56334968
s6_9261	camk family protein kinase	NS	0.55328423
s6_12845	camk family protein kinase	NS	-0.5392136
s6_3062	camp-dependent protein kinase catalytic	NS	0.72988595
s6_10042	camp-dependent protein kinase catalytic	NS	0.47354894
s6_35960	camp-dependent protein kinase catalytic	NS	-0.7666271
s6_24210	carbon catabolite derepressing protein	NS	-0.376029
s6_2554	carbon catabolite derepressing protein	NS	-0.3794785
s6_10937	carbon catabolite derepressing protein kinase	NS	0.92613408
s6_51845	casein kinase	NS	2.63479701
s6_11085	casein kinase	NS	2.34967385
s6_14170	casein kinase	NS	1.12632956
s6_33708	casein kinase	NS	1.08175353
s6_25157	casein kinase	NS	-0.4371571
s6_33926	casein kinase family protein	NS	1.02374004
s6_39233	casein kinase i isoform delta-like protein	NS	-0.5399455
s6_17154	cbl-interacting protein kinase	NS	-0.5061703
s6_2518	cbl-interacting serine threonine-protein kinase 19	NS	-0.5574288

s6_4289	ccaat-binding transcription factor subunit	NS	-0.8854114
s6_44909	cell division control protein 28	NS	0.70671593
s6_47074	cell division protein	NS	-1.2186022
s6_33594	cell division protein kinase	NS	-0.6707485
s6_2534	cgmp dependent protein kinase	NS	0.78797916
s6_28298	cgmp-dependent protein	NS	1.76559175
s6_2743	cgmp-dependent protein	NS	1.25254749
s6_13376	cgmp-dependent protein	NS	1.22211515
s6_16608	cgmp-dependent protein	NS	1.19781055
s6_50966	cgmp-dependent protein	NS	0.8489316
s6_10341	cgmp-dependent protein	NS	0.40312118
s6_35240	cgmp-dependent protein	NS	0.38180326
s6_2401	cgmp-dependent protein kinase	NS	1.80668286
s6_4214	cgmp-dependent protein kinase	NS	1.55438891
s6_35984	cgmp-dependent protein kinase	NS	0.82787612
s6_16253	cgmp-dependent protein kinase	NS	0.79935328
s6_35892	cgmp-dependent protein kinase 2-like	NS	-0.5931877
s6_22909	cgmp-dependent protein kinase egl-4-like isoform 1	NS	1.25684728
s6_3148	cgmp-dependent protein kinase i alpha	NS	0.50240891
s6_7176	cgmp-dependent protein kinase isozyme 1	NS	3.68407543
s6_28545	cgmp-dependent protein partial	NS	1.17443797
s6_584	cipk-like protein expressed	NS	1.52623437
s6_5219	cmgc cdk cdc2 protein kinase	NS	-0.7352868
s6_9524	cmgc family protein kinase	NS	1.043601
s6_5650	cmgc mapk family	NS	-0.4039184
s6_13098	cyclic gmp-dependent protein kinase	NS	0.8818908
s6_9206	Cyclic nucleotide-binding domain	NS	1.46343932
s6_28847	cyclin g-associated	NS	0.75542615
s6_25972	cyclin-dependent kinase 10	NS	-0.8616104
s6_6444	cyclin-dependent kinase 3	NS	1.85471703
s6_3707	cytidylate kinase	NS	0.98192521
s6_1529	diguanylate cyclase domain-containing protein	NS	0.41266129

s6_33671	dihydroxyacetone kinase	NS	0.68753127
s6_15094	domain and endonuclease exonuclease phosphatase family protein	NS	0.92554493
s6_33548	eif2 alpha kinase gcn2	NS	4.24250948
s6_5427	eukaryotic elongation factor-2 kinase	NS	-0.5677231
s6_22475	extracellular signal-regulated protein kinase	NS	-0.5381885
s6_10204	FAFL228Wp	NS	0.68101548
s6_29719	gliding motility related cam kinase	NS	0.9339328
s6_40066	ha-tagged protein kinase domain of mitogen-activated protein kinase kinase kinase	NS	2.73432639
s6_23061	hunk protein	NS	0.65796322
s6_10927	hypothetical protein	NS	1.53331373
s6_16396	hypothetical protein	NS	0.68897905
s6_17224	hypothetical protein	NS	0.48520886
s6_2991	hypothetical protein	NS	0.48088429
s6_4704	hypothetical protein GUITHDRAFT_164559	NS	0.61852951
s6_4633	hypothetical protein GUITHDRAFT_40846, partial	NS	2.37937038
s6_18241	hypothetical protein GUITHDRAFT_40846, partial	NS	0.78484127
s6_16473	hypothetical protein GUITHDRAFT_76731	NS	1.03682049
s6_53918	hypothetical protein GUITHDRAFT_77982	NS	0.84888229
s6_12752	hypothetical protein NCAS_0C02830	NS	0.95114101
s6_7794	hypothetical protein THAOC_02564	NS	1.90279324
s6_18776	inositol monophosphatase	NS	-1.116603
s6_40592	Inositol polyphosphate-related phosphatase	NS	0.66212473
s6_833	integral membrane sensor hybrid histidine kinase	NS	0.87106904
s6_51174	kinase family protein	NS	-0.4319232
s6_4860	kinase-like protein	NS	1.67126355
s6_2902	kinase-like protein	NS	1.47615966
s6_4851	leucine-rich repeat and iq domain-containing protein 3	NS	1.21075459
s6_13864	map kinase-interacting serine threonine-protein	NS	0.78164284
s6_3407	map microtubule affinity-regulating kinase 2	NS	0.39323976

s6_8630	map microtubule affinity-regulating kinase 4	NS	0.32818059
s6_18527	member of the inositol monophosphatase protein family	NS	0.85729017
s6_21784	mhck ef2 kinase domain family protein	NS	-2.293044
s6_28987	mitochondrial atp synthase f0 lipid binding subunit-like protein 3	NS	-0.6247175
s6_25052	mitochondrial pyruvate dehydrogenase kinase	NS	-0.3590392
s6_34465	mitogen activated protein kinase kinase kinase	NS	0.69179901
s6_14690	mitogen activated protein kinase kinase kinase 3	NS	0.46569548
s6_34371	mitogen-activated protein	NS	0.38953099
s6_18924	mitogen-activated protein kinase	NS	0.92320024
s6_9653	mitogen-activated protein kinase	NS	0.78859009
s6_7630	mitogen-activated protein kinase	NS	0.53364962
s6_29494	mitogen-activated protein kinase	NS	-0.4195409
s6_46758	mitogen-activated protein kinase	NS	-0.4897699
s6_8960	mitogen-activated protein kinase	NS	-0.7842464
s6_14851	mitogen-activated protein kinase 3	NS	1.16320372
s6_12915	myosin light chain kinase	NS	2.22167441
s6_25613	myosin light chain kinase	NS	1.4983274
s6_15791	myosin light chain kinase	NS	-0.754363
s6_54077	nek4 protein Serine/threonine-protein kinase Nek4	NS	-1.1560179
s6_7303	nima-related kinase 7	NS	-1.1189461
s6_8707	non-specific serine threonine protein kinase	NS	1.54303663
s6_4011	nuak snf1-like 2	NS	0.96258434
s6_35474	nucleoside diphosphate kinase 7-like	NS	-0.4301505
s6_279	ovarian-specific serine threonine-protein kinase	NS	-0.3586034
s6_2888	Paramyosin, putative	NS	0.72445863
s6_51298	phosphate dikinase	NS	3.08808174
s6_33547	phosphate dikinase	NS	1.66346925
s6_14453	phosphatidylinositol 3- and 4-kinase domain-containing protein	NS	0.46559803
s6_27447	phosphatidylinositol 3- root isoform	NS	0.90313341

s6_34611	phosphoenolpyruvate carboxylase kinase	NS	1.5639676
s6_781	phosphoenolpyruvate synthase	NS	1.00762787
s6_6310	phosphoinositide 3-kinase regulatory subunit 4-like	NS	1.54331577
s6_28626	phosphoinositide-dependent protein	NS	-0.4942233
s6_43078	phosphoinositide-dependent protein	NS	-0.7254442
s6_37659	pkinase-domain-containing protein	NS	0.90410173
s6_17873	probable serine threonine-protein kinase abkc-like	NS	0.515838
s6_20038	protein	NS	0.7016155
s6_3440	protein camp- catalytic chain	NS	0.4483526
s6_6542	protein cgmp- type i	NS	0.79150769
s6_15935	protein kinase	NS	2.81103367
s6_17584	protein kinase	NS	1.82337375
s6_5182	protein kinase	NS	1.65319195
s6_40107	protein kinase	NS	1.4560932
s6_40092	protein kinase	NS	1.11969923
s6_3686	protein kinase	NS	0.60772001
s6_9228	protein kinase	NS	0.52659247
s6_13785	protein kinase	NS	0.50438258
s6_293	protein kinase	NS	0.42988307
s6_5673	protein kinase	NS	0.38743948
s6_9204	protein kinase	NS	0.33289049
s6_3550	protein kinase	NS	-0.3953246
s6_1058	protein kinase	NS	-0.4248657
s6_9491	protein kinase	NS	-1.0535537
s6_4572	protein kinase 2	NS	0.69560651
s6_11842	protein kinase b-like protein	NS	0.4080949
s6_23199	protein kinase domain containing protein	NS	3.64839153
s6_6015	protein kinase domain containing protein	NS	2.17876764
s6_21915	protein kinase domain containing protein	NS	1.83006848
s6_243	protein kinase domain containing protein	NS	1.3502419
s6_12011	protein kinase domain containing protein	NS	1.17630465

s6_33753	protein kinase domain containing protein	NS	1.16139404
s6_34237	protein kinase domain containing protein	NS	1.07320252
s6_18025	protein kinase domain containing protein	NS	1.07137032
s6_43520	protein kinase domain containing protein	NS	0.88382998
s6_34765	protein kinase domain containing protein	NS	0.68426116
s6_12233	protein kinase domain containing protein	NS	0.64648863
s6_7045	protein kinase domain containing protein	NS	0.64067473
s6_8483	protein kinase domain containing protein	NS	0.54782934
s6_17670	protein kinase domain containing protein	NS	0.54632236
s6_35504	protein kinase domain containing protein	NS	0.48944526
s6_23886	protein kinase domain containing protein	NS	0.4822645
s6_13769	protein kinase domain containing protein	NS	0.47103171
s6_6007	protein kinase domain containing protein	NS	0.46533891
s6_40389	protein kinase domain containing protein	NS	0.45200921
s6_9651	protein kinase domain containing protein	NS	0.44066364
s6_38306	protein kinase domain containing protein	NS	-0.3780226
s6_29016	protein kinase domain containing protein	NS	-0.6278009
s6_27627	protein kinase domain containing protein	NS	-0.6574332
s6_24640	protein kinase domain containing protein	NS	-0.7005173
s6_14552	protein kinase domain containing protein	NS	-0.7993244
s6_13987	protein kinase domain containing protein	NS	-0.8577726
s6_8780	protein kinase domain protein	NS	0.6400958
s6_39440	protein kinase domain protein	NS	0.63185385
s6_880	protein kinase domain protein	NS	0.36681523
s6_40176	protein kinase domain-containing protein	NS	0.64667183
s6_23760	protein kinase domain-containing protein	NS	-0.6804664
s6_25010	protein kinase domain-containing protein	NS	-0.8580696
s6_15960	protein kinase family protein	NS	0.45926191
s6_20172	protein kinase family transcriptional partial	NS	2.93248973
s6_30180	protein kinase-like protein	NS	-0.7794892
s6_28864	protein-tyrosine kinase	NS	1.10043794
s6_3590	pyruvate dehydrogenase kinase	NS	-0.8543281

s6_732	pyruvate phosphate dikinase	NS	-0.5473402
s6_20965	rac-beta serine threonine-protein kinase-	NS	1.08604469
s6_1744	rac-beta serine threonine-protein kinase-	NS	-0.6142603
s6_4155	receptor-like protein kinase	NS	1.23343779
s6_9867	related to phosphatidylinositol 3-kinase	NS	0.99569876
s6_28568	ribosomal protein s6 kinase beta-1-like	NS	0.65395705
s6_2952	sensory box sensor histidine kinase	NS	0.94807466
s6_15834	serine threonine protein	NS	1.33452348
s6_1079	serine threonine protein	NS	0.67257359
s6_8650	serine threonine protein	NS	0.49323526
s6_10620	serine threonine protein	NS	0.36976562
s6_13954	serine threonine protein	NS	-0.9604627
s6_28044	serine threonine protein kinase	NS	1.85743107
s6_40741	serine threonine protein kinase	NS	0.87949099
s6_39354	serine threonine protein kinase	NS	0.65179762
s6_23253	serine threonine protein kinase	NS	0.44596038
s6_28231	serine threonine protein kinase	NS	0.39746252
s6_558	serine threonine protein kinase	NS	-0.3999104
s6_23700	serine threonine protein kinase	NS	-0.5000223
s6_15085	serine threonine protein kinase	NS	-0.6147977
s6_8490	serine threonine protein kinase	NS	-0.7991599
s6_25522	serine threonine protein kinase	NS	-0.949923
s6_14969	serine threonine protein kinase	NS	-0.9923991
s6_3844	serine threonine protein kinase ctr3	NS	1.61707072
s6_47667	serine threonine-protein kinase	NS	2.33279763
s6_1692	serine threonine-protein kinase	NS	1.52479218
s6_17485	serine threonine-protein kinase	NS	1.07587625
s6_4476	serine threonine-protein kinase	NS	0.53670748
s6_10789	serine threonine-protein kinase	NS	-0.4582742
s6_17667	serine threonine-protein kinase 16	NS	-0.4956416
s6_21594	serine threonine-protein kinase 6	NS	-0.7855981
s6_19468	serine threonine-protein kinase 9	NS	0.56829645

s6_1166	serine threonine-protein kinase chk1	NS	0.39639185
s6_10090	serine threonine-protein kinase dclk3-like	NS	-1.2339007
s6_42855	serine threonine-protein kinase h1	NS	1.8761985
s6_35897	serine threonine-protein kinase mark2- partial	NS	1.49779201
s6_34011	serine threonine-protein kinase nek4	NS	1.47869316
s6_13632	serine threonine-protein kinase nek5	NS	0.79845641
s6_29707	serine threonine-protein kinase nek8	NS	-0.5055104
s6_4614	serine threonine-protein kinase pepkr2	NS	2.0831067
s6_917	serine threonine-protein kinase pepkr2-like	NS	0.64987325
s6_9197	serine threonine-protein kinase prp4	NS	-0.5970636
s6_3261	serine_threonine protein kinase receptor	NS	1.16303221
s6_5296	serine-threonine protein	NS	0.4386825
s6_21540	serine-threonine protein	NS	-0.4620184
s6_30755	serine-threonine protein	NS	-0.6237931
s6_9002	serine-threonine protein plant-	NS	0.94709875
s6_16759	serine-threonine protein plant-	NS	0.35744191
s6_15725	serine-threonine protein plant-	NS	-0.5541655
s6_14887	serine-threonine protein plant-	NS	-0.6241852
s6_10567	serine-threonine protein plant-	NS	-0.6615726
s6_5284	Serine/threonine protein kinase	NS	0.42803452
s6_17793	shaggy-like kinase	NS	0.86809371
s6_29427	signal transduction histidine kinase	NS	0.93207999
s6_35980	sperm motility kinase w-like	NS	2.54745625
s6_13742	spindle assembly checkpoint kinase	NS	0.55393461
s6_40252	ste ste20 ysk protein kinase	NS	0.61472862
s6_15613	sterile alpha motif and leucine zipper containing kinase azk	NS	1.00418181
s6_3093	tccd-inducible-parp-like domain-containing protein	NS	1.72539637
s6_38358	tkl family protein kinase	NS	0.45765026
s6_28141	tousled-like kinase 2	NS	0.3806002
s6_28627	two-component hybrid sensor and regulator	NS	0.81960126
s6_19424	two-component hybrid sensor and regulator	NS	0.65003391

s6_11018	unusual protein kinase	NS	0.97878047
s6_5393	unusual protein kinase	NS	0.68669431

NS = Not significant

Supplementary Table 2.6 Annotations and expression levels of transcripts for ion transporters in IMK and IMK + CAS relative to ASW.

ID	Annotation	Log2(Fold Change)	
		IMK	CAS
s6_6660	ion transport protein	NS	2.8464387
s6_29463	voltage-gated sodium channel	NS	2.82598409
s6_11186	chloride carrier channel family	NS	2.76361612
s6_34065	voltage-gated cation	NS	2.52669749
s6_35937	voltage-gated sodium channel protein	NS	2.41214047
s6_10391	cation channel family protein	NS	2.33943744
s6_5492	ammonium transporter	NS	2.27966248
s6_4371	potassium sodium hyperpolarization-activated cyclic nucleotide-gated channel 4-like	NS	2.23081143
s6_32551	ammonium transporter	NS	2.03002431
s6_21960	ion transport protein	NS	2.01812916
s6_4379	sulfate transporter chloroplastic-like	NS	1.93734711
s6_40112	protein kinase domain containing protein	NS	1.93063866
s6_8054	Intracellular calcium-release channel	NS	1.84086236
s6_34137	voltage-gated sodium channel sns	NS	1.82978398
s6_2849	kef-type k+ transport membrane component	NS	1.82447968
s6_10871	voltage-gated sodium channel	NS	1.80589404
s6_17047	p-type atpase superfamily	NS	1.80416035
s6_39252	bacteriorhodopsin ii	NS	1.80332134
s6_7627	sulfate bicarbonate oxalate exchanger and transporter sat-1	NS	1.79817624
s6_27994	gamma-aminobutyric acid receptor subunit gamma-3	NS	1.74858177
s6_5924	p-type atpase superfamily	NS	1.73452494
s6_21873	cyclic nucleotide-binding protein	NS	1.72686004
s6_35189	sodium channel protein type 11 subunit alpha-like	NS	1.70457384
s6_12125	isoform cra_a	NS	1.70414662

s6_16819	voltage-gated ion channel superfamily	NS	1.70253606
s6_34545	ion transport protein	NS	1.67860229
s6_5094	conserved hypothetical protein	NS	1.64006639
s6_7107	conserved hypothetical protein	NS	1.63649597
s6_36139	conserved unknown protein	NS	1.63407133
s6_12331	voltage-gated sodium channel	NS	1.61693804
s6_54172	sodium channel protein type 5 subunit alpha	NS	1.59783032
s6_33766	cre-eat-6 protein	NS	1.58074418
s6_12982	potassium sodium hyperpolarization-activated cyclic nucleotide-gated	NS	1.57844297
s6_5792	glycoside pentoside hexuronide transporter	NS	1.5749291
s6_16850	voltage-gated sodium channel	NS	1.55535324
s6_17045	zip family transporter	NS	1.55129124
s6_12085	cation channel family protein	NS	1.54044047
s6_40058	voltage-gated sodium channel	NS	1.49763215
s6_8585	sodium calcium	NS	1.47013781
s6_28921	akt2 inward rectifier channel	NS	1.46274641
s6_3745	membrane transport	NS	1.45546719
s6_20127	af484082_1voltage-dependent non-l-type calcium channel alpha-1 subunit isoform a	NS	1.45395036
s6_9766	sodium calcium transport	NS	1.44575418
s6_9016	sodium calcium transport	NS	1.44510915
s6_1219	sodium channel protein	NS	1.43977779
s6_1055	voltage-gated ion channel superfamily	NS	1.42606522
s6_29162	voltage-gated sodium channel	NS	1.42376054
s6_5892	voltage-gated cation	NS	1.41421656
s6_21563	hyperpolarizaion-activated cyclic nucleotide-gated cation channel	NS	1.38519496
s6_25858	sodium channel protein type 11 subunit alpha	NS	1.36867165
s6_15330	voltage-gated cation	NS	1.32337803
s6_34567	cre-nnt-1 protein	NS	1.32218611
s6_18280	conserved hypothetical protein	NS	1.31104541

s6_11807	na+ h+ antiporter	NS	1.30734444
s6_11073	ion transport protein	NS	1.30416571
s6_28906	phospholipid-transporting atpase 3	NS	1.30060699
s6_6762	cation transporter component	NS	1.29053702
s6_33321	nad transhydrogenase-like	NS	1.28442805
s6_11102	vacuolar proton translocating atpase 116 kda subunit a	NS	1.27134422
s6_9827	voltage-gated ion channel superfamily	NS	1.26526781
s6_5869	voltage-gated ion channel superfamily	NS	1.25589084
s6_6765	conserved hypothetical protein	NS	1.2459151
s6_18284	conserved hypothetical protein	NS	1.23082173
s6_28642	voltage-gated ion channel superfamily	NS	1.22989321
s6_40453	voltage-gated ion channel superfamily	NS	1.22763986
s6_9489	conserved hypothetical protein	NS	1.22676413
s6_9432	ascidian calcium channel alpha1-subunit	NS	1.22516049
s6_40258	sodium channel protein type 2 subunit alpha-like	NS	1.22075371
s6_3334	guanylate cyclase activator 1a	NS	1.21884566
s6_23860	chloride channel	NS	1.21012604
s6_26520	conserved hypothetical protein	NS	1.20022662
s6_12787	voltage-gated ion channel superfamily	NS	1.19963286
s6_18506	hyperpolarization-activated cyclic nucleotide-modulated cation channel splice variant i	NS	1.1776613
s6_9337	sulfate transporter	NS	1.16901244
s6_6593	p-type atpase superfamily	NS	1.16043836
s6_10943	potassium channel	NS	1.15318553
s6_8391	sodium calcium	NS	1.14640118
s6_33576	sodium hydrogen exchanger	NS	1.14555376
s6_14742	voltage-gated ion channel superfamily	NS	1.14400084
s6_2885	two pore calcium channel protein 1-like	NS	1.13910797
s6_34408	conserved hypothetical protein	NS	1.13519553
s6_24018	ion transport protein	NS	1.13498192

s6_28123	voltage-gated ion channel superfamily	NS	1.1320583
s6_18800	transient receptor potential cation channel subfamily m member 2-like	NS	1.13074346
s6_692	neuronal acetylcholine receptor subunit alpha-2	NS	1.12995787
s6_2406	p-type partial	NS	1.12898958
s6_33540	hypothetical protein Pmar_PMAR028239	NS	1.12804186
s6_34647	bsc1 sodium channel protein	NS	1.1271673
s6_11034	ion transport protein	NS	1.12595912
s6_8007	conserved hypothetical protein	NS	1.11937307
s6_7232	voltage-dependent l-type calcium channel subunit alpha-1c	NS	1.11313214
s6_34227	voltage-dependent n-type calcium channel	NS	1.10974178
s6_8690	hypothetical protein Pmar_PMAR007653	NS	1.10730094
s6_36059	ion transport protein	NS	1.10444211
s6_11040	ion transport protein	NS	1.10389289
s6_33819	p-type	NS	1.10007797
s6_1731	voltage-gated sodium channel	NS	1.09423646
s6_42934	conserved hypothetical protein	NS	1.09306727
s6_9836	p-type atpase	NS	1.08747508
s6_34701	cation channel family protein	NS	1.08396755
s6_4962	ion transport protein	NS	1.0804369
s6_12456	sodium voltage- type alpha-like	NS	1.07973548
s6_31475	ion transport protein	NS	1.07722817
s6_724	conserved hypothetical protein	NS	1.07598841
s6_3890	cl- channel voltage-gated family protein	NS	1.07541605
s6_28350	cgmp-gated cation channel	NS	1.07449257
s6_7278	ion transport protein	NS	1.07201022
s6_9034	cl- channel voltage-gated family protein	NS	1.06578802
s6_658	voltage-dependent cation channel sc1	NS	1.0477021
s6_4562	voltage-gated cation	NS	1.03744828
s6_14828	cation channel family protein	NS	1.03721915

s6_6594	kef-type k+ transport system protein	NS	1.03022773
s6_17363	conserved hypothetical protein	NS	1.02917037
s6_16675	na+ h+ antiporter	NS	1.02613598
s6_10604	ion transport protein	NS	1.01584977
s6_10482	voltage-gated ion channel superfamily	NS	1.01387886
s6_7299	h(+) cl(-) exchange transporter 3-like	NS	1.0126442
s6_28065	k+ kef-type	NS	1.0086323
s6_12582	guanylate cyclase activator protein 1	NS	1.00730331
s6_356	ion transporter	NS	1.00489589
s6_39175	voltage-gated ion channel superfamily	NS	1.00478002
s6_7895	h+ transporting atpase	NS	0.98818532
s6_25472	cation channel family protein	NS	0.98304141
s6_17079	monovalent cation:proton antiporter-2 family	NS	0.97088743
s6_17718	potassium sodium hyperpolarization-activated cyclic nucleotide-gated	NS	0.96532904
s6_27563	two-pore calcium channel	NS	0.9549112
s6_2252	ion transport protein	NS	0.9456101
s6_7125	potassium voltage-gated channel subfamily c member 2	NS	0.94518484
s6_7037	voltagegated ion channel superfamily	NS	0.94069392
s6_2007	bach_halss ame: full=halorhodopsin short=hr	NS	0.93734283
s6_8648	voltage-gated sodium channel	NS	0.9332013
s6_40409	sodium calcium	NS	0.93152843
s6_2111	potassium sodium hyperpolarization-activated cyclic nucleotide-gated	NS	0.93026789
s6_9745	cgmp-gated cation channel	-2.7437142	0.92832765
s6_4152	cyclic nucleotide-binding protein	NS	0.92433236
s6_1906	sodium channel protein type 3 subunit alpha	NS	0.92044672
s6_29438	cgmp-gated cation channel	NS	0.90908166
s6_6880	cation transporter	NS	0.90541203
s6_33495	conserved hypothetical protein	NS	0.90348603
s6_967	anion exchanger family	NS	0.90031267

s6_14502	cation channel family protein	NS	0.8986878
s6_154	bach_halsd ame: full=halorhodopsin short=hr	NS	0.89377339
s6_43201	cation transporter component	NS	0.89266963
s6_2117	v-type h(+)-translocating pyrophosphatase	NS	0.89212066
s6_10067	sodium channel na bp	NS	0.88778666
s6_15528	cation channel family protein	NS	0.88528095
s6_6134	potassium partial	NS	0.87644667
s6_4786	cyclic nucleotide-binding protein	NS	0.87509484
s6_29319	ion transport protein	NS	0.87389391
s6_574	ae family transporter: anion exchange	NS	0.87383234
s6_31238	voltage-gated sodium channel	NS	0.87359576
s6_833	integral membrane sensor hybrid histidine kinase	NS	0.87106904
s6_9104	ion transport protein	NS	0.8661028
s6_33900	monovalent cation:proton antiporter-2 family	NS	0.86206644
s6_8273	adenylyl cyclase	NS	0.8583253
s6_34784	calcium voltage- t alpha 1i partial	NS	0.85743856
s6_21331	voltage-gated clc-type chloride	NS	0.85710605
s6_11426	ca- isoform d	NS	0.85498472
s6_28285	potassium voltage-gated channel subfamily a member 1	NS	0.83509212
s6_553	hypothetical protein	NS	0.82851378
s6_34278	cation channel family protein	NS	0.8268937
s6_40171	adenylyl cyclase	NS	0.82129304
s6_28627	two-component hybrid sensor and regulator	NS	0.81960126
s6_7007	adenylyl cyclase	NS	0.81293912
s6_27413	atp synthase alpha	NS	0.81113824
s6_9861	zinc transporter zupt	NS	0.80927208
s6_1540	nad mitochondrial precursor	NS	0.79960935
s6_7783	ammonium transporter	NS	0.79717709
s6_13413	two-pore calcium channel	NS	0.78814868
s6_688	monovalent cation:proton antiporter1 family	NS	0.78688109

s6_18775	h(+) cl(-) exchange transporter 7-like	NS	0.77895844
s6_35461	voltage-dependent sodium channel	NS	0.77131921
s6_7433	adenylate guanylate cyclase with integral membrane sensor	NS	0.76804944
s6_6468	potassium voltage-gated channel subfamily h member 2	NS	0.7673147
s6_8545	voltage-gated sodium channel	NS	0.76584311
s6_7809	trp cation partial	NS	0.76438341
s6_8342	cyclic nucleotide-binding protein	NS	0.75892966
s6_6083	plasma-membrane proton-efflux p-type atpase	NS	0.75351257
s6_23514	conserved hypothetical protein	NS	0.75179057
s6_34132	voltage-gated sodium channel	NS	0.75012308
s6_29805	potassium channel protein	NS	0.7494864
s6_12784	potassium channel	NS	0.73843481
s6_12734	rhodopsin 3 partial	NS	0.73718346
s6_5457	voltage-dependent t-type calcium channel subunit alpha-1h-like	NS	0.72822613
s6_4472	voltage-gated ion channel superfamily	NS	0.7146868
s6_18876	ion transport protein	NS	0.71237052
s6_40330	voltage-gated ion channel superfamily	NS	0.70662043
s6_8601	voltage-gated sodium channel	NS	0.70395803
s6_11468	conserved hypothetical protein	NS	0.68934186
s6_4110	conserved hypothetical protein	NS	0.68710278
s6_8469	conserved unknown protein	NS	0.68426877
s6_9579	cation channel family protein	NS	0.68424283
s6_17344	conserved hypothetical protein	NS	0.68384285
s6_8933	potassium sodium hyperpolarization-activated cyclic nucleotide-gated	NS	0.68009068
s6_8705	voltage-gated ion channel superfamily	NS	0.67505442
s6_34404	kef-type k+ transport nad-binding component	NS	0.67138378
s6_16502	mitochondrial phosphate carrier protein	NS	0.66988424
s6_6881	p-type transporter	NS	0.66956895

s6_12748	natural resistance-associated macrophage protein	NS	0.66556366
s6_28024	potassium sodium hyperpolarization-activated cyclic nucleotide-gated channel 1	NS	0.66479231
s6_15718	ion transporter	NS	0.65971476
s6_19424	two-component hybrid sensor and regulator	NS	0.65003391
s6_9948	sulfate transporter family protein	NS	0.64655109
s6_40344	cation channel family protein	NS	0.64438148
s6_32575	cation transporter	NS	0.63098465
s6_4582	sodium calcium	NS	0.62401248
s6_51410	p-type atpase superfamily	NS	0.61852412
s6_593	potassium voltage-gated channel subfamily b member 2	NS	0.61174514
s6_12176	bacterial type voltage activated sodium channel	NS	0.60780227
s6_6294	voltage-gated ion channel superfamily	NS	0.59516994
s6_10776	voltage-gated sodium channel	NS	0.59515289
s6_34768	cl- channel voltage-gated family protein	NS	0.58873721
s6_34586	calcium-binding protein cml19	NS	0.58419813
s6_23184	hypothetical protein Pmar_PMAR007653	NS	0.58392591
s6_15135	k channel inward rectifier conserved region 2 domain protein	NS	0.58092401
s6_9220	v-type h(+)-translocating pyrophosphatase	NS	0.5784801
s6_3166	potassium channel	NS	0.57511166
s6_51101	cation channel family	NS	0.57190297
s6_10826	sodium voltage- type isoform cra_a	NS	0.56508563
s6_51680	vacuolar proton translocating atpase 116 kda subunit a	NS	0.56297969
s6_10859	Sodium/potassium-transporting ATPase subunit alpha	NS	0.56131727
s6_27953	hypothetical protein	NS	0.56103653
s6_23645	polycystin cation channel family	NS	0.55021777
s6_17358	chloride carrier channel family	NS	0.54926111
s6_35781	voltage-dependent cation channel	NS	0.54636942

s6_2141	adenylyl cyclase	NS	0.5434649
s6_3510	voltage-gated sodium channel subunit	NS	0.52743623
s6_2962	calcium atpase serca-like	NS	0.52430676
s6_52041	atp synthase delta subunit	NS	0.52289262
s6_34242	voltage-gated sodium channel subunit	NS	0.5201597
s6_14363	cation channel family	NS	0.51197569
s6_30734	voltage-gated sodium channel	NS	0.50728233
s6_40493	bacterial type voltage activated sodium channel	NS	0.50720749
s6_4728	probable phospholipid-transporting atpase ib	NS	0.49424414
s6_23079	hypothetical protein Pmar_PMAR007873	NS	0.49393961
s6_6589	voltage-gated sodium channel	NS	0.49387162
s6_29054	sugar (glycoside-pentoside-hexuronide) transporter	NS	0.49160526
s6_12170	ion transporter	NS	0.48437988
s6_9439	voltage-gated sodium channel	NS	0.48099045
s6_15285	sulfate transporter chloroplastic-like	NS	0.47825485
s6_6162	ion transport protein	NS	0.47807381
s6_25886	sodium transporter	NS	0.47313469
s6_40461	cation channel family	NS	0.47174295
s6_29638	protein kvs- isoform a	NS	0.46431479
s6_15519	cation channel family protein	NS	0.45776298
s6_15158	ion transport protein	NS	0.45716664
s6_2833	polycystic kidney disease 2-like 1 protein	NS	0.45045834
s6_4666	calcium-activated potassium channel alpha	NS	0.44909732
s6_29731	conserved hypothetical protein	NS	0.4482654
s6_932	h(+) cl(-) exchange transporter 5 isoform 3	NS	0.44366115
s6_12195	ion transport protein	NS	0.44271306
s6_10900	ion transporter	NS	0.44226007
s6_14362	cation channel family protein	NS	0.4405704
s6_3499	v-type h(+)-translocating pyrophosphatase	NS	0.43836037
s6_13798	kiaa1120 protein	NS	0.43542445

s6_27927	atp synthase alpha	NS	0.43317488
s6_17762	conserved hypothetical protein	NS	0.4329047
s6_41129	voltage-gated shaker-like k+ channel kcna	NS	0.42377544
s6_40155	voltage-gated sodium channel	NS	0.4215363
s6_15785	copper transporter atpase	NS	0.42063128
s6_6770	calcium atpase serca-like	NS	0.42022928
s6_5379	ion transport protein	NS	0.41654267
s6_14573	cation channel family protein	NS	0.40495881
s6_7072	metal ion transporter family	NS	0.38446622
s6_35963	sodium potassium calcium exchanger 2	NS	0.3738891
s6_3774	na+ h+ antiporter	NS	0.3728177
s6_962	bach_hals4 ame: full=halorhodopsin short=hr	NS	0.3662139
s6_7168	hypothetical protein Pmar_PMAR007653	NS	0.36602591
s6_10422	mg2+ transporter	NS	0.36589018
s6_3621	cyclic nucleotide-gated cation channel cnga1-3 and related proteins	NS	0.36569243
s6_13751	conserved hypothetical protein	NS	0.36411314
s6_11069	metal ion transporter family	NS	0.35904354
s6_35280	k+ kef-type	NS	0.35587754
s6_10923	conserved hypothetical protein	NS	0.35581723
s6_33522	ion transport protein	NS	0.35299476
s6_16845	voltage-gated ion channel superfamily	NS	0.34336497
s6_28581	hypothetical protein Pmar_PMAR007873	NS	0.33857157
s6_2246	vacuolar atp synthase subunit	NS	0.31021911
s6_8097	vacuolar atp synthase 21 kda proteolipid	NS	-0.3077948
s6_35890	anion exchanger family	NS	-0.308735
s6_2861	major facilitator superfamily protein	NS	-0.3143427
s6_770	atp synthase cf1 epsilon subunit	NS	-0.3242933
s6_35663	cation diffusion facilitator family transporter containing protein	NS	-0.3259512
s6_20915	atp synthase cf0 b chain subunit ii	NS	-0.329613

s6_30706	ammonium transporter	NS	-0.3319845
s6_38002	chloroplast atp synthase subunit c	NS	-0.3328191
s6_2894	copper-transporting atpase p-	NS	-0.3330715
s6_28419	ion transport protein	NS	-0.351526
s6_11045	ion transport protein	NS	-0.3528412
s6_39084	atp synthase cf1 delta subunit	NS	-0.3557616
s6_10705	PREDICTED: uncharacterized protein LOC762549 isoform 1	NS	-0.3669405
s6_529	atp synthase gamma	NS	-0.378749
s6_20522	kef-type k+ transport nad-binding component	NS	-0.380786
s6_25002	mitochondrial atp synthase f0 lipid binding subunit-like protein 3	NS	-0.3844164
s6_15803	voltage-gated sodium channel	NS	-0.3852357
s6_38325	conserved hypothetical protein	NS	-0.3875655
s6_15103	ion transport protein	NS	-0.3878355
s6_5045	ammonium transporter	NS	-0.3999749
s6_28365	chromate ion transporter family	NS	-0.4033255
s6_27594	bile acid:sodium symporter family protein	NS	-0.4103607
s6_18455	metal tolerance protein	NS	-0.4108835
s6_38413	calcium-dependent protein kinase 1	NS	-0.4188616
s6_16600	atp synthase subunit b	NS	-0.4189052
s6_34156	voltage-dependent l-type calcium channel subunit alpha-1c	NS	-0.4207096
s6_691	coiled-coil domain containing 2-like	NS	-0.4408709
s6_6610	cation channel family protein	NS	-0.4484339
s6_40230	mitochondrial atp synthase f0 lipid binding subunit-like protein 3	NS	-0.450126
s6_2533	conserved hypothetical protein	NS	-0.454043
s6_23580	voltage-gated sodium channel	NS	-0.4542158
s6_31174	ion transport protein	NS	-0.4546497
s6_51708	vacuolar atp synthase subunit	NS	-0.4570501
s6_14724	cation channel family	NS	-0.4607199

s6_35136	na+ h+ antiporter	NS	-0.462022
s6_9039	mitochondrial atp synthase f1 delta subunit	NS	-0.4651426
s6_30713	zip family transporter	NS	-0.4671593
s6_23295	conserved hypothetical protein	NS	-0.4719866
s6_7410	potassium channel homolog	NS	-0.477947
s6_5173	mitochondrial import receptor subunit tom40	NS	-0.4824486
s6_38354	atp synthase alpha sodium ion specific	NS	-0.4907408
s6_29765	calcium ion transporter	NS	-0.4925507
s6_38776	atp synthase subunit	NS	-0.493059
s6_23784	ctr2 family transporter: copper ion ctr-type copper transporter	NS	-0.4935988
s6_496	voltage-gated sodium channel subunit	NS	-0.4941121
s6_7654	kef-type k+ transport nad-binding component	NS	-0.5148919
s6_14197	organic cation transporter	NS	-0.5158891
s6_31470	mg co ni transporter	NS	-0.5175903
s6_3042	voltage-gated sodium channel	-1.9112445	-0.5176598
s6_16257	zip-family zinc transporter	NS	-0.529447
s6_18919	hydrogen-transporting atp synthase	NS	-0.5353968
s6_52007	magnesium transporter nipa2-like	NS	-0.5391362
s6_42884	ion transporter	NS	-0.5429783
s6_5828	calcium proton exchanger family protein	NS	-0.5577977
s6_16538	ca2+ h+ antiporter	NS	-0.56349
s6_39280	atp synthase cf0 subunit i	NS	-0.5801545
s6_39443	atp f1 epsilon subunit	NS	-0.5838998
s6_9683	cac1m_musdo ame: full=muscle calcium channel subunit alpha-1 ame: full=mdl-alpha-1	NS	-0.5844276
s6_28099	k+-dependent na+ ca+ exchanger-like protein	NS	-0.5846465
s6_28286	voltage dependent anion channel	NS	-0.5863411
s6_3780	hypothetical protein Pmar_PMAR026893	NS	-0.5863805
s6_34739	divalent cation transporter	NS	-0.5876841
s6_14404	ammonium transporter	NS	-0.5902464

s6_28128	sss family transporter: sodium ion pantothenate	NS	-0.5929553
s6_10508	conserved hypothetical protein	NS	-0.5937731
s6_18229	potassium voltage-gated channel subfamily b member 1-like	NS	-0.6050435
s6_39193	opsin 2	NS	-0.6179683
s6_28987	mitochondrial atp synthase f0 lipid binding subunit-like protein 3	NS	-0.6247175
s6_14941	anion transporter	NS	-0.6303462
s6_24860	conserved hypothetical protein	NS	-0.6387953
s6_2570	organic cation transporter	NS	-0.6403529
s6_22045	ankyrin repeat-containing	NS	-0.6502889
s6_21501	inwardly rectifying k+	NS	-0.6595286
s6_16818	vacuolar atp synthase 16 kda proteolipid	NS	-0.6629688
s6_11696	cobalt and zinc h(+)-k(+) antiporter	NS	-0.6637049
s6_7609	atp-binding cassette sub-family b member mitochondrial	NS	-0.6663216
s6_5355	sco1 domain-containing protein	NS	-0.671252
s6_10828	solute carrier family 39 protein	NS	-0.6831401
s6_5720	sulfate permease family	NS	-0.686359
s6_16527	bacr3_halsd ame: full=archaerhodopsin-3 short=ar 3 flags: precursor	NS	-0.6960523
s6_6943	inorganic phosphate	NS	-0.714871
s6_241	voltage-dependent l type calcium channel alpha 1	NS	-0.7151408
s6_39162	atp synthase cf0 a chain	NS	-0.7228941
s6_33764	ammonium transporter	NS	-0.7358
s6_12483	neurotransmitter-gated ion-channel ligand-binding protein	NS	-0.7416037
s6_12614	bacr3_halsd ame: full=archaerhodopsin-3 short=ar 3 flags: precursor	NS	-0.7549905
s6_14575	hypothetical protein Pmar_PMAR007873	NS	-0.7888792
s6_17662	bile acid:na+ symporter family	NS	-0.7890782
s6_57443	ammonium	NS	-0.8661234

s6_11015	potassium channel tetramerisation domain containing	NS	-0.8668746
s6_12163	major facilitator superfamily protein	NS	-0.8703501
s6_21330	sulfate transporter	NS	-0.8774009
s6_16167	divalent cation transporter	NS	-0.8793441
s6_38230	chloroplast atp synthase	NS	-0.8824994
s6_11747	mg2+ transporter-e family	NS	-0.88779
s6_16652	af493793_1 sulphate transporter	NS	-0.8896658
s6_14671	ion transport protein	NS	-0.8911079
s6_50930	rhodopsin	NS	-0.9244223
s6_712	vacuolar atp synthase 16 kda proteolipid	NS	-0.9326315
s6_6985	ammonium	NS	-0.9352517
s6_48896	vacuolar atp synthase 16 kda proteolipid	NS	-0.9425393
s6_41226	nitrate transporter	NS	-0.9546087
s6_422	nitrate transporter	NS	-0.9640377
s6_13254	membrane protein	NS	-0.9780839
s6_43072	solute carrier family 22 member 15-like	NS	-1.0047216
s6_30780	major intrinsic protein	NS	-1.0370435
s6_51634	solute carrier family 22 member 8	NS	-1.0518534
s6_56281	ammonium transporter	NS	-1.1048015
s6_38207	ammonium transporter	NS	-1.112236
s6_34430	ammonium transporter	NS	-1.1564765
s6_47531	ankyrin unc44	NS	-1.1578197
s6_43218	major facilitator superfamily mfs_1	NS	-1.2311367
s6_40239	ammonium transporter	NS	-1.2545666
s6_420	nitrate transporter	NS	-1.4734192
s6_58513	nitrate transporter	NS	-1.5835972
s6_50951	ammonium transporter	NS	-1.708212
s6_44035	ammonium transporter	NS	-1.8317058
s6_55422	ammonium transporter	NS	-1.928497
s6_51281	ammonium transporter	NS	-1.9904485

s6_51578	ammonium transporter	-2.0523849	-2.2197376
s6_53768	ammonium transporter channel family	NS	-2.2449884
s6_51076	ammonium transporter partial	NS	-2.4735334
s6_38239	ammonium transporter channel family	NS	-3.1721517

NS = Not significant

Supplemental Table 2.7 Annotations and expression levels of transcripts involved in microtubule-based movement in IMK and CAS relative to ASW

ID	Annotation	Log2(Fold Change)	
		IMK	CAS
s6_345	light-harvesting partial	NS	1.97215825
psbI	Photosystem II reaction center protein I (psbI)	-5.9961161	1.40876777
s6_40562	light-harvesting partial	-1.0143584	0.9555766
s6_33558	light-harvesting partial	NS	0.90602154
s6_40514	cytochrome f	NS	0.82561172
s6_17857	light-harvesting partial	NS	0.72290738
s6_33888	light-harvesting partial	NS	0.68060458
s6_9936	light-harvesting partial	NS	0.52424864
s6_52041	atp synthase delta subunit	NS	0.52289262
s6_7938	light-harvesting partial	NS	0.35567922
s6_9594	light-harvesting partial	NS	0.270394
s6_770	atp synthase cf1 epsilon subunit	NS	-0.3242933
s6_20915	atp synthase cf0 b chain subunit ii	NS	-0.329613
s6_38002	chloroplast atp synthase subunit c	NS	-0.3328191
s6_39084	atp synthase cf1 delta subunit	NS	-0.3557616
s6_51621	light-harvesting partial	NS	-0.3783485
s6_529	atp synthase gamma	NS	-0.378749
s6_23562	light-harvesting partial	NS	-0.3804689
s6_4310	photosystem i subunit iii	NS	-0.3962404
s6_33899	light-harvesting partial	NS	-0.4017234
s6_27969	light-harvesting partial	NS	-0.4042531
s6_16600	atp synthase subunit b	NS	-0.4189052
s6_57498	light-harvesting partial	NS	-0.4246275
s6_35909	photosystem ii protein l	NS	-0.4250707
s6_4869	light-harvesting partial	NS	-0.4307639
s6_50949	ferredoxin-binding protein ii	NS	-0.4422315
s6_23160	oxygen-evolving enhancer protein 1 precursor	NS	-0.4516673
s6_47010	chaperone required for the assembly of the	NS	-0.4688535

	mitochondrial f1-atpase		
s6_12841	cytochrome b6-f complex iron-sulfur subunit	NS	-0.4703549
s6_50909	light-harvesting partial	NS	-0.4842495
s6_33999	chloroplast cytochrome b6	NS	-0.4869482
s6_28012	light-harvesting partial	NS	-0.4895433
s6_38776	atp synthase subunit	NS	-0.493059
s6_33872	photosystem i reaction center subunit iv	NS	-0.5095229
s6_2108	light-harvesting partial	NS	-0.521012
s6_53968	apocytochrome c-terminal	NS	-0.5213439
s6_51205	light-harvesting partial	NS	-0.5243747
s6_56907	light-harvesting partial	NS	-0.5368314
s6_55196	photosystem ii protein n	NS	-0.5423076
s6_26767	hypothetical protein BN8_01755	NS	-0.549162
s6_4650	light-harvesting partial	NS	-0.5569234
s6_27231	uncharacterized iron-regulated protein	NS	-0.5597985
s6_39280	atp synthase cf0 subunit i	NS	-0.5801545
s6_39443	atp f1 epsilon subunit	NS	-0.5838998
s6_157	light-harvesting partial	NS	-0.5869043
s6_56261	cytochrome b6-f complex iron-sulfur subunit	NS	-0.5933789
s6_41471	cytochrome b559 beta chain	NS	-0.6003548
s6_34572	chloroplast photosystem i protein e	NS	-0.6069899
s6_36987	photosystem i reaction center subunit xi	NS	-0.6327118
s6_33994	light-harvesting partial	NS	-0.6362574
s6_39101	photosystem ii protein l	NS	-0.6450618
s6_10134	light-harvesting partial	NS	-0.6582771
s6_5324	achain peridinin-chlorophyll a high-salt form	NS	-0.6634718
s6_24882	light-harvesting partial	NS	-0.6732852
s6_30786	light-harvesting partial	NS	-0.6817872
s6_27769	light-harvesting partial	NS	-0.6825739
s6_23001	light-harvesting partial	NS	-0.6892754
s6_26377	photosystem i reaction center subunit iv	NS	-0.6953689
s6_25516	light-harvesting partial	NS	-0.7217043

s6_39162	atp synthase cf0 a chain	NS	-0.7228941
s6_38665	apocytochrome c-terminal	NS	-0.7745362
s6_24485	cytochrome b559 beta chain	NS	-0.7978969
s6_2300	proteasome subunit beta	NS	-0.8015404
s6_6004	light-harvesting partial	NS	-0.8213259
s6_2951	light-harvesting partial	NS	-0.8321604
s6_39143	photosystem i subunit vii	NS	-0.858737
s6_38230	chloroplast atp synthase	NS	-0.8824994
s6_34244	light-harvesting partial	NS	-0.9007662
s6_51635	light-harvesting partial	NS	-0.9307829
s6_2125	pcp3_ampca ame: full=peridinin-chlorophyll a-binding protein 3 short=pcp	NS	-0.9325729
s6_3391	chloroplast atp synthase	NS	-0.9328221
s6_23030	photosystem i subunit vii	NS	-1.05777
s6_32715	light-harvesting partial	NS	-1.1367359
s6_28011	light-harvesting partial	NS	-1.1441659
s6_39810	cytochrome b559 beta chain	NS	-1.2025381
s6_40062	light-harvesting partial	NS	-1.2033079
s6_58522	light-harvesting partial	NS	-1.2821925
s6_51120	light-harvesting partial	NS	-1.8059531

NS = not significant

CHAPTER 3: SINGLE-CELL DISSOCIATION OF CNIDARIAN TISSUE TO EVALUATE CNIDARIAN-SYMBIODINIACEAE SYMBIOSIS ESTABLISHMENT

This chapter has been derived and summarized from methods and research articles, referenced below, where I am a co-author:

Jinkerson, R. E., Russo, J. A., Newkirk, C. R., **Kirk, A. L**., Chi, R. J., Martindale, M. Q., Grossman, A. R., Hatta, M., & Xiang, T. (2022). Cnidarian-Symbiodiniaceae symbiosis establishment is independent of photosynthesis. Current Biology: CB, 32(11), 2402–2415.e4. © 2022 The Authors. Published by Elsevier Inc.

Kirk, A. L., & Xiang, T. (2022). Single-cell dissociation of the model cnidarian sea anemone Exaiptasia diaphana. *STAR Protocols*, *3*(4), 101897. https://doi.org/10.1016/j.xpro.2022.101897. © 2022 The Authors.

3.1 Introduction

Exaiptasia diaphana (Aiptasia) sea anemone serves as a laboratory model for studying cnidarian-Symbiodiniaceae symbiosis (Baumgarten et al., 2015; Lehnert et al., 2014), a foundational relationship for the survival and biodiversity of coral reef ecosystems (Davy et al., 2012; Muscatine & Porter, 1977). Aiptasia and other cnidarians, such as corals, have multiple tissue layers and cell types performing specific functions (Figure 1.1). The outer tissue layer, the ectoderm, is associated with marine bacteria and can contain cnidocytes, or stinging cells. The inner tissue layer, the endoderm, is made of gastrodermal cells that may harbor endosymbiotic Symbiodiniaceae algal cells (Davy et al., 2012). During symbiosis establishment, algal symbionts infect these host gastrodermal cells, proliferate throughout the gastrodermis by an unknown mechanism, and are maintained at a steady density through nutrient regulation by the host (Xiang

et al., 2020). The endosymbiotic algae conduct photosynthesis and translocate products to the cnidarian hosts in exchange for protection and inorganic nutrients (Cresswell et al., 2017; Venn et al., 2008; Zawada et al., 2019). Despite the importance of this symbiosis to reef ecosystems (Buerger et al., 2020; Muscatine & Porter, 1977), the cellular mechanisms governing each stage of symbiosis establishment are largely unknown due to limited cellular biological techniques in the field of cnidarian-algal symbiosis.

Tissue dissociation is an important experimental tool to break down complex tissues into their individual cells for fluorescence microscopy, flow cytometry (Leelatian et al., 2017), or single-cell RNA-sequencing (Rodriguez de la Fuente et al., 2021). While Aiptasia has emerged as a versatile model for cellular biological analyses in cnidarian-algal symbiosis (Lehnert et al., 2012; Rädecker et al., 2018; Weis et al., 2008; Xiang et al., 2020), there is no published protocol available for the generation of Aiptasia single-cells. An efficient protocol for processing adult Aiptasia into a single-cell suspension will make possible single-cell analysis of cnidarian tissue types, including symbiotic and symbiont-free gastrodermal cells. Such comparisons will provide a better understanding of the infection, proliferation, and maintenance stages of cnidarian-algal symbiosis establishment.

In this chapter, we describe an optimized protocol to dissociate adult Aiptasia tissue to generate a single-cell suspension of symbiotic and symbiont-free host cells for fluorescent staining, microscopy, and flow cytometry. While optimized for Aiptasia, this protocol is also applicable to coral tissues. To demonstrate the feasibility of this protocol for investigating the stages of symbiosis establishment, this method was used to visualize the intracellular localization of the recently generated Symbiodiniaceae photosynthesis mutant *ORANGE 1* (*ora1*) in both adult Aiptasia and juvenile coral polyp tissue (Jinkerson et al., 2022). In Jinkerson et al. (2022), six

Symbiodiniaceae algal mutants deficient in photosynthesis were generated using UV mutagenesis from the wild type *Breviolum minutum* (strain SSB01) and used to evaluate the impact of photosynthesis on the stages of symbiosis establishment. Using the single-cell dissociation protocol (Kirk & Xiang, 2022) in combination with the photosynthesis mutant *ora1*, we confirm that symbiosis establishment is independent of photosynthesis (Jinkerson et al., 2022). The photosynthetically deficient *ora1* algae was visualized within both intact Aiptasia and coral host cells. These results demonstrate the application of cellular biological techniques such as single-cell dissociation as a means to uncover the essential mechanisms in cnidarian-Symbiodiniaceae symbiosis.

3.2 Materials and Methods

3.2.1 Symbiodiniaceae strains

Clonal and axenic *Breviolum minutum* strain SSB01 (Clade B) (Xiang et al., 2013) was used in this study. Symbiodiniaceae liquid cultures were grown without agitation at 27 °C on a 12 hr-light/12 hr-dark cycle with an irradiance of ~10 or 50 µmol photons m^{-2} s^{-1} of photosynthetically active radiation (PAR) provided by Percival SciWhite LED tiles in MB supplemented with glucose (Millipore-Sigma G8270). Photosynthesis mutant *ORANGE 1 (ora1)* was generated from wild type *B. minutum* and maintained in liquid culture as previously described (Jinkerson et al., 2022; Russo et al., 2023).

3.2.2 *Acropora tenuis* coral

Colonies of the coral *Acropora tenuis* (referred to as *Acropora*) were collected from Seoko Island (26°37’41”N, 127°51’38”E, Okinawa, Japan) under collecting permit #30-78 and #2-57 by Okinawa prefecture and maintained as described previously (Wolfowicz et al., 2016). Symbiont-

free gametes from the colonies were mixed to form planulae after coral spawning on June 12, 2019 and on May 22, 2021 as previously reported in (Jinkerson et al., 2022).

3.2.3 *Exaiptasia diaphana* clonal strains

Anemones utilized in this study were from clonal strains *Exaiptasia diaphana* (Aiptasia) H2 and CC7. Aposymbiotic Aiptasia were rendered free of endogenous algae via short term cold shock (Lehnert et al., 2012) followed by menthol treatment (Matthews et al., 2016) and maintained within polycarbonate tanks filled with artificial seawater (ASW) at 27 °C in continuous darkness.

For protocol optimization and evaluation, Aiptasia previously inoculated with wild type (WT) *Breviolum minutum* (clonal axenic strain SSB01 (Xiang et al., 2013)) were maintained and allowed to reach stable state density in 27 °C, 12 hr-light/12 hr-dark (~10 μmol photons m^{-2} s^{-1} of PAR) prior to single-cell dissociation.

To assess the impact of photosynthesis on symbiosis establishment, Aiptasia previously inoculated with wild type *B. minutum* or photosynthesis mutant *ora1* (Jinkerson et al., 2022) were maintained in 27 °C continuous darkness for up to three months prior to single-cell dissociation.

3.2.4 Single-cell dissociation and microscopy

To visualize Symbiodiniaceae algal cells within dissociated Aiptasia or *Acropora* host cells, *ora1* or WT *B. minutum* associated adult Aiptasia and *Acropora* juvenile polyps were used along with aposymbiotic animals as controls. All samples were washed in calcium- and magnesium-free artificial seawater (CMF-ASW) three times and then allowed to incubate in the CMF-ASW for 10 minutes. After incubation of Aiptasia, the tentacles were dissected off the body of the anemone and diced into small pieces, which were subsequently centrifuged at 70 × *g* for 5 minutes to remove CMF-ASW. Alternatively, coral polyps were crushed gently to break-up the $CaCO_3$ skeletons and then centrifuged at 200 × *g* for 5 minutes to remove the CMF-ASW. To each

tissue sample, 100 µl of 0.5% pronase from *Streptomyces griseus* (MilliporeSigma 10165921001) in CMF-ASW with EGTA (ethylene glycol-bis (β-aminoethyl ether)-N,N,N′,N′-tetraacetic acid, MilliporeSigma 324626) was added. The solution was mixed by pipetting up and down eight times and allowed to incubate for 20 minutes with gentle agitation, followed by mixing eight more times with a pipette. The dissociated tissue samples were centrifuged again at 70 × *g* for 5 minutes, and the pronase solution was removed. The dissociated tissue samples were gently resuspended in 50 µl of cell permeable Hoechst 33342 fluorescent nucleic acid stain at a concentration of 12 $\mu g \cdot ml^{-1}$ in CMF-ASW with EGTA, which stained the host nuclei if present. Dissociated tissue samples were incubated in the staining solution for 30 minutes in the dark at 25 °C, followed by centrifugation at 70 × *g* for 5 minutes and the removal of 40 µl of staining solution. The dissociated tissue was gently suspended in the remaining staining solution and immediately imaged with a Zeiss Axio Observer inverted microscope either in bright-field mode or Texas Red filter set for chlorophyll fluorescence (546/12 nm excitation, 590 nm long-pass fluorescence emission), and fluorescence filter set for Hoechst 33342 fluorescent nucleic acid stain (365 nm excitation, 445/50 nm band pass fluorescence emission). Controls were completed by dissociating aposymbiotic Aiptasia tentacles, mixing the single-cell suspension with *ora1* algae grown *in vitro*, and staining the sample with Hoechst 33342 fluorescent nucleic acid stain.

3.2.5 Flow cytometry

The Amnis FlowSight Imaging Flow Cytometer (Luminex) was used with excitation by the 488 nm (0.01 mW) and 405 nm (3.00 mW) lasers, with side scatter (SSC, 3.00 mW). Following dissociation, single-cell suspensions of aposymbiotic and WT *B. minutum* associated Aiptasia were centrifuged at 100 × *g* for 10 minutes. The supernatant was removed, and the cells were resuspended in 1 mL of 3.3x phosphate buffered saline (PBS) (Gibco™ 10010072). The cell

suspensions were filtered through a 40 µm cell strainer into 1.5 mL tube and resuspended with gentle agitation before applying to the FlowSight. Symbiotic and symbiont-free host cells were discriminated from debris by the combination of side scatter and fluorescence positive for Hoechst nuclei stain (ex. 405 nm, em 430-505 nm). From this positive host cell population, symbiotic host cell populations were separated from symbiont-free host cells by algal endogenous fluorescence (ex. 488 nm, em. 640-745 nm). All analysis was completed using the IDEAS application version 6.2.

3.3 Results

3.3.1 Dissociation of Aiptasia tissue produces intact host cells

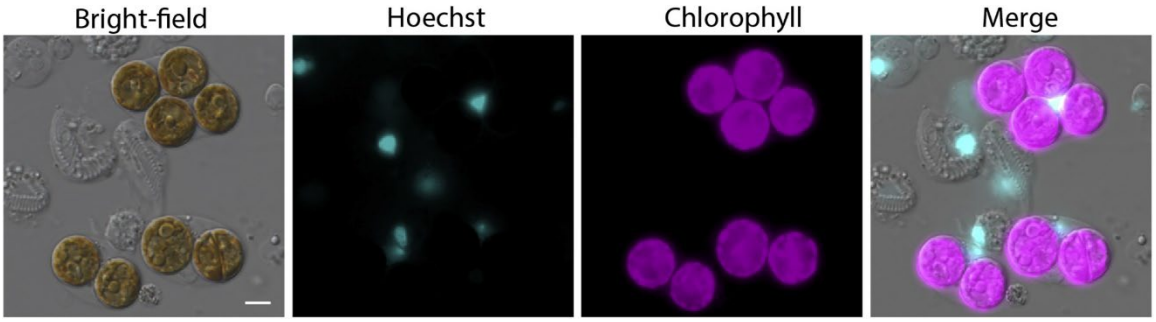

Figure 3.1 Host cell types remain intact following single-cell dissociation of adult Aiptasia. Representative microscopy images of CC7 Aiptasia cells after dissociation depicting symbiotic host cells enclosing *B. minutum* algae and symbiont-free Aiptasia cells. Cyan, cell-permeable Hoechst 33342 fluorescent nucleic acid stain; magenta, algal chlorophyll fluorescence. Scale bar, 5 µm.

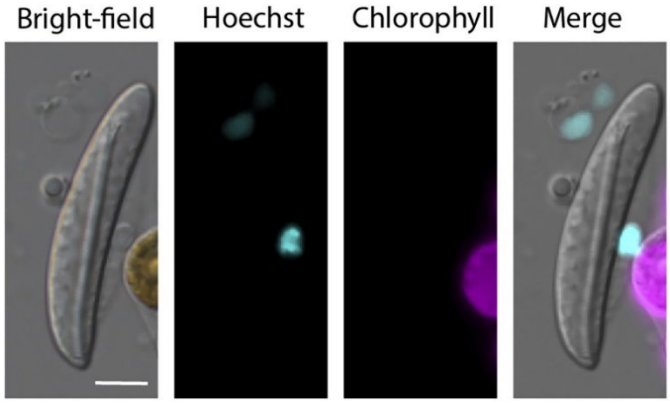

Figure 3.2 Representative microscopy images of CC7 Aiptasia cells after dissociation depicting an intact host nematocyst cell and symbiont-free Aiptasia cells.
Cyan, cell-permeable Hoechst 33342 fluorescent nucleic acid stain; magenta, algal chlorophyll fluorescence. Scale bar, 5 μm.

To optimize the single-cell dissociation of adult Aiptasia tissue, tentacles from Aiptasia previously inoculated with wild type *B. minutum* were dissected from the animals. Tentacle tissue was used to avoid excess mucus produced from the body of the anemones (Brown & Bythell, 2005), which interferes with downstream processing of the single-cell tissue suspension. The typical single-cell suspension resulting from the dissociation of adult Aiptasia tissue is shown in Figure 3.1 & 3.2. The host membrane can easily be observed using differential interference contrast (DIC) imaging and is useful, in combination with the presence of host nuclei stained with Hoechst 33342, to confirm that host cells are intact. Both symbiont-free (Figure 3.1 & 3.2) and symbiotic (Figure 3.1) Aiptasia host cells are observed in the single-cell suspension. The algal chlorophyll fluorescence is used to identify symbiotic cells, where the presence of stained host nuclei between the algae and host membrane indicates intact host gastrodermal cells.

3.3.2 Single-cell suspension of Aiptasia is applicable for flow cytometry

To evaluate the dissociation protocol for use in single-cell analysis, dissociated aposymbiotic and inoculated Aiptasia tissue samples were stained with Hoechst 33342 and

separated using imaging flow cytometry. Intact host cells were identified and gated from cell debris using side scatter (SSC) and the fluorescence from the nuclei stain (ex. 405 nm). Host cells were further separated into symbiont-free and symbiotic populations using the endogenous algal fluorescence of *B. minutum* algae at excitation of 488 nm (Figure 3.3). From the dissociated single-cell suspension of *B. minutum*-inoculated Aiptasia tissue, approximately 10% of the total cell population was associated with *B. minutum* algae. In contrast, no *B. minutum* algal cells were observed in the aposymbiotic cell suspension sample.

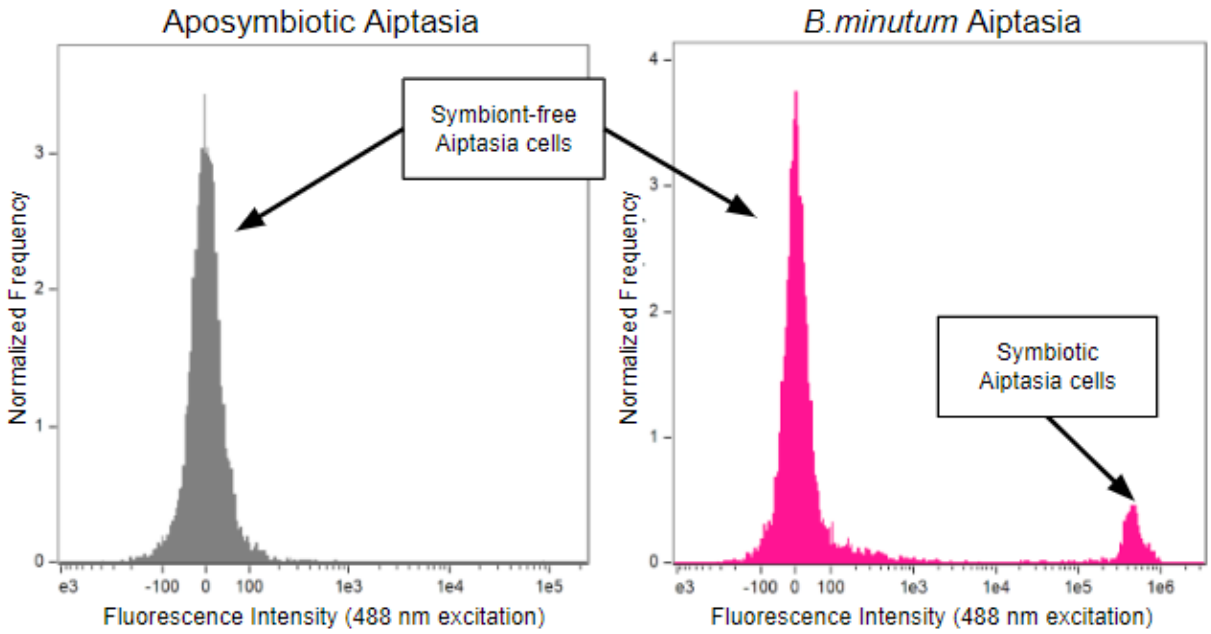

Figure 3.3 Symbiotic and symbiont-free Aiptasia cells identified via flow cytometry.
Expected populations of host cells after dissociation of aposymbiotic (left panel) and *B. minutum*-associated (right panel) Aiptasia tissue. Populations were gated with excitation by the Amnis FlowSight Imaging Flow Cytometer (Luminex) 488 nm laser (chlorophyll autofluorescence), 405 nm laser (Hoechst nuclei stain), and side scatter (intact cells).

3.3.3 Symbiodiniaceae mutant localizes within cnidarian host gastrodermal cells

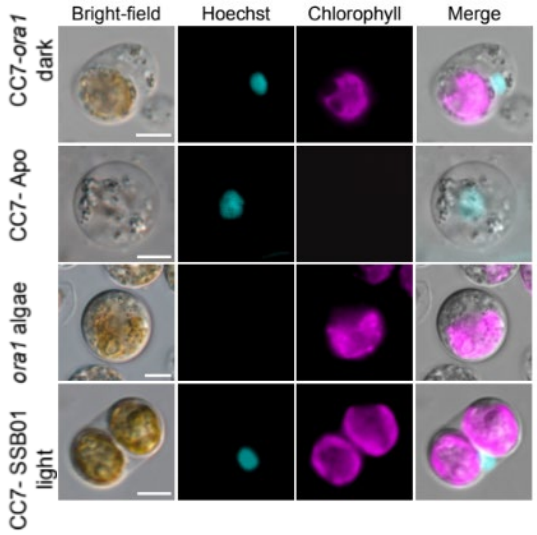

Figure 3.4 Photosynthesis mutant *ora1* establishes symbiosis within Aiptasia host.
(A) Representative microscopy images of a dissociated Aiptasia CC7 cell enclosing an *ora1* mutant cell from an animal kept in the dark, aposymbiotic CC7 host cell only, ora1 cells only, and a CC7 cell enclosing two SSB01 (*B. minutum*) cells from an animal kept in the light. Cyan: cell-permeable Hoechst 33342 fluorescent nucleic acid stain. Magenta: algal chlorophyll fluorescence. Scale bar: 5 μm.

To determine how photosynthesis impacts the stages of symbiosis establishment, aposymbiotic Aiptasia were inoculated with *ora1* multiple times and were maintained in 24-hour dark conditions for approximately three months as previously reported (Jinkerson et al., 2022). The *ora1*-associated Aiptasia were monitored using whole animal fluorescent microscopy which revealed high densities of algae in the animals despite the absence of photosynthesis. To determine if the photosynthetically deficient *ora1* algal cells observed in whole animal microscopy were intracellularly localized, the *ora1*-associated Aiptasia were dissociated into single cells following the three-month dark maintenance. The single cell suspension was scanned via DIC bright-field and fluorescent microscopy for intact host cells containing both *ora1* algae and positive for host nuclei stain. The photosynthesis mutant *ora1* was observed within intact Aiptasia host cells as indicated by the presence of the host membrane enclosing the alga and stained host nucleus (Figure

3.4). Similarly, following the dissociation of WT *B. minutum* SSB01-associated Aiptasia, WT SSB01 algal cells were observed intracellularly (Figure 3.4). In controls, *ora1* algal cells were mixed with dissociated aposymbiotic Aiptasia tissue, but no co-localization of algae and host nuclei was observed. Additionally, Hoechst 33342 staining of control algal cultures does not stain algal nucleus (Figure 3.4) due to the thick cell walls of Symbiodiniaceae algae (Tortorelli, Oakley, et al., 2022). Here, the data indicate that infection and maintenance of symbionts in Aiptasia is independent of photosynthesis.

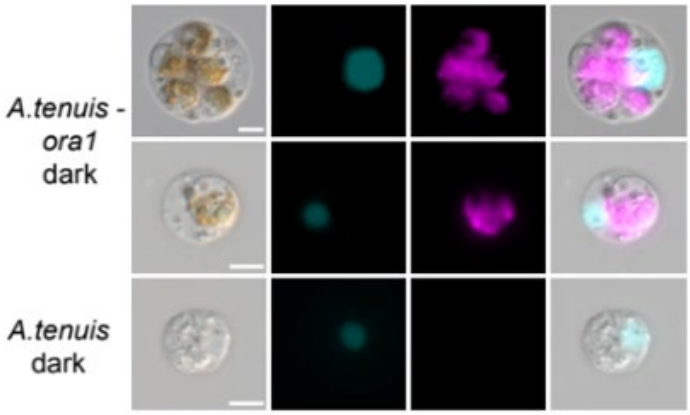

Figure 3.5 Photosynthesis mutant *ora1* infects and proliferates within coral host cells. Representative microscopy images of dissociated coral *A. tenuis* polyp cells containing *ora1* cells from animals kept in the dark (top and middle panel), and an aposymbiotic coral cell without algae. Cyan: cell-permeable Hoechst 33342 fluorescent nucleic acid stain. Magenta: algal chlorophyll fluorescence. Scale bar: 5 μm.

The effects of photosynthesis on symbiosis establishment was next examined in *Acropora* juvenile coral polyps. Five photosynthesis mutants, including *ora1*, were added to individual coral polyps and observed within coral tentacles via whole animal fluorescent microscopy (Jinkerson et al., 2022). To confirm that the observed algal cells were intracellular, *Acropora* polyps associated with *ora1* were dissociated into a single-cell suspension. Following dissociation, intact *Acropora* host cells were observed that were symbiont-free or contained one or more *ora1* algal cells (Figure

3.5). Up to five *ora1* algal cells were observed intracellularly localized in a single *Acropora* cell (Figure 3.5). Together with the increase in *ora1* densities observed *in hospite* in Jinkerson et al. (2022), this data suggests proliferation of the symbionts without photosynthesis. Therefore, establishment including infection, proliferation, and maintenance, proceeds without photosynthesis in *Acropora* juveniles.

3.4 Discussion

In this work, we detail and evaluate a protocol optimized for the generation of a single-cell suspension from adult Aiptasia tissue. We demonstrate that dissociated Aiptasia cells are amenable for cellular biological analyses, such as DIC microscopy and imaging flow cytometry, and can be used to evaluate the fundamental biology of cnidarian-algal symbiosis establishment. For example, Symbiodiniaceae photosynthesis mutant *ora1* was visualized within both Aiptasia and coral host cells, indicating that photosynthesis is not required for the infection or maintenance stages of symbiosis establishment in these cnidarians. These results demonstrate how cellular biological techniques can provide unique insights into the cnidarian-Symbiodiniaceae relationship that were previously unknown.

3.4.1 Single-cell dissociation of Aiptasia is for cellular biological analyses

In previous research, coral *Acropora tenuis* has been used for single-cell dissociation and analyses, including flow cytometry and RNA-seq (Kawamura et al., 2021). However, the slow growth and calcium carbonate skeletons of *Acropora* and other reef-building corals limits the throughput and efficiency of single-cell analyses and application of cellular biological techniques (Weis et al., 2008). As an alternative, the model sea anemone Aiptasia has proven easy to culture and experimentally manipulate in the laboratory (Bucher et al., 2016; Lehnert et al., 2014;

Mansfield et al., 2017). We found that Aiptasia cells can withstand enzymatic dissociation and staining procedures for fluorescent microscopy (Figure 3.1 & 3.2) and flow cytometry (Figure 3.3). Our results suggest that symbiotic and symbiont-free Aiptasia cells can be easily gated using fluorescent staining and imaging flow cytometry for downstream analysis. These findings allow for future protocol development, including single-cell RNA-seq, that may reveal essential genes for symbiosis establishment. For instance, in the soft coral *Xenia sp.*, researchers have used single-cell transcriptomics to identify states of endosymbiotic host cells (Hu et al., 2020). The successful generation of a single-cell suspension from adult Aiptasia, containing symbiotic and symbiont-free host cells, is invaluable to the field of cnidarian-algal symbiosis and can be used to decouple the interactions between host and symbiont.

3.4.2 Photosynthesis is not needed for symbiosis establishment

We used the cellular-level resolution provided by this single-cell dissociation protocol to investigate the impact of photosynthesis on the stages of symbiosis establishment. Contradicting studies have suggested that photosynthesis may impact symbiosis establishment (Wolfowicz et al., 2016; Xiang et al., 2018) and symbiont maintenance in the host tissue (Fransolet et al., 2014; Jones, 2004; Lehnert et al., 2014; Zaquin et al., 2019). Many of these studies utilize chemical treatments such as DCMU (3-(3,4-dichlorophenyl)-1,1-dimethylurea) that could stress the host animals, or researchers attempt to maintain dark conditions which inevitably have incidental light exposure. The photosynthesis mutant *ora1* (Jinkerson et al., 2022) avoids these confounding variables. In Jinkerson et al. (2022) *ora1* algae was observed associating with both Aiptasia and *Acropora*. However, whole animal fluorescent microscopy of symbiont-containing hosts did not provide enough resolution to determine the cellular localization of the symbionts. For instance, *ora1* algal cells could be residing within the host gastrovascular cavity instead of enclosed within the

gastrodermal cells of the host (Figure 1.1). Utilizing single-cell dissociation and fluorescent microscopy of *ora1*-associated animals, we discovered that *ora1* localizes intracellularly in both Aiptasia (Figure 3.4) and *Acropora* (Figure 3.5) despite the loss of photosynthesis. However, while photosynthesis mutant *ora1* proliferated in *Acropora*, *ora1* did not proliferate in Aiptasia without photosynthesis (Jinkerson et al., 2022). This difference observed in adult Aiptasia and juvenile coral polyps could be due to differences in the translocation of fixed carbon or other key nutrients from the host to the algal symbionts. Symbiodiniaceae algae are capable of surviving varying trophic states (Xiang et al., 2018), but without photosynthesis, the algae must be supplied with nutrients to proliferate. Juvenile coral polyps may contain stored nutrients that allow them to survive in nature prior to obtaining symbionts from the water column (Graham et al., 2013; Harii et al., 2007). Without photosynthesis, the algal symbionts may obtain fixed carbon from the juvenile coral polyps as 1) a stimulant for symbiont growth, 2) in exchange for translocating essential nutrients to the host, or 3) by parasitizing the host, but no evidence of parasitism was observed (Jinkerson et al., 2022). These results suggest that cnidarian-algal symbiosis establishment is independent of photosynthesis but the extent at which it proceeds is dependent on the cnidarian species.

In summary, this study highlights how single-cell dissociation of adult Aiptasia can be used to investigate the essential mechanisms of cnidarian-Symbiodiniaceae symbiosis. Here, we indicate that host-symbiont interactions and mechanisms other than photosynthesis may be more critical for symbiosis establishment. Advancing the cellular and molecular tools in the field of cnidarian-algal symbiosis will help researchers probe these and other unanswered questions in symbiosis.

CHAPTER 4: DYNAMICS OF SYMBIONT PROLIFERATION IN CNIDARIAN-SYMBIODINIACEAE SYMBIOSIS

4.1 Abstract

Cnidarian-Symbiodiniaceae symbiosis occurs on a cellular level where algal symbionts must rapidly proliferate in host tissue to reach an optimal biomass. However, the fundamental cellular events responsible for symbiont proliferation are not well known. Here, we demonstrate that symbiont division and primary infections of host cells are the drivers of symbiont proliferation *in hospite*. UV mutagenesis was used to isolate a green *Breviolum minutum* mutant *gr02*, that is visually distinct from the brown wild type (WT) *in hospite*. The green mutant *gr02* and WT *B. minutum* were co-inoculated into the model host sea anemone *Exaiptasia diaphana* (Aiptasia), and the patterns of symbiont proliferation were determined through symbiont tracking in live hosts. Both homogenous symbiont clusters, represented by either brown-only or green-only algae, and mixed clusters containing brown and green symbionts were observed within host tissue. Quantification of these cluster types reveals homogenous clusters are the majority throughout proliferation. Moreover, we show for the first time that two symbiont species can co-occupy a host cell across three cnidarians. Taken together, these results reveal new insights into how symbionts proliferate in cnidarian hosts, as well as lay the foundation for future research into *in hospite* interactions between symbiont species using the green mutant tool.

4.2 Introduction

Symbiotic relationships rely on intimate host-microbe interactions involving the growth and spread of symbionts throughout host tissues. This proliferation of symbionts within

multicellular hosts establishes a dynamic homeostasis that is essential for mutualistic relationships at the foundation of diverse ecosystems (Herre et al., 1999). In coral reef ecosystems, corals and other cnidarians, such as sea anemones and jellyfish, form symbioses with dinoflagellate algae in the family Symbiodiniaceae (LaJeunesse et al., 2018; Muscatine & Porter, 1977). During cnidarian-Symbiodiniaceae symbiosis establishment, algal symbionts are engulfed into gastrodermal cells lining the gut cavity of cnidarian hosts where inorganic nutrients and algal photosynthates are exchanged (Davy et al., 2012). Algal symbionts then proliferate to a steady-state density within the host (Muscatine et al., 1997) thereby exchanging sufficient nutrients to not only meet the energetic demands of the host but also support coral reef biodiversity (Falkowski et al., 1984, 1993). The rapid proliferation of acquired symbionts is important for the stability of cnidarian-algal symbiosis (Baird & Marshall, 2002; Gabay et al., 2018; C. R. Newkirk et al., 2018; Rädecker et al., 2021; Toller et al., 2001) and in turn coral reef ecosystems, but the cellular events responsible for symbiont proliferation in a healthy symbiosis are not well understood.

Algal symbionts are initially acquired at low densities, appearing sparsely across host tissue (Gabay et al., 2018; Jinkerson et al., 2022). Symbiont population is then regulated by host-symbiont nutritional balance (Cui et al., 2019; Krueger et al., 2020; Xiang et al., 2020) and cell cycle coordination (Tivey et al., 2020; Wilkerson et al., 1988). Previous studies have observed clusters of symbionts within host cells during symbiont proliferation (Jinkerson et al., 2022), indicating that symbionts may divide intracellularly and are maintained in the host cell for some period of time. Other research indicates that symbionts undergo inter-cellular division where host and symbiont coordinate mitotic division such as in the coral *Pocillopora damicornis* (Camaya, 2020). The division of symbionts could also result in selective expulsion, as to limit the intracellular population of symbionts (Baghdasarian & Muscatine, 2000). Expulsion of competent

symbionts has been observed under natural, un-stressed conditions (Davy et al., 2012; Hoegh-Guldberg et al., 1987), but how symbiont division and expulsion influence symbiont proliferation *in hospite* is not clear.

Symbionts must spread to new areas of the host gastrodermis during proliferation to populate the host (Tivey et al., 2022). Following initial engulfment into host tissue, the spread of algal symbionts could be aided by cell-to-cell migration, where symbionts migrate between adjacent host cells, or through expulsion into the gastrovascular cavity and subsequent infection of a distant host cell. This infection could be primary, where an alga is engulfed into an unoccupied host cell, or secondary, where an alga is engulfed into a host cell already occupied by an endosymbiotic alga. Indeed, other studies have observed two or more symbiont cells co-occurring in a single host cell, occupying separate symbiosomes (Barott et al., 2015; Muscatine et al., 1998). However, it is difficult to distinguish if these co-occurring cells are the result of intracellular symbiont division, cell-to-cell migration, or secondary infection events.

A combination of cellular mechanisms could contribute to the proliferation of symbionts in cnidarian-Symbiodiniaceae symbiosis: (1) intracellular division of symbionts within the host cell, (2) inter-cellular division of symbiont and host cell, (3) cell-to-cell migration, (4) primary infection, or (5) secondary infection events (Figure 4.3A). Visually observing the various cellular dynamics over the course of proliferation has been challenging due to the genetic intractability of Symbiodiniaceae limiting genetic manipulation of symbionts. Here, we used classical UV mutagenesis (Russo et al., 2023) to generate a Symbiodiniaceae pigment mutant *GREEN02* (*gr02*) that is green in color and visually distinct from the brown color of the wild type (WT) *B. minutum*. These contrasting symbiont phenotypes allow for cellular events during symbiont proliferation to be distinguished within host tissue.

In this study, co-inoculations of WT *B. minutum* and *gr02* in the sea anemone *Exaiptasia diaphana* (Aiptasia) were used to investigate the driving mechanism of symbiont proliferation during symbiosis establishment. Quantification of symbiont clusters *in hospite*, reveals that secondary infections of symbionts occur rarely during proliferation. The spread of symbionts is instead driven by intracellular symbiont division and primary infections of unoccupied host cells. Moreover, we have demonstrated the versatility of the green mutant in evaluating aspects of cnidarian-algal symbiosis. For the first time, two Symbiodiniaceae species were observed co-localized within a host cell across three cnidarians. Taken together, these results highlight the cyclical cellular events occurring during symbiont proliferation and demonstrate the potential for intracellular interactions and competition between symbiont genotypes *in hospite*.

4.3 Methods

4.3.1 Symbiodiniaceae strains

Three clonal and axenic strains of Symbiodiniaceae were used in this study: *Symbiodinium linucheae* strain SSA01 (Clade A) (Bieri et al., 2016), *Symbiodinium necroappetens* strain SSA02 (Clade A), and *Breviolum minutum* strain SSB01 (Clade B) (Xiang et al., 2013). Other Symbiodiniaceae strains include *Cladocopium goreaui* strain LHI-33 (Clade C) and *Durusdinium trenchii* strain CCMP2556 (Clade D). Symbiodiniaceae liquid cultures were grown without agitation at 27 °C on a 12 hr-light/12 hr-dark cycle with an irradiance of ~10 or 50 µmol photons m^{-2} s^{-1} of photosynthetically active radiation (PAR) provided by Percival SciWhite LED tiles in Daigo's IMK minimal medium for marine microalgae (Wako Pure Chemicals, Osaka, Japan) made with artificial seawater, 37.4 $g \cdot L^{-1}$, marine broth (MB) (Millipore-Sigma 76448) medium, or MB

supplemented with 2 $g \cdot L^{-1}$ glucose (Millipore-Sigma G8270). *C. goreaui* (LHI-33) and *D. trenchii* (CCMP2556) were cultured in Daigo's IMK.

4.3.2 *Exaiptasia diaphana* clonal strains

Anemones utilized in this study were from clonal strains of *Exaiptasia diaphana* (Aiptasia) H2 and CC7 rendered aposymbiotic (free of endogenous algae) via short term cold shock (Lehnert et al., 2012) followed by menthol treatment (Matthews et al., 2016). Aposymbiotic Aiptasia were maintained within polycarbonate tanks filled artificial seawater (ASW) at 27 °C in continuous darkness and transferred to 12 hr-light/12 hr-dark (10 μmol photons m^{-2} s^{-1} of PAR) ~2 weeks prior to inoculations. The animals were fed and their water changed 2x weekly unless otherwise noted. Aposymbiotic status was confirmed prior to every inoculation using fluorescent microscopy to detect algal chlorophyll fluorescence.

4.3.3 *Pseudodiploria strigosa* and *Colpophyllia natans* coral

Larvae of the coral *Pseudodiploria strigosa* and *Colpophyllia natans* were kindly provided by the Baker lab from the University of Miami. Aposymbiotic larvae were washed with filtered ASW and settled into 6-well polypropylene plates (~10–20 polyps per well). Larvae were incubated overnight with 1 μM of the neuropeptide Hym-248 (Iwao et al., 2002) in ASW at 27 °C and washed with filtered ASW following attachment and metamorphosis. Coral polyps intended for inoculation experiments were confirmed algae free with fluorescent microscopy.

4.3.4 *Cassiopea xamachana* jellyfish

Cassiopea xamachana polyps were collected from the Florida Keys, rendered aposymbiotic, and propagated as previously reported (C. Newkirk et al., 2022). Aposymbiotic polyps intended for inoculation studies were maintained in 6-well polypropylene plates with filtered ASW in 24-hour dark at 27°C. Two weeks prior to inoculations, polyps were placed in 12

hr-light/12 hr-dark (50 μmol photons m^{-2} s^{-1} of PAR) and algae-free status confirmed with fluorescent microscopy.

4.3.5 Generation of SSB01 accessory pigment mutant

As previously reported (Jinkerson et al., 2022), mutants of the *B. minutum* SSB01 background were created using UV mutagenesis and grown on solid MB media with 0.5 $g \cdot L^{-1}$ glucose in low light (~5-10 μmol photons m^{-2} s^{-1} of PAR) up to 45 days. Plates were screened for colonies with distinctively altered color phenotype compared to brown WT *B. minutum* and confirmed by secondary screen on solid media. In this study, mutant *GREEN02* (*gr02*) was identified and cultured in MB under 12 hr-light/12 hr-dark (50 μmol photons m^{-2} s^{-1} of PAR).

4.3.6 Algal growth studies in culture

To compare the photoautotrophic growth of WT *B. minutum* and green mutant *gr02* in Figure 4.1, three replicates were inoculated for each strain at an initial concentration of 1.5 $x10^5$ $cells \cdot ml^{-1}$ in liquid MB and grown under 12 hr-light/12 hr-dark (50 μmol photons m^{-2} s^{-1} of PAR) at 27 °C. Samples were taken every 7 days for cell counting using the Countess II FL Automated Cell Counter (Invitrogen) up to day 21.

4.3.7 Analyses of photosynthetic function

Algal samples of WT *B. minutum* and *gr02* grown photoautotrophically in MB under 27 °C 12 h light / 12 h dark (50 μmol photons m^{-2} s^{-1} of PAR) were sampled at approximately 10^6 cells and allowed 30 minutes of dark adaptation before measuring the maximum quantum yields of photosystem II (PSII), $F_v/F_m = (F_m–F_0)/F_m$ (Joliot et al., n.d.) using an Aquapen AP-100 (Photon Systems Instruments).

4.3.8 Inoculation of Aiptasia with Symbiodiniaceae

For inoculations of aposymbiotic CC7 or H2 Aiptasia, individual anemones were settled on day 0 in each well of a 6-well polypropylene plate and inoculated with single or mixed Symbiodiniaceae strains at a final concentration of $1x10^5$ cells·ml^{-1}. Single inoculations of WT *B. minutum* and *gr02* were completed by adding each algal strain separately to individual anemones. For mixed inoculations, Symbiodiniaceae algae were combined in the following pairs: *gr02* with WT *B. minutum*, *gr02* with *S. linucheae* (SSA01), *gr02* with *S. necroappetens* (SSA02), *gr02* with *C. goreaui* (LHI-33), and *gr02* with *D. trenchii* (CCMP2556). Individual algal strains were mixed at a 1:1 ratio prior to inoculations for all algal pairs except *gr02* with *C. goreaui* (LHI-33) or *D. trenchii* (CCMP2556). Animals were first inoculated with either *C. goreaui* (LHI-33) or *D. trenchii* (CCMP2556) and the algae allowed to propagate followed by addition of *gr02.* After an incubation period of 24 hours, all inoculated anemones were washed in sterile ASW and transferred to new, clean 6-well plates. All infected Aiptasia were kept at 27 °C in 12 hr-light/12 hr-dark (10 μmol photons m^{-2} s^{-1} of PAR).

4.3.9 Inoculation of coral polyps with Symbiodiniaceae

Algae-free polyps were inoculated by incubating for two days with either single Symbiodiniaceae strains (WT *B. minutum* or *gr02*) or a mixture of strains (*gr02* and *D. trenchii*) at a concentration of $1x10^4$ cells·ml^{-1}. After two days of incubation, the polyps were washed with ASW and maintained in 12 hr-light/12 hr-dark (10 μmol photons m^{-2} s^{-1} of PAR).

4.3.10 Inoculation of *Cassiopea* polyps with Symbiodiniaceae

Algae-free polyps of *Cassiopea* were acclimated to light (50 μmol photons m^{-2} s^{-1} of PAR) at least two-weeks prior to inoculations. Mixed inoculations were completed by first infecting the polyps with a high density ($4x10^5$ cells/mL) of *gr02* three times weekly until algae

was maintained within the polyps. Following *gr02* infections, brown Symbiodiniaceae *D. trenchii* (CCMP2556) was added at a concentration of $1x10^5$ cells. Inoculated *Cassiopea* polyps were maintained in 12 hr-light/12 hr-dark (50-70 µmol photons m^{-2} s^{-1} of PAR).

4.3.11 Algal cells per protein density

Aiptasia containing either WT *B. minutum* or *gr02* strains at steady state were maintained at a temperature of 27 °C 12 h light / 12 h dark (5-10 µmol photons m^{-2} s^{-1} of PAR) light cycle inside of a I-36 VL Percival Incubator before use. Individual anemones were placed into a 2 mL microcentrifuge tube and centrifuged for approximately 5 minutes at a speed of 15000 rpm until ASW supernatant could be removed from the pellet containing the anemone body. Anemones were then resuspended in 500 uL of .01% SDS and subsequently pulverized and homogenized with the plunger of a 1 mL syringe followed by vigorous pipetting up and down to break down clumps of tissue. Cell concentration of the homogenized solution was taken by hand using a hemocytometer and brightfield. Protein concentration was then performed using Pierce Rapid Gold BCA Protein Assay Kit (Thermo Scientific A53225)

4.3.12 Pigment extraction and chromatography analysis

To extract pigments for thin-layer chromatography (TLC), samples of WT *B. minutum* and *gr02* ($2x10^7$ cells each) grown for 16 days in MB (24 hour, 50 µmol photons m^{-2} s^{-1} light) were centrifuged at 500 *x g* for 5 minutes to remove the growth media. Each cell pellet was then frozen in liquid nitrogen and ground for 30 seconds with a mortar and pestle. Grinding and freezing was repeated three times, and the algal cells were washed from the mortar with the addition of 200 uL of ethanol and quick grinding. The mixture of algae and ethanol was then transferred to a 1.5 mL tube and allowed to incubate in the dark at 4 °C for ~24 hours for pigment extraction.

Separation of pigment extracts was completed with TLC. The pigment extracts were concentrated via lyophilization, and the final volume brought to 30 uL with ethanol. Extracts were spotted in lines 1 cm in length on a TLC Silica gel 60 F254 plate (MilliporeSigma 1055700001). The TLC plates were then run in a mobile phase of hexane and acetone (60:40, v/v) until separation was observed.

4.3.13 Algal cell quantification in host tissue

To quantify the number and composition of algal clusters from mixed inoculations with WT *B. minutum* and *gr02* in Aiptasia from Figures 4.2 and 4.3, infected anemones were incubated with 1:1 ASW and 0.37 M $MgCl_2$ solution until fully relaxed. Each tentacle of the Aiptasia was scanned for algae using a Leica DM6 fluorescence microscope either in bright-field mode or with a Texas Red filter set (534–59 nm excitation and 630–69 nm emission). Algae were categorized as "brown" or "green" based on both color under bright-field, *gr02* appearing bright green and WT *B. minutum* appearing brown, and the noticeably lower fluorescence from *gr02* when compared to WT *B. minutum* under fluorescence. Algal cells that made direct contact with one another in groups of eight or less were identified as a cluster. Quantification of *in hospite* algal clusters were repeated weekly for single and mixed infections until clusters were no longer distinguishable.

4.3.14 Time-series symbiont tracking in Aiptasia

To observe the cellular events of proliferation in host tissues, *gr02*/ WT *B. minutum*-associated H2 Aiptasia were tracked across three days of symbiont proliferation. Prior to inoculations with *gr02*/WT, animal tentacles were cut such that a fork would produce on the end of one or multiple tentacles. This allowed for the tentacles to be identified and the animal to be mounted on a slide in the same position across multiple days. Following inoculations with a 1:1 ratio of WT/*gr02*, the algae was allowed to proliferate for ~2 weeks. On day 14 post-inoculation,

animals were relaxed with ASW/$MgCl_2$ and mounted between two coverslips for imaging on a Leica DM6 microscope in bright-field. Whole animal images were taken at 40x magnification using the tile scan feature in LASX. All animals were washed with filtered ASW and placed in a clean 6-well plate following imaging each day. Image analysis was performed in LASX Office where sections of host tissue were identified across days 14, 15, and 16.

4.3.15 Single-cell dissociation of cnidarians

To better visualize and confirm algal clusters within host cells in Figures 4.2 and 4.4, the three cnidarians (Aiptasia, *P. strigosa*, and *Cassiopea*) associated with mixed Symbiodiniaceae pairs were dissociated into single-cells as reported in (Jinkerson et al., 2022) and (Kirk & Xiang, 2022). Tentacles of adult Aiptasia were dissected and coral skeletons were crushed prior to enzymatic digestion. *Cassiopea* polyps metamorphosed into adult ephyra prior to dissociation, and the ephyra were chopped into small pieces to prepare for enzymatic digestion. Animal tissues were incubated with 0.25-0.5% pronase from *Streptomyces griseus* (MilliporeSigma 10165921001) in CMF-ASW with EGTA (ethylene glycol-bis (β-aminoethyl ether)-N,N,N′,N′-tetraacetic acid, MilliporeSigma 324626) and 15 ug/mL of cell permeable Hoechst 33342 fluorescent nuclei stain for the host nuclei. The solution was mixed well by pipetting and incubated for 15-30 minutes with gentle agitation until the tissue samples appeared homogenized. The pronase-staining solution was removed from dissociated tissue by centrifugation at 70 *x g* and the single-cells were resuspended in 16 uL CMF-ASW+EGTA for immediate imaging.

4.3.16 Microscopy

Whole animal imaging of Aiptasia, *P. strigosa*, *C. natans*, and *Cassiopea* polyps and ephyra was completed with a Nikon SMZ-25 fluorescence stereoscope in bright-field or blue-light

excitation (GFP2 filter set; 480/40 nm excitation, 510 nm long-pass fluorescence emission) of endogenous algal chlorophyll. Images were captured with a Nikon DS-Ri2 Color CMOS Camera. To identify symbiont clusters in host tissue of adult Aiptasia (Figures 4.2 & 4.3), animals were viewed with a Leica DM6 fluorescence microscope either in bright-field mode or with a Texas Red filter set (534–59 nm excitation and 630–69 nm emission) and imaged with a Leica DMC6200 pixel shift camera.

Dissociated cnidarian tissue was observed with a Zeiss Axio Observer inverted microscope either in bright-field mode or Texas Red filter set for chlorophyll fluorescence (546/12 nm excitation, 590 nm long-pass fluorescence emission), and fluorescence filter set for Hoechst 33342 fluorescent nucleic acid stain (365nm excitation, 445/50 nm band pass fluorescence emission).

4.3.17 Statistical analysis

All statistical tests were performed using Python (2.7.11; https://www.python.org), SciPy (0.17.0; https://www.scipy.org), Pandas (0.18.1; https://pandas.pydata.org/) packages integrated in Jupyter Notebook, or R statistical computing software (version 4.1.1; R Core Team 2021). Statistical tests used and number of repeats are indicated in the figure legends or in the text.

4.4 Results

4.4.1 *Breviolum minutum* green mutant *gr02* lacks peridinin

UV mutagenesis techniques were used to generate mutants in wild type (WT) *Breviolum minutum* (Jinkerson et al., 2022; Russo et al., 2023). The green mutant *GREEN02*, *gr02*, was identified due to its bright green appearance when compared to the WT *B. minutum* that is brown in color (Figure 4.1A). To determine if the green mutant *gr02* displays similar physiology as the WT *B. minutum*, we assessed each algal genotype *in vitro* and *in hospite*. The green mutant is

visually distinct in both bright-field and fluorescent microscopy from the WT. Under 561 nm excitation, the green mutant has reduced autofluorescence when compared to WT *B. minutum* (Figure 4.1A). Photosynthetic pigments are responsible for the fluorescence of dinoflagellate algae (Anthony et al., 2023; Kato et al., 2020). Evaluation of algal pigment extracts using thin-layer chromatography (TLC) reveals that *gr02* lacks the pigment peridinin, visible in the WT as a bright orange band (Figure 4.1B). This absence of peridinin in *gr02* was also confirmed through UHPLC (Supplementary Figure 4.1). Peridinin is an accessory pigment found in the light harvesting complex of dinoflagellates and absorbs light in the blue-green region (Carbonera et al., 2014), and the loss of peridinin corresponds to the reduced auto-fluorescence in *gr02* compared to WT (Figure 4.1A). Even without peridinin, *gr02* maintains a maximum quantum efficiency of photosystem II indicated by F_v/F_m and is able to grow photoautotrophically similar to WT (Figure 4.1CD).

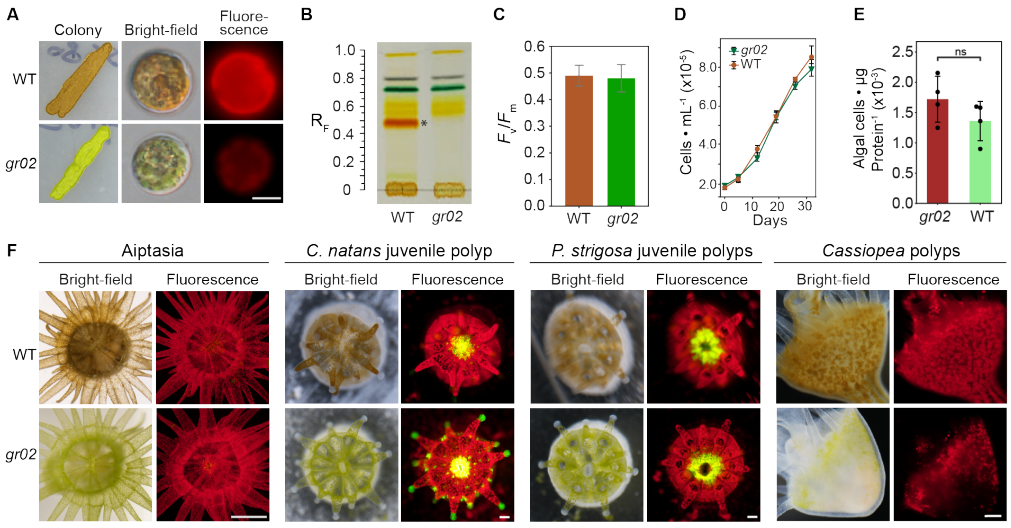

Figure 4.1 *Breviolum minutum* mutant *gr02* exhibits a bright green color and forms symbioses with cnidarian hosts.
(A) Representative images of wild type *B. minutum* (WT) and green mutant *GREEN02* (*gr02*) cells grown on agar media plates and cells grown in liquid medium. Scale bar, 5 µm. (B) Chromatograms of pigment extracts from WT and *gr02* on a silica gel 60 TLC plate. Asterisk

indicates the band of peridinin. (C) Maximum PSII efficiencies F_v/F_m of WT and gr02. Error bars represent standard deviation (+/- SD) from 6 biological replicates. (D) Growth curve of WT and *gr02* in liquid MB medium under 10 µmol photons m^{-2} s^{-1}. Error bars represent +/- SD from 3 biological replicates. (E) Algal population densities of WT or *gr02* in Aiptasia tissue. Error bars represent +/- SD from 3 biological replicates. (F) Representative microscopic images of sea anemone Exaiptasia diaphana (Aiptasia), coral polyp *Pseudodiploria strigosa*, coral polyp *Colpophyllia natans*, and *Cassiopea xamachana* (*Cassiopea*) infected with WT or *gr02* in the light. A top-down view of animals in bright-field and fluorescence is shown. Chlorophyll autofluorescence from algal cells is in red. Scale bars represent 1 mm for Aiptasia and 100 µm for coral polyps, and 200µm for Cassiopea, respectively.

4.4.2 Green mutant *gr02* forms symbiosis with cnidarian hosts.

WT *B. minutum* has previously been shown to establish symbiosis with a variety of cnidarian hosts including sea anemones, jellyfish, and coral (Bucher et al., 2016; Jinkerson et al., 2022; LaJeunesse et al., 2018). We next assessed the ability of the green mutant *gr02* to establish symbiosis with four cnidarian species: sea anemone *Exaiptasia diaphana* (Aiptasia), juvenile coral polyp *Pseudodiploria strigosa*, juvenile coral polyp *Colpophyllia natans,* and jellyfish *Cassiopea xamachana*. In all cases, *gr02* was able to infect, proliferate, and be maintained, resulting in visibly bright green anemones, coral polyps, and jellyfish polyps (Figure 4.1F). *Cassiopea* polyps required multiple inoculations before the green mutant was able to establish symbiosis; once *gr02* was acquired, the density of symbionts in *gr02*-associated *Cassiopea* did not appear to reach that of WT-associated *Cassiopea*. In contrast, analysis of symbiont population densities in Aiptasia associated with *gr02* or WT *B. minutum* revealed that both *gr02* and WT reach similar densities *in hospite* (Figure 4.1E, *p*-value= 0.403, two-tailed t test). These data demonstrate that *gr02* can form symbiosis with various cnidarian hosts despite the loss of peridinin and is the first evidence of a clonal Symbiodiniaceae mutant retaining its ability to infect, photosynthetically proliferate, and be maintained in various cnidarian hosts.

4.4.3 Mixed symbiont clusters form during symbiont proliferation

Clusters of Symbiodiniaceae algae have been observed within cnidarian host tissue (Gabay et al., 2018; Tivey et al., 2022), and sequencing has shown that multiple Symbiodiniaceae genotypes and species often associate with hosts (Pootakham et al., 2021; Silverstein et al., 2012). Prior to the generation of the green mutant *gr02*, the individual genotypes of Symbiodiniaceae cells in these *in hospite* clusters could not be distinguished. We next assessed the ability for green mutant *gr02* and WT *B. minutum* to establish symbiosis concurrently and be visually distinguished using bright-field and fluorescence microscopy in host tissue. Following the co-inoculation of *gr02* and WT *B. minutum* in Aiptasia, algal cells were visible as red fluorescence dots in host tentacles, depicted in the top-view of the whole animal in Figure 4.2A. The tentacles of *gr02*/WT-associated Aiptasia were then scanned utilizing high-resolution bright-field and fluorescence microscopy to identify clusters of algae, defined as groups of algae that appeared to touch one another and maintain clear separation from other symbiont clusters (Supplementary Figure 4.2). Four days post-inoculation (dpi), homogeneous clusters of brown-only WT *B. minutum* or green-only *gr02* cells were observed in the anemone tentacles (Figure 4.2). As proliferation proceeded, mixed-genotype clusters of both green *gr02* and brown WT formed in the tentacles (Figure 4.2BC).

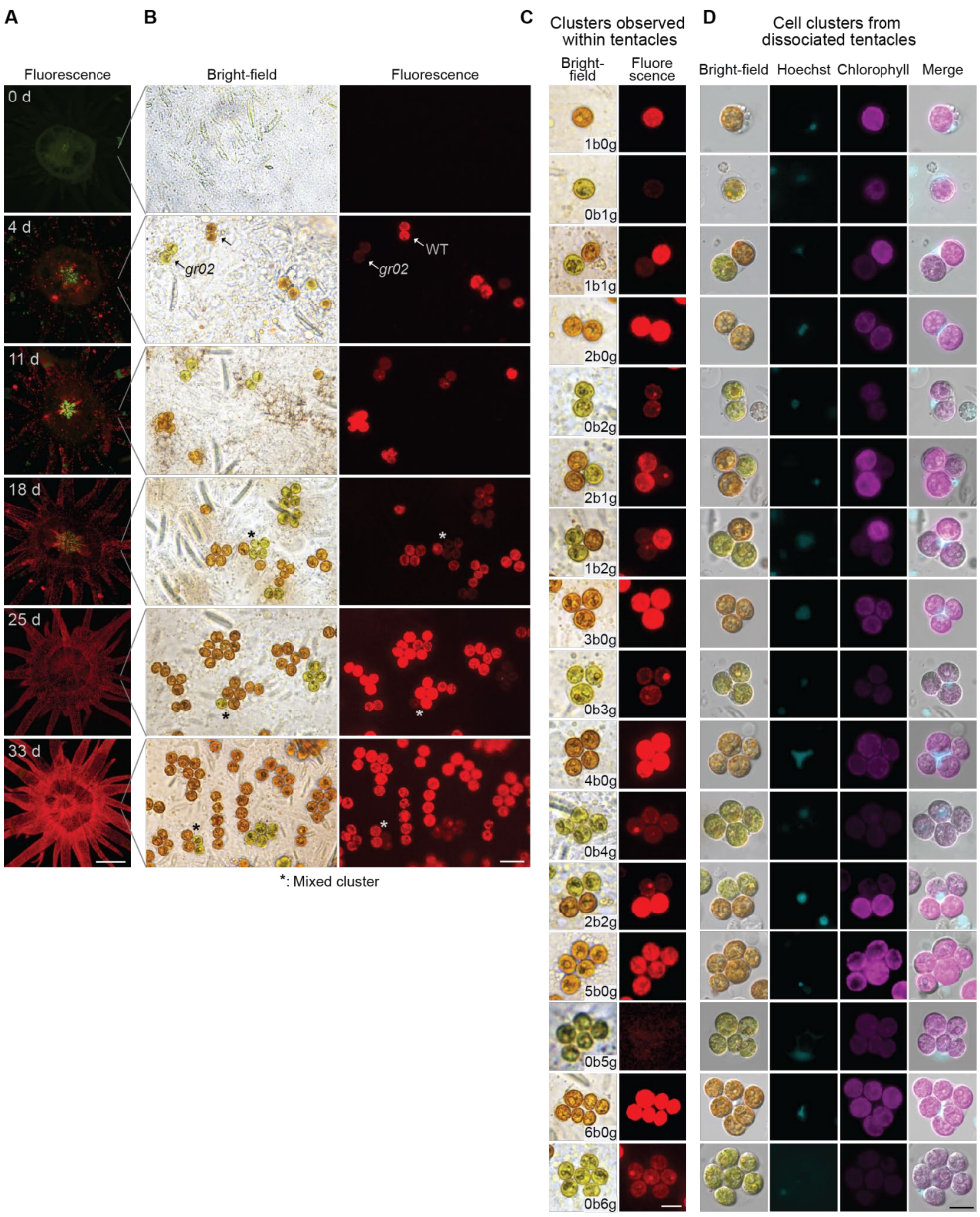

Figure 4.2 Mixed-genotype symbiont clusters form during proliferation *in hospite*.
(A-B) Representative microscopic images of sea anemones Aiptasia inoculated with WT *B. minutum* and green mutant *gr02*. (A) top-down view of animals in fluorescence; (B) bright-field and fluorescence images of algal symbiont clusters within the gastrodermis of host tentacles. Green algal cells are *gr02*; brown cells are WT. Scale bars, 1 mm for A; 20 µm for B. (C) Representative microscopic images of cell clusters with various compositions of WT (brown) and *gr02* (green) symbionts within Aiptasia tentacles. Scale bar, 10 µm. (D) Representative microscopy images of individual dissociated Aiptasia cells containing symbionts with various compositions of WT (brown) and *gr02* (green) symbionts. Cyan, cell-permeable Hoechst 33342 fluorescent nucleic acid stain; magenta, algal chlorophyll fluorescence. Scale bars, 10 µm.

To verify that symbiont clusters observed in host tissue are localized intracellularly, *gr02*/WT-associated Aiptasia tentacles were dissected and dissociated into a single-cell suspension using enzymatic digestion (Kirk & Xiang, 2022). Symbiont clusters ranging in size from one to six algal cells were observed within host tentacle tissue (Figure 4.2C) and within dissociated host cells (Figure 4.2D). Various combinations of mixed genotype clusters were also observed in dissociated tissue, matching the variety of cluster types found in host tentacles (Figure 4.2BCD). This is the first evidence of two Symbiodiniaceae genotypes co-localizing in a single host cell. The host cell membrane can be seen enveloping the stained host nucleus and the endosymbiotic algal cells (Figure 4.2D). These data indicate that two symbiont genotypes can co-occur within a host cell where *in hospite* interactions and competition between symbionts may occur.

4.4.4 Primary infections and intercellular division aids symbiont proliferation *in hospite*

We next evaluated the quantity and composition of algal clusters that formed during the course of *gr02*/WT proliferation in Aiptasia. This comprehensive assessment encompassed the entirety of the host animal, as depicted in Figure 4.2A, as well as a closer examination of the tentacles, as illustrated in Figure 4.2B. Through quantification of homogeneous and mixed genotype clusters of *gr02* and WT *B. minutum*, proliferation events such as division, migration, and infection can be distinguished in the host tissue (Figure 4.3A). For example, homogenous algal clusters likely form by initial infection of an alga followed by mitotic cell division. In contrast, mixed symbiont clusters can only occur through infection of distinct algal cells into one host cell. By comparing the abundance of homogenous and mixed clusters of algae, the primary mechanism of algal proliferation can be elucidated.

Following inoculation of *gr02*/WT into aposymbiotic Aiptasia, homogenous clusters were the majority cluster type observed when compared to mixed clusters during early (2-11 dpi) and

late (12-40 dpi) stages of proliferation (Figure 4.3B, Supplementary Figure 4.3, ***$p<0.001$, two-sided Mann Whitney U). Algae within mixed clusters occurred rarely following initial infection, indicating that a single algal genotype is most commonly engulfed into a host cell (primary infection). Additionally, the low abundance of mixed clusters throughout proliferation suggests that secondary infection is a minor mechanism.

Homogeneous clusters containing ~1-4 symbionts were observed frequently during early proliferation, while larger clusters of 5-8 symbionts appeared more often at later time points (Figure 4.3B, Supplementary Figure 4.3). Homogenous doublets are abundant throughout proliferation while singlets appear initially and decrease in overall percent abundance (Figure 4.3B). The cell counts of symbionts associated with both homogenous and mixed clusters increase during proliferation (Figure 4.3D), but the percent abundance of cells in mixed clusters remains relatively low (Figure 4.3CE). Taken together, these results suggest that intracellular symbiont division produces growing homogeneous clusters during initial proliferation. New clusters of symbionts are then formed from the infection of symbionts into primarily unoccupied host cells, and rarely, host cells already occupied by an alga.

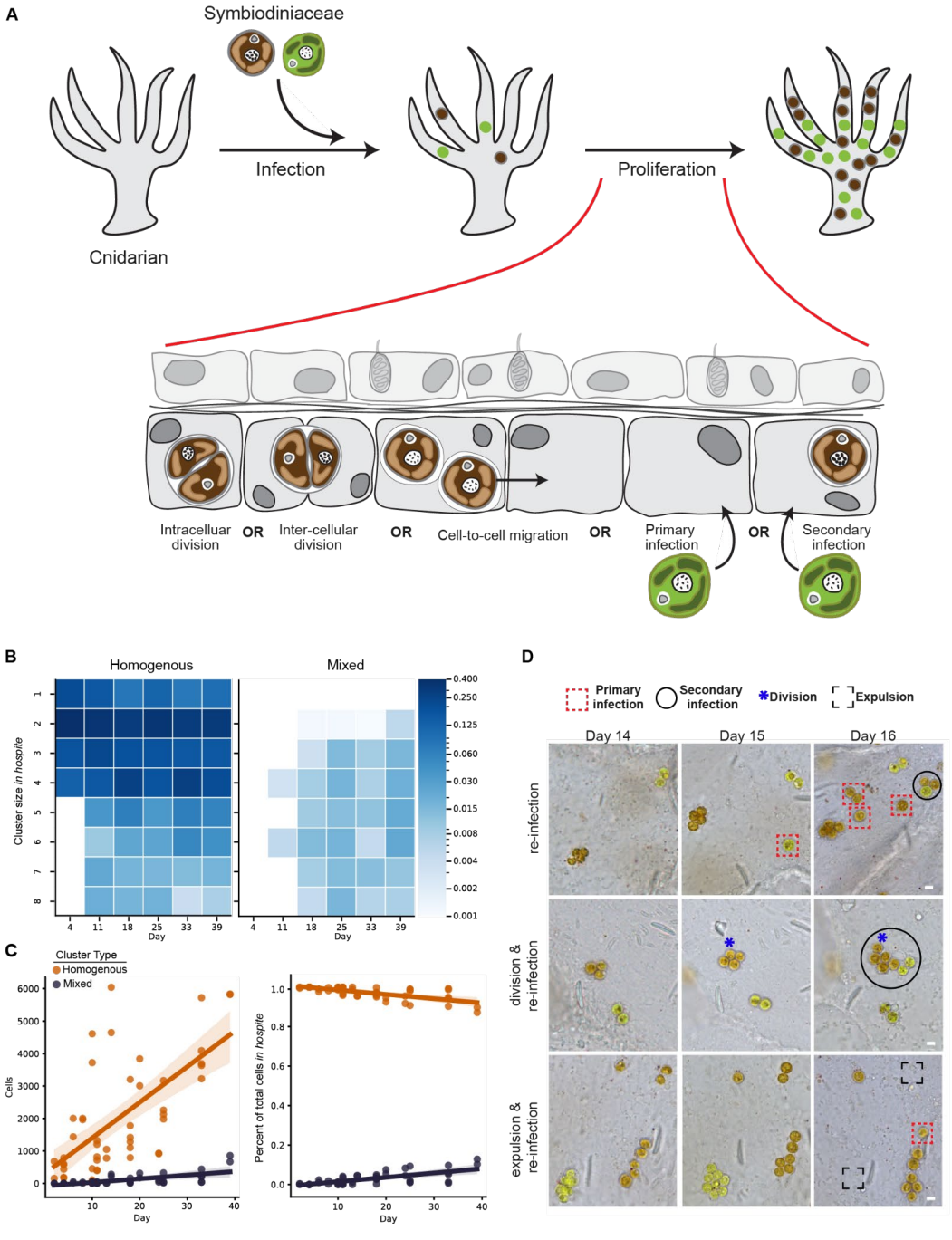

Figure 4.3 Proliferation in Aiptasia is driven by primary symbiont infection followed by division within host cells.

(A) Cartoon depicting the cellular events possible during symbiont proliferation in cnidarian host tissue. Establishment of symbiosis begins when Symbiodiniaceae algae infect or are engulfed into the gastrodermal cells of the host. Following infection, symbionts may proliferate through a combination of cellular events including 1) intracellular division within host cells; 2) inter-cellular division between, or coordinated with, host cells; 3) cell-to cell migration across adjacent host

gastrodermal cells; 4) primary infection of host cells from the gastrodermal cavity; or 5) secondary infection of a host cell already containing an algal symbiont. (B) Representative heatmaps depicting the percent abundance of symbiont cells associated with homogenous (left panel) or mixed clusters (right panel) present in a WT/*gr02*-associated Aiptasia sea anemone during proliferation. (C) Regression plots showing the symbiont cell count (left panel) and percent abundance of symbiont cells associated with homogenous (orange) or mixed clusters (dark blue) in the tentacles of WT/*gr02* inoculated Aiptasia sea anemones (n=10) during proliferation. (D) Representative microscopic images depicting three sections of WT/*gr02* associated Aiptasia tentacles tracked across two days of proliferation. Top-panels show instances of primary (red squares) and secondary (black circle) infections. Middle panels depict symbiont intracellular division (blue asterisk) and secondary infection events. Bottom panels show loss, or expulsion (black square), of symbionts from sections of host tissue as well as primary infection. Scale bars, 5 μm.

The number of symbiont clusters increases during proliferation *in hospite* (Supplementary Figure 4.4). To determine if new symbiont clusters are formed from cell-to-cell migration of symbionts across the gastrodermal tissue layer or through primary and/or secondary infections following expulsion into the gastrovascular cavity, we tracked symbiont clusters across sections of host tissue (n=3) during two days of proliferation. Aiptasia associated with *gr02* and WT *B. minutum* were imaged in the same position on day 14, 15, and 16 post-inoculation. On day 15 and 16 of proliferation, symbionts appear in previously unoccupied host tissue (Figure 4.3D, top panels). It is unlikely that these symbionts moved through cell-to-cell migration or were produced from inter-cellular division due to the (1) absence of surrounding symbionts available for migration and (2) stability of present symbiont clusters across timepoints. Therefore, the majority of appearing symbionts in these panels likely result from primary infections. Two secondary infections into occupied host cells (Figure 4.3D, top and middle panels) were also observed. Additionally, intracellular symbiont division is observed during proliferation (Figure 4.3D, middle panels), resulting in an expanding symbiont cluster that is maintained during the tracking period. Finally, the loss of symbiont clusters (Figure 4.3D, bottom panels) was observed. Here, two

clusters are observed on days 14 and 15 but are absent from day 16 imaging; the missing clusters were likely expelled into the gastrovascular cavity, as they could not be located in the tissue surrounding the tracked area. It is unlikely that these missing algal clusters were degraded by the host, as we did not observe any visual deterioration in the symbiont cells prior to their disappearance on day 16. Taken together, these results support that new symbiont clusters are most frequently formed by primary infections of unoccupied host cells following possible expulsion into the gastrovascular cavity.

To confirm that symbiont cell-to-cell migration is not responsible for symbiont spread, a hypothetical model depicting the formation of algal clusters was generated to compare frequent migration vs. frequent infection. The patterns of symbiont clusters formed in the frequent cell-to-cell migration model do not match the observed cluster composition in host tissue (Figure 4.2B, Supplementary Figure 4.5). In contrast, the model depicting frequent infection events most closely resembles observed symbiont cluster patterns. While cell-to-cell migration could have occurred, but was not captured during imaging, the model indicates that it is only a minor mechanism in proliferation responsible for local changes in symbiont clusters.

4.4.5 Two Symbiodiniaceae species co-occur in the same host cell across three cnidarians

A wide range of Symbiodiniaceae species can establish symbiotic relationships with cnidarians hosts (Jinkerson et al., 2022; LaJeunesse et al., 2018; Xiang et al., 2013), and in nature multiple Symbiodiniaceae species can co-occur in hosts (McIlroy et al., 2019, 2022; Silverstein et al., 2012; Thornhill et al., 2006). We observed single-species mixed clusters (Figure 4.2C), and now we sought to determine if more than one symbiont species would co-localize within a single host cell. To tackle this question, aposymbiotic Aiptasia were co-inoculated with four pairs of Symbiodiniaceae species including 1) *Cladocopium goreaui* and *gr02*; 2) *Durusdinium trenchii*

and *gr02*; 3) *Symbiodinium necroappetens* and *gr02*; and 4) *Symbiodinium linucheae* and *gr02*. For each symbiont pair, algal cells were observed within the host animal following inoculation as seen in the whole animal bright-field and fluorescence images in Figure 4.4A. Subsequently, the tentacles of Aiptasia associated with mixed symbiont species were dissociated into single-cell suspensions and evaluated for intact host cells (Supplementary Figure 4.6). In the four symbiont pairs tested, the green mutant *gr02* and another Symbiodiniaceae species were observed co-localized, as indicated by the intact cell membrane and the presence of a stained host nucleus (Figure 4.4A).

To further validate the co-localization of Symbiodiniaceae species, we expand to other cnidarians such as the coral *Pseudodiploria strigosa*, a reef building coral in the Caribbean, and the upside-down jellyfish *Cassiopea xamachana*, isolated from the Florida Keys. Aposymbiotic, juvenile *P. strigosa* polyps were co-inoculated with mixed Symbiodiniaceae species: *D. trenchii* and *gr02*. Following inoculation, the two species of Symbiodiniaceae were observed within *P. strigosa* polyp tissue using bright-field and fluorescence microscopy (Figure 4.4C). Green mutant *gr02* and *D. trenchii* associated coral polyps were then dissociated into a single cell suspension (Kirk & Xiang, 2022) where *gr02* and *D. trenchii* were observed co-localized within the same coral host cell (Figure 4.4C). To confirm if our finding holds true in *Cassiopea*, we inoculated aposymbiotic *Cassiopea* polyps with high densities of *gr02*, followed by inoculation of *D. trenchii*. Interestingly, *Cassiopea* metamorphosed from polyps to adult ephyra approximately two weeks after the acquisition of *D. trenchii*. The ephyra associated with *gr02* and *D. trenchii* were dissociated into a single-cell suspension, where *Cassiopea* host cells containing *gr02* and *D. trenchii* concurrently were observed (Figure 4.3B). We demonstrate for the first time that multiple species of Symbiodiniaceae symbionts can co-exist in the same cnidarian host cell.

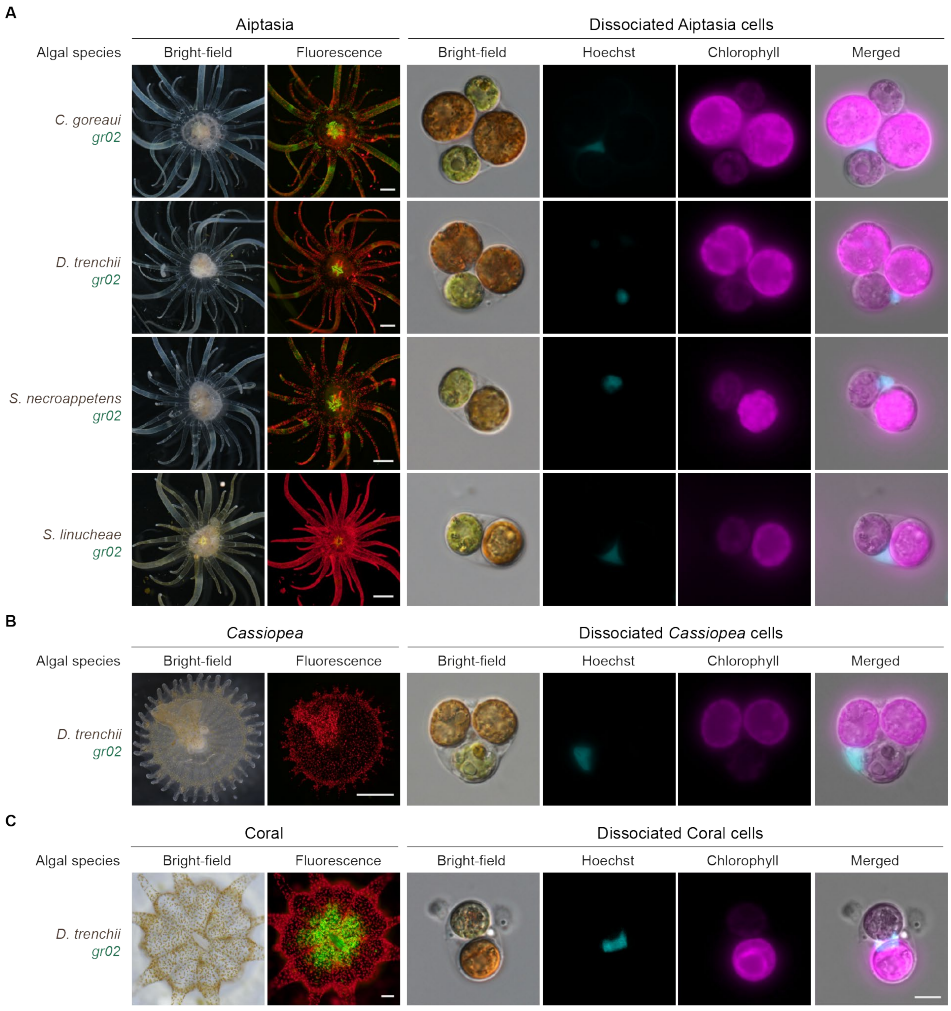

Figure 4.4 Two Symbiodiniaceae species co-exist within single cells of cnidarian hosts. Representative top-down microscopic images of symbiotic (A) sea anemone Aiptasia, (B) jellyfish *Cassiopea xamachana* ephyra, and (C) juvenile coral polyp *Pseudodiploria strigosa* with two co-occurring Symbiodiniaceae species. Top panels show four pairs of Symbiodiniaceae associated with Aiptasia including *Breviolum minutum* green mutant *gr02* and *Cladocopium goreaui* strain LHI-33; *gr02* and *Durusdinium trenchii* strain CCMP-2556, *gr02* and *Symbiodinium necroappetens* strain SSA02; *gr02* and *Symbiodinium linucheae* strain SSA01. Red, algal chlorophyll fluorescence. Scale bars represent 1 mm for Aiptasia, 1 mm for *Cassiopea*, and 100 µm for Coral respectively (left panels). Representative microscopic images of dissociated Aiptasia, *Cassiopea*, and coral host cells enclosing two species of Symbiodiniaceae algae (right panels), where green cells are *gr02* and brown cells are LHI-33, CCMP-2556, SSA02, or SSA01, respectively. Cyan, cell-permeable Hoechst 33342 fluorescent nucleic acid stain; magenta, algal chlorophyll fluorescence. Scale bars, 5 µm.

4.5 Discussion

In this work, we used the newly generated green mutant *gr02* to investigate the patterns of symbiont proliferation in host tissues during cnidarian-algal symbiosis establishment. We observed that algae are initially engulfed into unoccupied host cells and subsequently proliferate through intracellular symbiont division, and additional primary infection events establish algal cells in new areas of cnidarian host tissue. While secondary infections occurred rarely (Figure 4.3), we discovered cnidarian cells concurrently harboring two Symbiodiniaceae genotypes (Figure 4.2) or two Symbiodiniaceae species (Figure 4.4). These results demonstrate how the green mutant tool can be utilized in uncovering fundamental mechanisms essential to cnidarian-Symbiodiniaceae relationships.

4.5.1 Symbiont proliferation *in hospite* is driven by intercellular division and primary infections of symbionts

Previous studies have suggested that proliferation of symbionts in cnidarian hosts is accomplished through a series of cellular events involving mitotic cell division and symbiont migration (Davy et al., 2012; Tivey et al., 2020, 2022). However, the contributions of the various cellular mechanisms (Figure 4.4A) could not be observed without a means to distinguish between algal cells *in hospite*. With the green mutant *gr02* and WT *B. minutum*, we were able to parse out the details of proliferation within the model host sea anemone Aiptasia. Through simple bright-field and fluorescence microscopy, two symbiont genotypes can easily be distinguished in Aiptasia tissue and monitored across timepoints without needing to sacrifice host animals or sequence symbionts. We demonstrate that algal symbionts are initially acquired through primary infection of unoccupied host gastrodermal cells. The intracellular division of symbionts within the host cytoplasm then produces homogenous clusters of up to six symbionts confirmed within a single

host cell (Figure 4.2). A small proportion of healthy symbionts may then be expelled into the gastrovascular cavity (Davy et al., 2012). Symbionts expelled in host egesta have been shown to maintain their ability to infect host tissues (Maruyama et al., 2022),. This suggests that prior to exiting the host oral cavity, expelled symbionts may first travel through the gastrovascular cavity to previously unoccupied areas of host tissue and subsequently infect host cells. While it is possible that these traveling symbionts will infect a host cell already occupied by an algal symbiont, we discovered that these secondary infections are rare (Supplementary Figure 4.3). This could be due to the high abundance of unoccupied host cells at this stage of symbiosis establishment, resulting in primary infections being most common (Figure 4.3C). It is through this repeated sequence of primary infections, intracellular division, and expulsion into the gastrovascular cavity that symbionts proliferate across the gastrodermal tissue layer in cnidarian hosts.

4.5.2 Symbiodiniaceae species can co-localize in host cells across three cnidarians

Diverse Symbiodiniaceae communities have been shown to proliferate and be maintained within cnidarian host tissues, the composition of which may depend on host-specificity or responses to environmental stress (McIlroy et al., 2019, 2022; Silverstein et al., 2012; Thornhill et al., 2006). Our discovery of two Symbiodiniaceae genotypes co-localized into a single host cell poses interesting possibilities for *in hospite* interactions and competition between symbionts (McIlroy et al., 2019). We found that four pairs of Symbiodiniaceae species not only infect host tissue but also co-localize into host cells. The co-occurrence of Symbiodiniaceae species has implications for how natural symbiont populations in hosts could be achieved. Studies suggest that host-specificity regulates the composition of symbiont species *in hospite* (Gabay et al., 2018, 2019), but our work reveals that symbiont-symbiont direct or indirect interactions within co-occupied host cells or adjacent host cells may play a role in symbiont community dynamics.

As global warming continues to devastate coral reef ecosystems, understanding how symbiont communities are regulated *in hospite* has become increasingly important (Herrera et al., 2021; Howells et al., 2011). Under heat stress, corals and other cnidarians experience bleaching where algal symbionts are lost from host tissues. Symbiont compositions *in hospite* have been shown to shift during heat stress; for instance, the heat-tolerant *Durusdinium trenchii* (Silverstein et al., 2015) often occurs at low levels with heat sensitive Symbiodiniaceae species such as *Cladocopium goreaui* and emerges as the dominant species following bleaching events (Berkelmans & van Oppen, 2006; Silverstein et al., 2015). Our study shows that both heat-tolerant and heat-sensitive Symbiodiniaceae species will co-localize within a single host cell across three cnidarian species. It is unclear how these Symbiodiniaceae species with differing thermotolerances would respond to heat stress within a single host cell, but the green mutant provides an avenue for future research of possible intracellular Symbiodiniaceae interactions within cnidarian hosts.

4.5.3 The green mutant *gr02* is a powerful tool in the study of symbiosis

The generation of Symbiodiniaceae mutants with dysfunctional phenotypes has previously been used to investigate fundamental aspects of cnidarian-Symbiodiniaceae biology (Buerger et al., 2020; Jinkerson et al., 2022). Our study is the first to apply UV mutagenesis techniques to generate a visually distinct Symbiodiniaceae mutant with similar physiology to the WT *B. minutum*. This work establishes the green mutant as a tool for investigating the mechanisms important in cnidarian-Symbiodiniaceae relationships and demonstrates the research applications of mutant Symbiodiniaceae algae. Further generation of Symbiodiniaceae mutants can help researchers to not only understand essential genes for symbiosis but also reveal key steps in other biological mechanisms. For example, the photosynthesis mutant in *B. minutum*, *lbr1*, is a chlorophyll c deficient mutant, leading to the discovery of *CHLOROPHYLL C SYNTHASE*

responsible for chlorophyll c biosynthesis (Jinkerson et al., 2024). Here, we discovered that the bright green color exhibited by the green mutant *gr02*, is due to the absence of the carotenoid peridinin (Figure 4.1, Supplementary Figure 4.1). The green mutant therefore provides an interesting opportunity for future research into the peridinin biosynthesis pathway important for the development of new drugs and cosmetics (Oliveira et al., 2022).

4.6 Conclusion

In our work we provide an in-depth analysis of the cellular events during symbiont proliferation in cnidarian-Symbiodiniaceae symbiosis. We demonstrate that a cycle of primary infection and intracellular division is responsible for the growth and spread of symbionts in cnidarian hosts, and we show that symbiont cells can be found closely associated in host tissues regardless of species. Additional research is needed to determine the extent to which the host cell provides a niche for symbiont competition. With the green mutant, these and other foundational questions regarding symbiosis can be answered.

4.7 Chapter 4: Acknowledgements

I would like to thank Dr. Tingting Xiang for her significant contributions to this chapter: conceptualization, experimental design, completion of experiments, chapter revisions, and guidance in manuscript preparation. I also would like to extend my gratitude to Dr. Robert Jinkerson and Joseph Russo for their help in conceptualization, experimental design, data analysis, and manuscript preparation. Appreciation also goes to Dr. Jinkerson for the model provided in Supplementary Figure 4.5 and Joseph Russo for the generation of the green mutant, *gr02*, and his help with experiments for this project. I would like to specifically thank Tori Stoenner for her

animal husbandry, inoculations of *Cassiopea*, and microscopic top-down images of *Cassiopea* polyps. Special thanks to the Baker lab at the University of Miami, notably Emily Yeager and Andrew Baker, for the coral larvae used in this chapter. Thanks to Dr. Johan Andersen-Ranberg at the University of Copenhagen for his analysis of pigments from the green mutant by UHPLC.

4.8 Chapter 4 Supplementary Figures and Tables

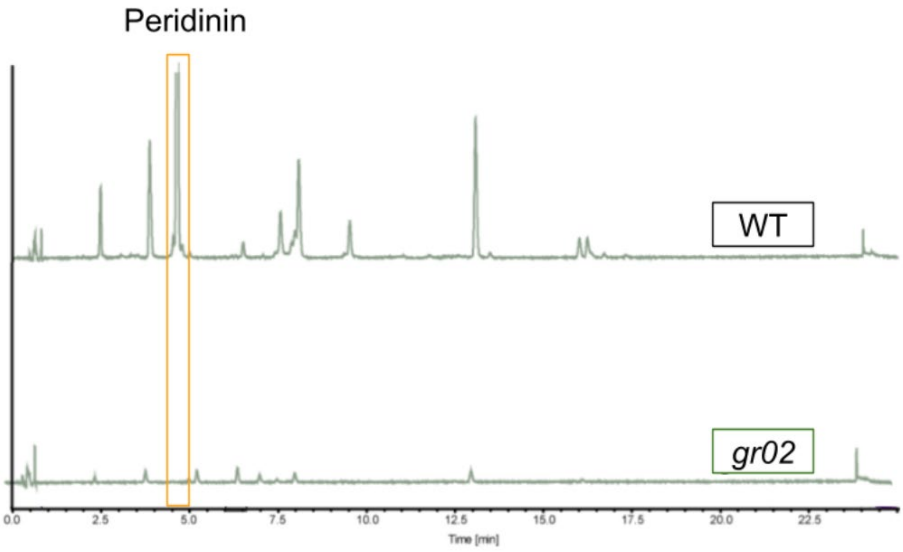

Supplemental Figure 4.1 UHPLC Chromatogram analyses of pigment extracts from WT *B. minutum* and green mutant *gr02* completed by Dr. Andersen-Ranberg.

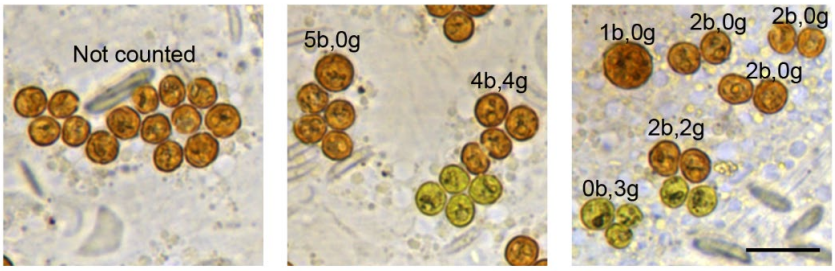

Supplemental Figure 4.2 Representative microscopic images depicting example Symbiodiniaceae algal clusters WT *B. minutum* and green mutant *gr02* for quantification. Scale bar, 20 µm.

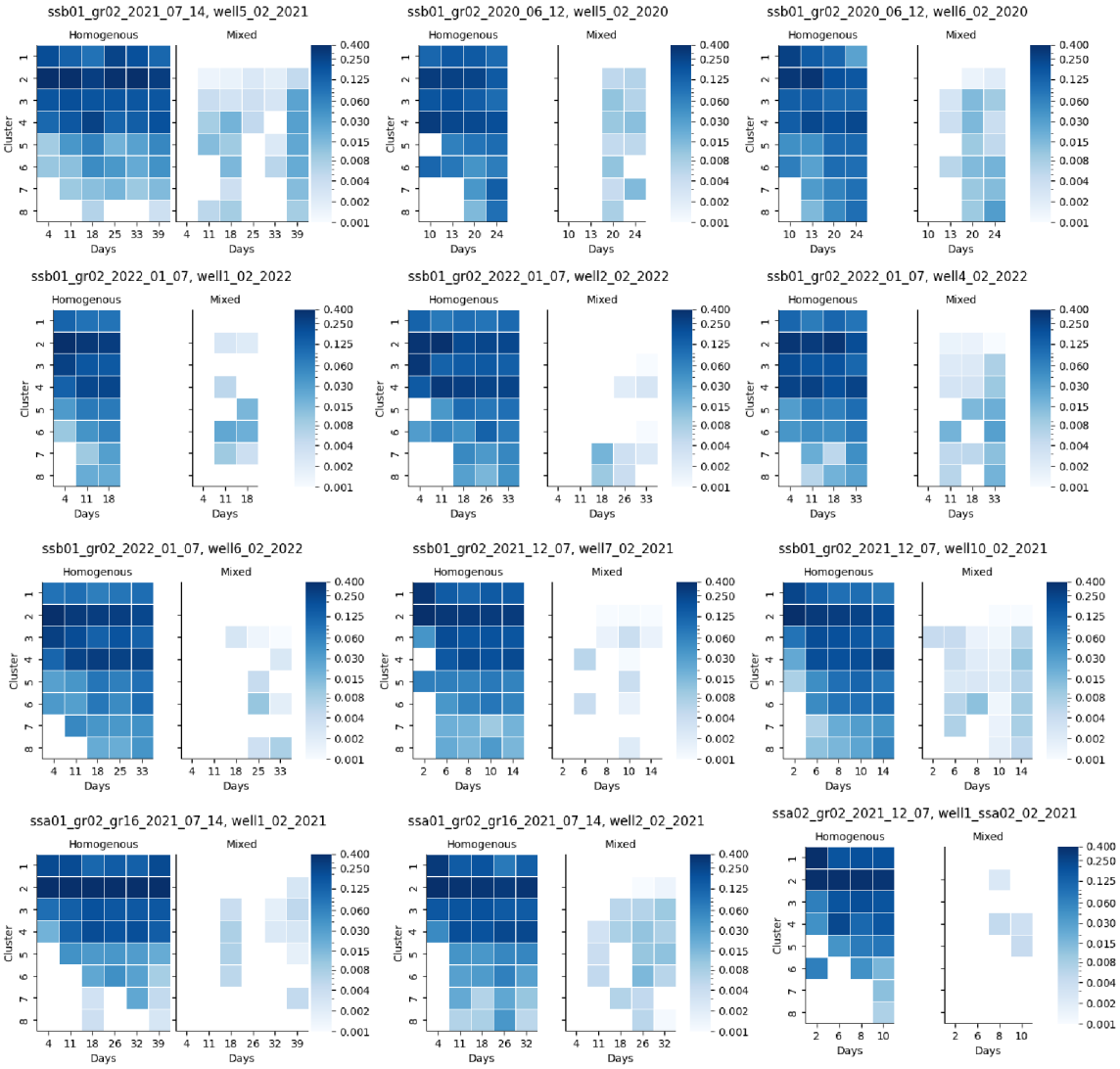

Supplemental Figure 4.3 Heatmaps representing the percent abundance of Symbiodiniaceae cells associated with homogenous or mixed algal clusters *in hospite* of Aiptasia across three pairs of Symbiodiniaceae: WT *B. minutum* (SSB01) and *gr02*; *S. necroappetens* (SSA02) and *gr02*; and 4) *Symbiodinium linucheae* (SSA01) and *gr02*.

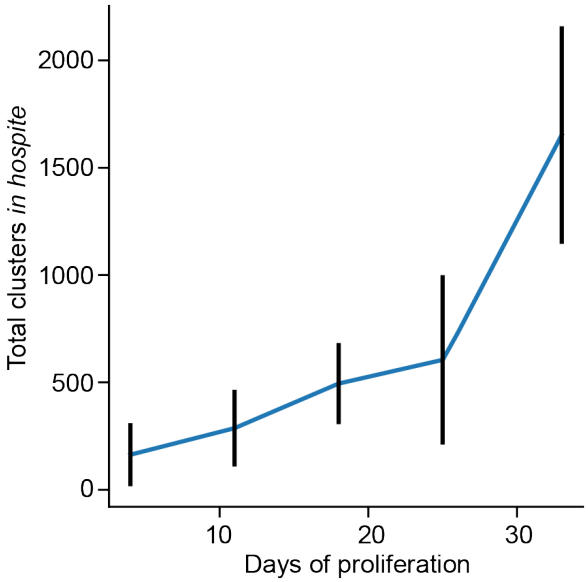

Supplemental Figure 4.4 Line plot depicting the total clusters of Symbiodiniaceae algae (y-axis) over the days of proliferation (x-axis) in Aiptasia associated with WT *B. minutum* and *gr02* across 5 biological replicates. Error bars represent +/- standard deviation.

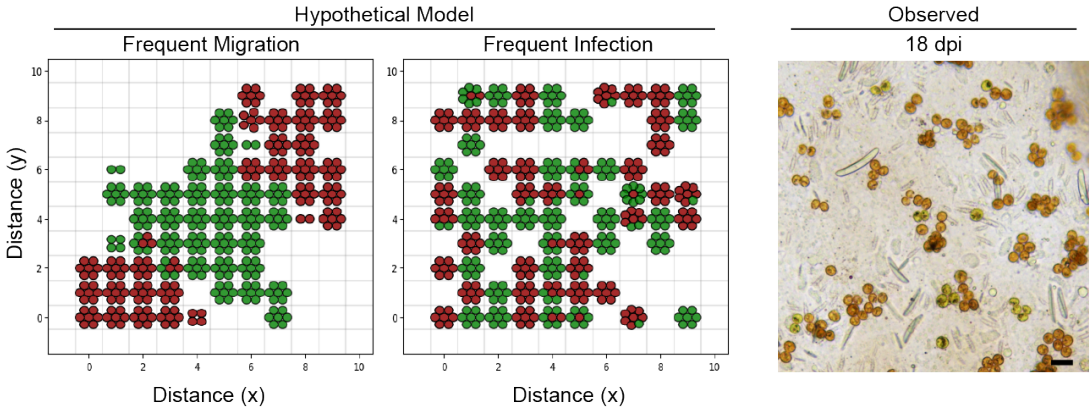

Supplemental Figure 4.5 Hypothetical model and observed cluster patterns during symbiont proliferation.

Model depicting proliferation from frequent migration (migration 1%, infection 0.01%, left panel) or frequent infection (migration 0.01%, infection 1%, middle panel) are shown. Right panel shows a representative microscopic image of an Aiptasia tentacle 18 days post-inoculation with WT *B. minutum* and *gr02*. Scale bar, 20 µm. This model was kindly provided by Robert Jinkerson at UC Riverside.

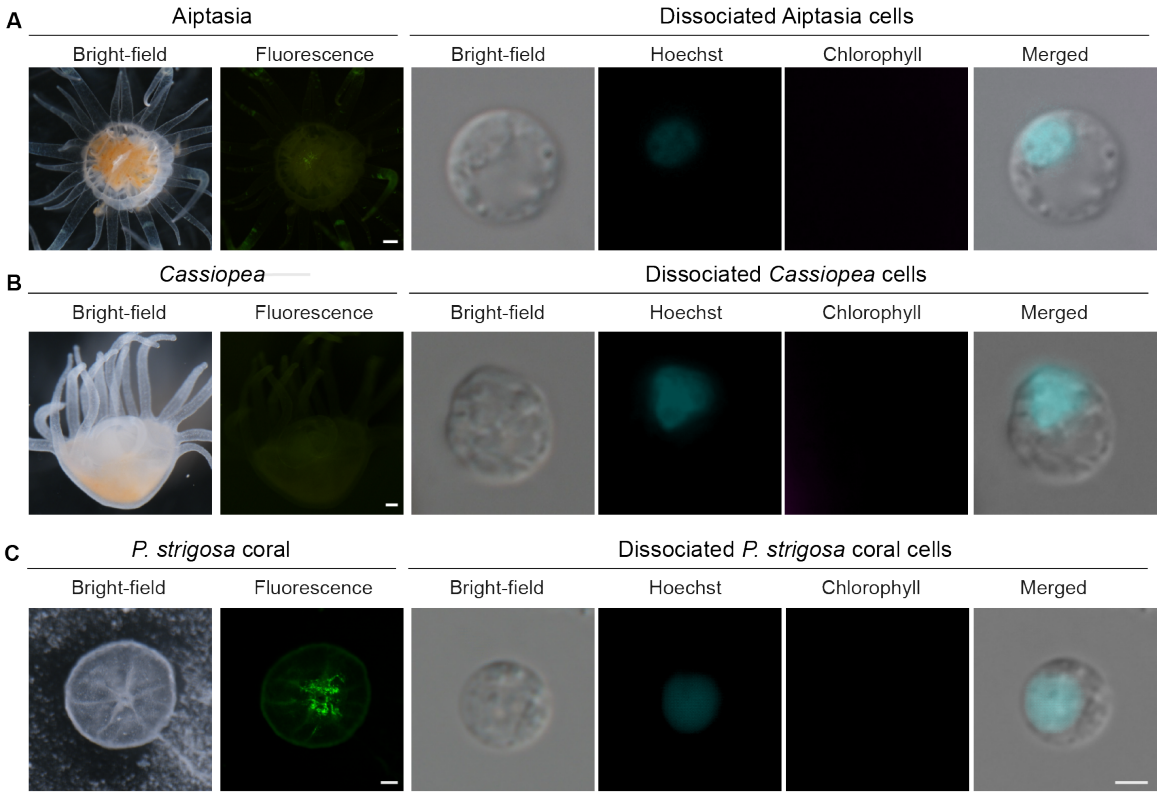

Supplemental Figure 4.6 Algae-free Aiptasia, *Cassiopea*, and *P. strigosa* animals and dissociated cells.

Representative top-down bright-field and chlorophyll fluorescence microscopic images of aposymbiotic (A) sea anemone *Exaiptasia diaphana* (Aiptasia), scale bar, 500µm; (B*) Cassiopea xamachana* (*Cassiopea*), scale bar 100µm; and (C) coral *Pseudodiploria strigosa*, scale bar 100µm. Representative microscopic images of dissociated single cells (right panels) from Aiptasia, *Cassiopea*, and coral. Cyan, cell-permeable Hoechst 33342 fluorescent nucleic acid stain; magenta, algal chlorophyll fluorescence. Scale bar, 2µm.

CHAPTER 5: FUTURE DIRECTIONS

In this dissertation, I used a variety of *in vitro* and *in hospite* analyses to investigate cnidarian-Symbiodiniaceae symbiosis. In chapter two, *Breviolum minutum* was shown to have significant transcriptome reprogramming with organic nutrient supplementation *in vitro*, shedding light on the trophic shifts that Symbiodiniaceae algae may experience during symbiosis establishment (Kirk et al., 2020). In chapter three, I established a single-cell dissociation protocol, effective for the analysis of symbiotic and symbiont-free adult Aiptasia cells (Kirk & Xiang, 2022). With this protocol the cellular localization of photosynthesis mutant *ora1* was determined, and it was concluded that photosynthesis is not required for symbiosis establishment (Jinkerson et al., 2022). Finally, in chapter four, I characterized the newly generated green mutant *gr02* and completed co-inoculations with WT *B. minutum* and other Symbiodiniaceae species to analyze infection and proliferation mechanisms in cnidarian-Symbiodiniaceae symbiosis.

Symbiodiniaceae physiology is an important component in the establishment of a healthy symbiosis (Kishimoto et al., 2020; Wood-Charlson et al., 2006; Xiang et al., 2018). It has been difficult to determine the physiological and molecular responses of the diverse Symbiodiniaceae species due to the presence of bacteria and other contaminants in some species isolates. The isolation of clonal, axenic strains of Symbiodiniaceae allows for comparative analysis of characteristics in controlled trophic conditions as shown in chapter two (Kirk et al., 2020). Other studies have shown the free-living Symbiodiniaceae (strain SSE01) grows best in photoautotrophic conditions while symbiotic species (strains SSB01 and SSA02) grows best in heterotrophic conditions (Xiang et al., 2013). These differences in metabolic strategies observed among Symbiodiniaceae species has implications for the evolution of cnidarian-Symbiodiniaceae symbiosis and how the relationship will respond to ongoing environmental perturbations.

Currently there are limited strains of Symbiodiniaceae that have been isolated and cultured axenically (Bieri et al., 2016; LaJeunesse, 2001; Parkinson et al., 2015; Santos et al., 2001; Steinke et al., 2011; Xiang et al., 2013) out of the many species identified (LaJeunesse et al., 2018). Continued isolation of clonal, axenic strains of Symbiodiniaceae would benefit the field of cnidarian-Symbiodiniaceae symbiosis by improving our understanding of Symbiodiniaceae diversity and physiology *in vitro* and *in hospite*.

The Aiptasia-Symbiodiniaceae model system has proven invaluable to the study of cnidarian-Symbiodiniaceae symbiosis (Bucher et al., 2016; Burriesci et al., 2012; Kishimoto et al., 2020; Xiang et al., 2020). With an available transcriptome and genome assembly (Baumgarten et al., 2015; Lehnert et al., 2012), essential mechanisms associated with symbiosis can be investigated in Aiptasia. In an effort to enhance the tools available in the Aiptasia-Symbiodiniaceae model system, I developed the first single-cell dissociation protocol for adult Aiptasia in chapter three (Kirk & Xiang, 2022), where both symbiotic and aposymbiotic anemones and coral polyps can be processed. As in other biological systems (Bawa et al., 2022; McNulty et al., 2023; Tang et al., 2009), single-cell analysis of the Aiptasia-Symbiodiniaceae system may reveal key insights into fundamental mechanisms essential to symbiosis. Future research analyzing the multiple tissue types in Aiptasia (Figure 1.1) using single cell RNA-seq may give insights into the unique features of gastrodermal cells that support symbionts. Additional efforts to culture isolated single cells of Aiptasia would further expand the toolkit available to researchers. Cultured tissues and cells have proven useful biological research (Segeritz & Vallier, 2017), and cultured Aiptasia cells would allow for high-throughput, reproducible assays of cnidarian tissue types, including symbiotic and symbiont-free host cells. The optimization of cellular biological techniques is therefore essential to the study of cnidarian-Symbiodiniaceae symbiosis.

The composition of Symbiodiniaceae communities in cnidarian hosts has been challenging to investigate due to the similar appearance of Symbiodiniaceae genotypes and species *in hospite*. In chapter four, I introduce the green mutant *gr02* that makes possible the visual distinction of Symbiodiniaceae species in host tissue. In this work, I highlight the proliferation mechanisms of WT *B. minutum* and green mutant *gr02* in Aiptasia. Future research using the Aiptasia-*gr02* model system could shed light on species-specific symbiont proliferation patterns in cnidarian-Symbiodiniaceae symbiosis. Additional experiments using co-infections of green mutant *gr02* with various Symbiodiniaceae species in Aiptasia could be completed to compare how symbiont composition impacts the symbiont proliferation *in hospite*. This can establish if symbiont species compete within host tissues or if hosts preferentially select for specific Symbiodiniaceae species during the proliferation period. Further research into symbiosis breakdown could also be accomplished with the Aiptasia-*gr02* system or through the generation of other Symbiodiniaceae mutants. For instance, the heat tolerant *D. trenchii* and *gr02* were shown to co-occur in cnidarian hosts. Observing how the *in hospite* symbiont cluster patterns of these two co-occurring symbionts shift during temperature stress may reveal if symbionts are selectively expelled from host tissue during heat stress events. Other research has attempted to generate heat tolerant Symbiodiniaceae mutants to aid in coral reef recovery (Buerger et al., 2020). UV mutagenesis, as described in chapter three and four, may also provide a means to generate resilient symbiont strains. In summary, additional investigations utilizing the green mutant and the generation of a Symbiodiniaceae mutant library would allow researchers to answer fundamental questions about symbiosis and guide efforts to bioengineer a thermally tolerant symbiosis.

5.1 Overall Conclusions

Coral reefs are dramatically declining in the face of anthropogenic climate change. Rising sea surface temperatures have resulted in the breakdown of symbiosis in reefs around the globe, causing a decline in bio-productivity of these marine ecosystems (Hoegh-Guldberg, 1999; Hoegh-Guldberg & Ormond, 2018; Hughes et al., 2018). The foundation of coral reefs is the symbiosis between cnidarian hosts and Symbiodiniaceae algae, but many questions still remain surrounding the basic biology of this relationship (Weis, 2019). With my work, I have contributed to the basic understanding of cnidarian-Symbiodiniaceae symbiosis through cellular biological protocols and analyses (Jinkerson et al., 2022; Kirk et al., 2020; Kirk & Xiang, 2022). I have provided a better understanding of symbiont trophic transitions, giving insight into how symbionts may respond to the nutritional environments they encounter when free-living and in symbiosis. I also developed the first single-cell dissociation protocol for adult Aiptasia, broadening the cellular biological techniques available in the Aiptasia-Symbiodiniaceae model system. Finally, I utilized some of the first Symbiodiniaceae mutants to be created with UV mutagenesis to elucidate the mechanisms of symbiont infection and proliferation. With this work, I established that symbionts proliferate throughout host tissue via a series of primary infections and intracellular divisions. I also present the first evidence of two Symbiodiniaceae species co-occurring within a cnidarian host cell, which has broad implications for symbiont communities in host tissues. The accumulation of my contributions increases our knowledge of cnidarian-Symbiodiniaceae symbiosis and can aid researchers and conservationists to develop effective solutions to mitigate further coral reef decline.

REFERENCES

Ahmad, M., Xue, Y., Lee, S. K., Martindale, J. L., Shen, W., Li, W., Zou, S., Ciaramella, M., Debat, H., Nadal, M., Leng, F., Zhang, H., Wang, Q., Siaw, G. E.-L., Niu, H., Pommier, Y., Gorospe, M., Hsieh, T.-S., Tse-Dinh, Y.-C., … Wang, W. (2016). RNA topoisomerase is prevalent in all domains of life and associates with polyribosomes in animals. *Nucleic Acids Research*, *44*(13), 6335–6349. https://doi.org/10.1093/nar/gkw508

Anthony, C. J., Lock, C., & Bentlage, B. (2023). Rapid, high-throughput phenotypic profiling of endosymbiotic dinoflagellates (Symbiodiniaceae) using benchtop flow cytometry. In *bioRxiv* (p. 2022.12.06.519248). https://doi.org/10.1101/2022.12.06.519248

Baghdasarian, G., & Muscatine, L. (2000). Preferential expulsion of dividing algal cells as a mechanism for regulating algal-cnidarian symbiosis. *The Biological Bulletin*, *199*(3), 278–286. https://doi.org/10.2307/1543184

Baird, A. H., & Marshall, P. A. (2002). Mortality, growth and reproduction in scleractinian corals following bleaching on the Great Barrier Reef. *Marine Ecology Progress Series*, *237*, 133–141. https://doi.org/10.3354/meps237133

Bai, Y., Cao, T., Dautermann, O., Buschbeck, P., Cantrell, M. B., Chen, Y., Lein, C. D., Shi, X., Ware, M. A., Yang, F., Zhang, H., Zhang, L., Peers, G., Li, X., & Lohr, M. (2022). Green diatom mutants reveal an intricate biosynthetic pathway of fucoxanthin. *Proceedings of the National Academy of Sciences of the United States of America*, *119*(38), e2203708119. https://doi.org/10.1073/pnas.2203708119

Baker, A. C. (2003). Flexibility and Specificity in Coral-Algal Symbiosis: Diversity, Ecology, and Biogeography of Symbiodinium. *Annual Review of Ecology, Evolution, and Systematics*, *34*, 661–689. http://www.jstor.org/stable/30033790

Barott, K. L., Venn, A. A., Perez, S. O., Tambutté, S., & Tresguerres, M. (2015). Coral host cells acidify symbiotic algal microenvironment to promote photosynthesis. *Proceedings of the National Academy of Sciences of the United States of America*, *112*(2), 607–612. https://doi.org/10.1073/pnas.1413483112

Baumgarten, S., Simakov, O., Esherick, L. Y., Liew, Y. J., Lehnert, E. M., Michell, C. T., Li, Y., Hambleton, E. A., Guse, A., Oates, M. E., Gough, J., Weis, V. M., Aranda, M., Pringle, J. R., & Voolstra, C. R. (2015). The genome of Aiptasia, a sea anemone model for coral symbiosis. *Proceedings of the National Academy of Sciences of the United States of America*, *112*(38), 11893–11898. https://doi.org/10.1073/pnas.1513318112

Bawa, G., Liu, Z., Yu, X., Qin, A., & Sun, X. (2022). Single-Cell RNA Sequencing for Plant Research: Insights and Possible Benefits. *International Journal of Molecular Sciences*, *23*(9). https://doi.org/10.3390/ijms23094497

Berkelmans, R., & van Oppen, M. J. H. (2006). The role of zooxanthellae in the thermal tolerance of corals: a "nugget of hope" for coral reefs in an era of climate change. *Proceedings of the Royal Society B: Biological Sciences*, *273*(1599), 2305–2312. https://doi.org/10.1098/rspb.2006.3567

Bieri, T., Onishi, M., Xiang, T., Grossman, A. R., & Pringle, J. R. (2016). Relative Contributions of Various Cellular Mechanisms to Loss of Algae during Cnidarian Bleaching. *PloS One*, *11*(4), e0152693. https://doi.org/10.1371/journal.pone.0152693

Black, B. E., Jansen, L. E. T., Maddox, P. S., Foltz, D. R., Desai, A. B., Shah, J. V., & Cleveland, D. W. (2007). Centromere identity maintained by nucleosomes assembled with histone H3 containing the CENP-A targeting domain. *Molecular Cell*, *25*(2), 309–322. https://doi.org/10.1016/j.molcel.2006.12.018

Brading, P., Warner, M. E., Smith, D. J., & Suggett, D. J. (2013). Contrasting modes of inorganic carbon acquisition amongst Symbiodinium (Dinophyceae) phylotypes. *The New Phytologist*, *200*(2), 432–442. https://doi.org/10.1111/nph.12379

Brown, B. E., & Bythell, J. C. (2005). Perspectives on mucus secretion in reef corals. *Marine Ecology Progress Series*, *296*, 291–309. https://doi.org/10.3354/meps296291

Bucher, M., Wolfowicz, I., Voss, P. A., Hambleton, E. A., & Guse, A. (2016). Development and Symbiosis Establishment in the Cnidarian Endosymbiosis Model Aiptasia sp. *Scientific Reports*, *6*, 19867. https://doi.org/10.1038/srep19867

Buerger, P., Alvarez-Roa, C., Coppin, C. W., Pearce, S. L., Chakravarti, L. J., Oakeshott, J. G., Edwards, O. R., & van Oppen, M. J. H. (2020). Heat-evolved microalgal symbionts increase coral bleaching tolerance. *Science Advances*, *6*(20), eaba2498. https://doi.org/10.1126/sciadv.aba2498

Burriesci, M. S., Raab, T. K., & Pringle, J. R. (2012). Evidence that glucose is the major transferred metabolite in dinoflagellate-cnidarian symbiosis. *The Journal of Experimental Biology*, *215*(Pt 19), 3467–3477. https://doi.org/10.1242/jeb.070946

Camaya, A. P. (2020). Stages of the symbiotic zooxanthellae–host cell division and the dynamic role of coral nucleus in the partitioning process: a novel observation elucidated by electron microscopy. *Coral Reefs* , *39*(4), 929–938. https://doi.org/10.1007/s00338-020-01912-y

Carbonera, D., Di Valentin, M., Spezia, R., & Mezzetti, A. (2014). The Unique Photophysical Properties of the Peridinin-Chlorophyll-a-Protein. *Current Protein & Peptide Science*, *15*(4), 332–350. https://www.ingentaconnect.com/content/ben/cpps/2014/00000015/00000004/art00004

Carucci, D. J., Witney, A. A., Muhia, D. K., Warhurst, D. C., Schaap, P., Meima, M., Li, J. L.,

Taylor, M. C., Kelly, J. M., & Baker, D. A. (2000). Guanylyl cyclase activity associated with putative bifunctional integral membrane proteins in Plasmodium falciparum. *The Journal of Biological Chemistry*, *275*(29), 22147–22156. https://doi.org/10.1074/jbc.M001021200

Castilho, B. A., Shanmugam, R., Silva, R. C., Ramesh, R., Himme, B. M., & Sattlegger, E. (2014). Keeping the eIF2 alpha kinase Gcn2 in check. *Biochimica et Biophysica Acta*, *1843*(9), 1948–1968. https://doi.org/10.1016/j.bbamcr.2014.04.006

Champoux, J. J. (2001). DNA Topoisomerases: Structure, Function, and Mechanism. *Annual Review of Biochemistry*, *70*(1), 369–413. https://doi.org/10.1146/annurev.biochem.70.1.369

Chen, J. E., Barbrook, A. C., Cui, G., Howe, C. J., & Aranda, M. (2019). The genetic intractability of Symbiodinium microadriaticum to standard algal transformation methods. *PloS One*, *14*(2), e0211936. https://doi.org/10.1371/journal.pone.0211936

Conti-Jerpe, I. E., Thompson, P. D., Wong, C. W. M., Oliveira, N. L., Duprey, N. N., Moynihan, M. A., & Baker, D. M. (2020). Trophic strategy and bleaching resistance in reef-building corals. *Science Advances*, *6*(15), eaaz5443. https://doi.org/10.1126/sciadv.aaz5443

Cook, C. B., & D'elia, C. F. (1987). Are natural populations of zooxanthellae ever nutrient-limited? *Symbiosis* . https://dalspace.library.dal.ca/bitstream/handle/10222/76973/VOLUME%204-NUMBERS%201-2-3-1987-PAGE%20199.pdf?sequence=1

Cresswell, A. K., Thomson, D. P., Trevenen, E. J., & Renton, M. (2017). A functional-structural coral model. *Proceedings of the 22nd International Congress on Modelling and Simulation*, 1–7. https://www.researchgate.net/profile/Anna-Cresswell/publication/321569815_A_functional-structural_coral_model/links/5a2750d5a6fdcc8e866e601b/A-functional-structural-coral-

model.pdf

Cui, G., Liew, Y. J., Konciute, M. K., Zhan, Y., Hung, S.-H., Thistle, J., Gastoldi, L., Schmidt-Roach, S., Dekker, J., & Aranda, M. (2022). Nutritional control regulates symbiont proliferation and life history in coral-dinoflagellate symbiosis. *BMC Biology*, *20*(1), 103. https://doi.org/10.1186/s12915-022-01306-2

Cui, G., Liew, Y. J., Li, Y., Kharbatia, N., Zahran, N. I., Emwas, A.-H., Eguiluz, V. M., & Aranda, M. (2019). Host-dependent nitrogen recycling as a mechanism of symbiont control in Aiptasia. *PLoS Genetics*, *15*(6), e1008189. https://doi.org/10.1371/journal.pgen.1008189

Cunning, R., & Baker, A. C. (2020). Thermotolerant coral symbionts modulate heat stress-responsive genes in their hosts. *Molecular Ecology*, *29*(15), 2940–2950. https://doi.org/10.1111/mec.15526

Dagenais-Bellefeuille, S., & Morse, D. (2013). Putting the N in dinoflagellates. *Frontiers in Microbiology*, *4*, 369. https://doi.org/10.3389/fmicb.2013.00369

Dautermann, O., Lyska, D., Andersen-Ranberg, J., Becker, M., Fröhlich-Nowoisky, J., Gartmann, H., Krämer, L. C., Mayr, K., Pieper, D., Rij, L. M., M.-L. Wipf, H., Niyogi, K. K., & Lohr, M. (2020). An algal enzyme required for biosynthesis of the most abundant marine carotenoids. In *Science Advances* (Vol. 6, Issue 10). https://doi.org/10.1126/sciadv.aaw9183

Davy, S. K., Allemand, D., & Weis, V. M. (2012). Cell biology of cnidarian-dinoflagellate symbiosis. *Microbiology and Molecular Biology Reviews: MMBR*, *76*(2), 229–261. https://doi.org/10.1128/MMBR.05014-11

D'Elia, C. F., Domotor, S. L., & Webb, K. L. (1983). Nutrient uptake kinetics of freshly isolated zooxanthellae. *Marine Biology*, *75*(2), 157–167. https://doi.org/10.1007/BF00405998

Demidchik, V., Shabala, S., Isayenkov, S., Cuin, T. A., & Pottosin, I. (2018). Calcium transport

across plant membranes: mechanisms and functions. *The New Phytologist*, *220*(1), 49–69. https://doi.org/10.1111/nph.15266

Edgar, R. C. (2004). MUSCLE: a multiple sequence alignment method with reduced time and space complexity. *BMC Bioinformatics*, *5*, 113. https://doi.org/10.1186/1471-2105-5-113

Falkowski, P. G., Dubinsky, Z., Muscatine, L., & McCloskey, L. (1993). Population Control in Symbiotic Corals. *Bioscience*, *43*(9), 606–611. https://doi.org/10.2307/1312147

Falkowski, P. G., Dubinsky, Z., Muscatine, L., & Porter, J. W. (1984). Light and the Bioenergetics of a Symbiotic Coral. *Bioscience*, *34*(11), 705–709. https://doi.org/10.2307/1309663

Foo, S. A., Liddell, L., Grossman, A., & Caldeira, K. (2020). Photo-movement in the sea anemone Aiptasia influenced by light quality and symbiotic association. *Coral Reefs* , *39*(1), 47–54. https://doi.org/10.1007/s00338-019-01866-w

Fox, M. D., Elliott Smith, E. A., Smith, J. E., & Newsome, S. D. (2019). Trophic plasticity in a common reef-building coral: Insights from δ13C analysis of essential amino acids. *Functional Ecology*, *33*(11), 2203–2214. https://doi.org/10.1111/1365-2435.13441

Fransolet, D., Roberty, S., & Plumier, J.-C. (2012). Establishment of endosymbiosis: The case of cnidarians and Symbiodinium. *Journal of Experimental Marine Biology and Ecology*, *420-421*, 1–7. https://doi.org/10.1016/j.jembe.2012.03.015

Fransolet, D., Roberty, S., & Plumier, J.-C. (2014). Impairment of symbiont photosynthesis increases host cell proliferation in the epidermis of the sea anemone Aiptasia pallida. *Marine Biology*, *161*(8), 1735–1743. https://doi.org/10.1007/s00227-014-2455-1

Gabay, Y., Parkinson, J. E., Wilkinson, S. P., Weis, V. M., & Davy, S. K. (2019). Inter-partner specificity limits the acquisition of thermotolerant symbionts in a model cnidarian-dinoflagellate symbiosis. *The ISME Journal*, *13*(10), 2489–2499.

https://doi.org/10.1038/s41396-019-0429-5

Gabay, Y., Weis, V. M., & Davy, S. K. (2018). Symbiont Identity Influences Patterns of Symbiosis Establishment, Host Growth, and Asexual Reproduction in a Model Cnidarian-Dinoflagellate Symbiosis. *The Biological Bulletin*, *234*(1), 1–10. https://doi.org/10.1086/696365

Gierz, S. L., Gordon, B. R., & Leggat, W. (2016). Integral Light-Harvesting Complex Expression In Symbiodinium Within The Coral Acropora aspera Under Thermal Stress. *Scientific Reports*, *6*, 25081. https://doi.org/10.1038/srep25081

Gornik, S. G., Ford, K. L., Mulhern, T. D., Bacic, A., McFadden, G. I., & Waller, R. F. (2012). Loss of nucleosomal DNA condensation coincides with appearance of a novel nuclear protein in dinoflagellates. *Current Biology: CB*, *22*(24), 2303–2312. https://doi.org/10.1016/j.cub.2012.10.036

Graham, E. M., Baird, A. H., Connolly, S. R., Sewell, M. A., & Willis, B. L. (2013). Rapid declines in metabolism explain extended coral larval longevity. *Coral Reefs* , *32*(2), 539–549. https://doi.org/10.1007/s00338-012-0999-4

Gregio, A. P. B., Cano, V. P. S., Avaca, J. S., Valentini, S. R., & Zanelli, C. F. (2009). eIF5A has a function in the elongation step of translation in yeast. *Biochemical and Biophysical Research Communications*, *380*(4), 785–790. https://doi.org/10.1016/j.bbrc.2009.01.148

Hambleton, E. A., Guse, A., & Pringle, J. R. (2014). Similar specificities of symbiont uptake by adults and larvae in an anemone model system for coral biology. *The Journal of Experimental Biology*, *217*(Pt 9), 1613–1619. https://doi.org/10.1242/jeb.095679

Harii, S., Nadaoka, K., Yamamoto, M., & Iwao, K. (2007). Temporal changes in settlement, lipid content and lipid composition of larvae of the spawning hermatypic coral Acropora tenuis.

Marine Ecology Progress Series, *346*, 89–96. https://doi.org/10.3354/meps07114

Hartung, F., Suer, S., Knoll, A., Wurz-Wildersinn, R., & Puchta, H. (2008). Topoisomerase 3alpha and RMI1 suppress somatic crossovers and are essential for resolution of meiotic recombination intermediates in Arabidopsis thaliana. *PLoS Genetics*, *4*(12), e1000285. https://doi.org/10.1371/journal.pgen.1000285

Harvey, S. H., Krien, M. J. E., & O'Connell, M. J. (2002). Structural maintenance of chromosomes (SMC) proteins, a family of conserved ATPases. *Genome Biology*, *3*(2), REVIEWS3003. https://doi.org/10.1186/gb-2002-3-2-reviews3003

Henderson, A., & Hershey, J. W. (2011). Eukaryotic translation initiation factor (eIF) 5A stimulates protein synthesis in Saccharomyces cerevisiae. In *Proceedings of the National Academy of Sciences* (Vol. 108, Issue 16, pp. 6415–6419). https://doi.org/10.1073/pnas.1008150108

Herre, E. A., Knowlton, N., Mueller, U. G., & Rehner, S. A. (1999). The evolution of mutualisms: exploring the paths between conflict and cooperation. *Trends in Ecology & Evolution*, *14*(2), 49–53. https://doi.org/10.1016/s0169-5347(98)01529-8

Herrera, M., Klein, S. G., Campana, S., Chen, J. E., Prasanna, A., Duarte, C. M., & Aranda, M. (2021). Temperature transcends partner specificity in the symbiosis establishment of a cnidarian. *The ISME Journal*, *15*(1), 141–153. https://doi.org/10.1038/s41396-020-00768-y

Hirano, T. (2002). The ABCs of SMC proteins: two-armed ATPases for chromosome condensation, cohesion, and repair. *Genes & Development*, *16*(4), 399–414. https://doi.org/10.1101/gad.955102

Hirokawa, N., Noda, Y., Tanaka, Y., & Niwa, S. (2009). Kinesin superfamily motor proteins and intracellular transport. *Nature Reviews. Molecular Cell Biology*, *10*(10), 682–696. https://doi.org/10.1038/nrm2774

Hoegh-Guldberg, O. (1999). Climate change, coral bleaching and the future of the world's coral reefs. *Marine and Freshwater Research*, *50*(8), 839–866. https://doi.org/10.1071/mf99078

Hoegh-Guldberg, O. (2011). The Impact of Climate Change on Coral Reef Ecosystems. In Z. Dubinsky & N. Stambler (Eds.), *Coral Reefs: An Ecosystem in Transition* (pp. 391–403). Springer Netherlands. https://doi.org/10.1007/978-94-007-0114-4_22

Hoegh-Guldberg, O., McCloskey, L. R., & Muscatine, L. (1987). Expulsion of zooxanthellae by symbiotic cnidarians from the Red Sea. *Coral Reefs* , *5*(4), 201–204. https://doi.org/10.1007/BF00300964

Hoegh-Guldberg, O., & Ormond, R. (2018). Consensus statement on coral bleaching climate change. *International Coral Reef Society*.

Hoegh-Guldberg, O., Poloczanska, E. S., Skirving, W., & Dove, S. (2017). Coral Reef Ecosystems under Climate Change and Ocean Acidification. *Frontiers in Marine Science*, *4*, 321. https://doi.org/10.3389/fmars.2017.00158

Howells, E. J., Beltran, V. H., Larsen, N. W., Bay, L. K., Willis, B. L., & van Oppen, M. J. H. (2011). Coral thermal tolerance shaped by local adaptation of photosymbionts. *Nature Climate Change*, *2*(2), 116–120. https://doi.org/10.1038/nclimate1330

Hughes, T. P., Anderson, K. D., Connolly, S. R., Heron, S. F., Kerry, J. T., Lough, J. M., Baird, A. H., Baum, J. K., Berumen, M. L., Bridge, T. C., Claar, D. C., Eakin, C. M., Gilmour, J. P., Graham, N. A. J., Harrison, H., Hobbs, J.-P. A., Hoey, A. S., Hoogenboom, M., Lowe, R. J., … Wilson, S. K. (2018). Spatial and temporal patterns of mass bleaching of corals in the Anthropocene. *Science*, *359*(6371), 80–83. https://doi.org/10.1126/science.aan8048

Hughes, T. P., Kerry, J. T., Álvarez-Noriega, M., Álvarez-Romero, J. G., Anderson, K. D., Baird, A. H., Babcock, R. C., Beger, M., Bellwood, D. R., Berkelmans, R., Bridge, T. C., Butler, I.

R., Byrne, M., Cantin, N. E., Comeau, S., Connolly, S. R., Cumming, G. S., Dalton, S. J., Diaz-Pulido, G., … Wilson, S. K. (2017). Global warming and recurrent mass bleaching of corals. *Nature*, *543*(7645), 373–377. https://doi.org/10.1038/nature21707

Hu, M., Zheng, X., Fan, C.-M., & Zheng, Y. (2020). Lineage dynamics of the endosymbiotic cell type in the soft coral Xenia. *Nature*, *582*(7813), 534–538. https://doi.org/10.1038/s41586-020-2385-7

Imbs, A. B., Yakovleva, I. M., Dautova, T. N., Bui, L. H., & Jones, P. (2014). Diversity of fatty acid composition of symbiotic dinoflagellates in corals: evidence for the transfer of host PUFAs to the symbionts. *Phytochemistry*, *101*, 76–82. https://doi.org/10.1016/j.phytochem.2014.02.012

Iwao, K., Fujisawa, T., & Hatta, M. (2002). A cnidarian neuropeptide of the GLWamide family induces metamorphosis of reef-building corals in the genus Acropora. *Coral Reefs* , *21*(2), 127–129. https://doi.org/10.1007/s00338-002-0219-8

Jacobovitz, M. R., Rupp, S., Voss, P. A., Maegele, I., Gornik, S. G., & Guse, A. (2021). Dinoflagellate symbionts escape vomocytosis by host cell immune suppression. *Nature Microbiology*, *6*(6), 769–782. https://doi.org/10.1038/s41564-021-00897-w

Jeong, H. J., Yoo, Y. D., Kang, N. S., Lim, A. S., Seong, K. A., Lee, S. Y., Lee, M. J., Lee, K. H., Kim, H. S., Shin, W., Nam, S. W., Yih, W., & Lee, K. (2012). Heterotrophic feeding as a newly identified survival strategy of the dinoflagellate Symbiodinium. *Proceedings of the National Academy of Sciences of the United States of America*, *109*(31), 12604–12609. https://doi.org/10.1073/pnas.1204302109

Jiang, P.-L., Pasaribu, B., & Chen, C.-S. (2014). Nitrogen-deprivation elevates lipid levels in Symbiodinium spp. by lipid droplet accumulation: morphological and compositional

analyses. *PloS One*, *9*(1), e87416. https://doi.org/10.1371/journal.pone.0087416

Jinkerson, R. E., Poveda-Huertes, D., Cooney, E. C., Cho, A., Ochoa-Fernandez, R., Keeling, P. J., Xiang, T., & Andersen-Ranberg, J. (2024). Biosynthesis of chlorophyll c in a dinoflagellate and heterologous production in planta. *Current Biology: CB*, *34*(3), 594–605.e4.

Jinkerson, R. E., Russo, J. A., Newkirk, C. R., Kirk, A. L., Chi, R. J., Martindale, M. Q., Grossman, A. R., Hatta, M., & Xiang, T. (2022). Cnidarian-Symbiodiniaceae symbiosis establishment is independent of photosynthesis. *Current Biology: CB*, *32*(11), 2402–2415.e4. https://doi.org/10.1016/j.cub.2022.04.021

Joliot, P., Béal, D., & Delosme, R. (1998). In vivo Measurements of Photosynthetic Activity: Methods. In *The Molecular Biology of Chloroplasts and Mitochondria in Chlamydomonas* (pp. 433–449). https://doi.org/10.1007/0-306-48204-5_22

Joliot, P., & Delosme, R. (1974). Flash-induced 519 nm absorption change in green algae. *Biochimica et Biophysica Acta*, *357*(2), 267–284. https://doi.org/10.1016/0005-2728(74)90066-8

Jones, R. J. (2004). Testing the photoinhibition model of coral bleaching using chemical inhibitors. *Marine Ecology Progress Series*, *284*, 133–145. https://doi.org/10.3354/meps284133

Kampranis, S. C., & Maxwell, A. (1996). Conversion of DNA gyrase into a conventional type II topoisomerase. *Proceedings of the National Academy of Sciences of the United States of America*, *93*(25), 14416–14421. https://doi.org/10.1073/pnas.93.25.14416

Kato, H., Tokutsu, R., Kubota-Kawai, H., Burton-Smith, R. N., Kim, E., & Minagawa, J. (2020). Characterization of a Giant PSI Supercomplex in the Symbiotic Dinoflagellate Symbiodiniaceae. *Plant Physiology*, *183*(4), 1725–1734. https://doi.org/10.1104/pp.20.00726

Kautza, A., Mazeika, S., & Sullivan, P. (2016). The energetic contributions of aquatic primary producers to terrestrial food webs in a mid-size river system. *Ecology*, *97*(3), 694–705. https://doi.org/10.1890/15-1095.1

Kawamura, K., Nishitsuji, K., Shoguchi, E., Fujiwara, S., & Satoh, N. (2021). Establishing Sustainable Cell Lines of a Coral, Acropora tenuis. *Marine Biotechnology* , *23*(3), 373–388. https://doi.org/10.1007/s10126-021-10031-w

Keshavmurthy, S., Tee, H. S., Kao, K.-W., Wang, J.-T., & Chen, C. A. (2020). Specificity trumps flexibility-location-based stable associations between Symbiodiniaceae genera and Platygyra verweyi (Scleractinia; Merulinidae). *PeerJ*, *8*, e8791. https://doi.org/10.7717/peerj.8791

Kirk, A. L., Clowez, S., Lin, F., Grossman, A. R., & Xiang, T. (2020). Transcriptome reprogramming of Symbiodiniaceae Breviolum minutum in response to organic nutrients casein amino acids supplementation. *Frontiers in Physiology*, *11*, 1301. https://doi.org/10.3389/fphys.2020.574654

Kirk, A. L., & Xiang, T. (2022). Single-cell dissociation of the model cnidarian sea anemone Exaiptasia diaphana. *STAR Protocols*, *3*(4), 101897. https://doi.org/10.1016/j.xpro.2022.101897

Kishimoto, M., Baird, A. H., Maruyama, S., Minagawa, J., & Takahashi, S. (2020). Loss of symbiont infectivity following thermal stress can be a factor limiting recovery from bleaching in cnidarians. *The ISME Journal*, *14*(12), 3149–3152. https://doi.org/10.1038/s41396-020-00742-8

Kovacević, G., Franjević, D., Jelencić, B., & Kalafatić, M. (2010). Isolation and cultivation of endosymbiotic algae from green hydra and phylogenetic analysis of 18S rDNA sequences.

Folia Biologica, *58*(1-2), 135–143. https://doi.org/10.3409/fb58_1-2.135-143

Krueger, T., Fisher, P. L., Becker, S., Pontasch, S., Dove, S., Hoegh-Guldberg, O., Leggat, W., & Davy, S. K. (2015). Transcriptomic characterization of the enzymatic antioxidants FeSOD, MnSOD, APX and KatG in the dinoflagellate genus Symbiodinium. *BMC Evolutionary Biology*, *15*, 48. https://doi.org/10.1186/s12862-015-0326-0

Krueger, T., Horwitz, N., Bodin, J., Giovani, M.-E., Escrig, S., Fine, M., & Meibom, A. (2020). Intracellular competition for nitrogen controls dinoflagellate population density in corals. *Proceedings. Biological Sciences / The Royal Society*, *287*(1922), 20200049. https://doi.org/10.1098/rspb.2020.0049

LaJeunesse, T. C. (2001). Investigating The Biodiversity, Ecology, And Phylogeny Of Endosymbiotic Dinoflagellates In The Genus *Symbiodinium* Using The Its Region: In Search Of A "Species" Level Marker. *Journal of Phycology*, *37*(5), 866–880. https://doi.org/10.1046/j.1529-8817.2001.01031.x

LaJeunesse, T. C., Parkinson, J. E., Gabrielson, P. W., Jeong, H. J., Reimer, J. D., Voolstra, C. R., & Santos, S. R. (2018). Systematic Revision of Symbiodiniaceae Highlights the Antiquity and Diversity of Coral Endosymbionts. *Current Biology: CB*, *28*(16), 2570–2580.e6. https://doi.org/10.1016/j.cub.2018.07.008

Lajeunesse, T. C., Parkinson, J. E., & Reimer, J. D. (2012). A genetics-based description of Symbiodinium minutum sp. nov. and S. psygmophilum sp. nov. (Dinophyceae), two dinoflagellates symbiotic with cnidaria. *Journal of Phycology*, *48*(6), 1380–1391. https://doi.org/10.1111/j.1529-8817.2012.01217.x

Lam, C. M. C., New, D. C., & Wong, J. T. Y. (2001). cAMP In The Cell Cycle Of The Dinoflagellate Crypthecodinium Cohnii (Dinophyta). *Journal of Phycology*, *37*(1), 79–85.

https://doi.org/10.1046/j.1529-8817.2001.037001079.x

Leal, M. C., Hoadley, K., Pettay, D. T., Grajales, A., Calado, R., & Warner, M. E. (2015). Symbiont type influences trophic plasticity of a model cnidarian-dinoflagellate symbiosis. *The Journal of Experimental Biology*, *218*(Pt 6), 858–863. https://doi.org/10.1242/jeb.115519

Lee, A. S. Y., Kranzusch, P. J., & Cate, J. H. D. (2015). eIF3 targets cell-proliferation messenger RNAs for translational activation or repression. *Nature*, *522*(7554), 111–114. https://doi.org/10.1038/nature14267

Lee, J. J. (1995). Living sands: the symbiosis of protists and algae can provide good models for the study of host symbiont interactions. *Bioscience*, *45*, 252+. https://go.gale.com/ps/i.do?id=GALE%7CA16999554&sid=googleScholar&v=2.1&it=r&linkaccess=abs&issn=00063568&p=AONE&sw=w

Leelatian, N., Doxie, D. B., Greenplate, A. R., Sinnaeve, J., Ihrie, R. A., & Irish, J. M. (2017). Preparing Viable Single Cells from Human Tissue and Tumors for Cytomic Analysis. *Current Protocols in Molecular Biology / Edited by Frederick M. Ausubel ... [et Al.]*, *118*, 25C.1.1–25C.1.23. https://doi.org/10.1002/cpmb.37

Leggat, W., Hoegh-Guldberg, O., Dove, S., & Yellowlees, D. (2007). Analysis of an EST library from the dinoflagellate (Symbiodinium sp.) symbiont of reef-building corals 1. *Journal of Phycology*, *43*(5), 1010–1021. https://doi.org/10.1111/j.1529-8817.2007.00387.x

Lehnert, E. M., Burriesci, M. S., & Pringle, J. R. (2012). Developing the anemone Aiptasia as a tractable model for cnidarian-dinoflagellate symbiosis: the transcriptome of aposymbiotic A. pallida. In *BMC Genomics* (Vol. 13, Issue 1). https://doi.org/10.1186/1471-2164-13-271

Lehnert, E. M., Mouchka, M. E., Burriesci, M. S., Gallo, N. D., Schwarz, J. A., & Pringle, J. R.

(2014). Extensive differences in gene expression between symbiotic and aposymbiotic cnidarians. *G3* , *4*(2), 277–295. https://doi.org/10.1534/g3.113.009084

Leutenegger, S. (1984). Symbiosis in benthic foraminifera; specificity and host adaptations. *Journal of Foraminiferal Research*, *14*(1), 16–35. https://doi.org/10.2113/gsjfr.14.1.16

Levin, N. A., Bjornsti, M. A., & Fink, G. R. (1993). A novel mutation in DNA topoisomerase I of yeast causes DNA damage and RAD9-dependent cell cycle arrest. *Genetics*, *133*(4), 799–814. https://www.ncbi.nlm.nih.gov/pubmed/8385050

Li, H., & Durbin, R. (2009). Fast and accurate short read alignment with Burrows–Wheeler transform. *Bioinformatics*. https://academic.oup.com/bioinformatics/article-abstract/25/14/1754/225615

Li, T., Chen, X., & Lin, S. (2021). Physiological and transcriptomic responses to N-deficiency and ammonium: Nitrate shift in Fugacium kawagutii (Symbiodiniaceae). *The Science of the Total Environment*, *753*, 141906. https://doi.org/10.1016/j.scitotenv.2020.141906

Lobban, C. S., Modeo, L., Verni, F., & Rosati, G. (2005). Euplotes uncinatus (Ciliophora, Hypotrichia), a new species with zooxanthellae. *Marine Biology*, *147*(5), 1055–1061. https://doi.org/10.1007/s00227-005-0024-3

Love, M. I., Huber, W., & Anders, S. (2014). Moderated estimation of fold change and dispersion for RNA-seq data with DESeq2. *Genome Biology*, *15*(12), 550. https://doi.org/10.1186/s13059-014-0550-8

Löwe, J., Cordell, S. C., & van den Ent, F. (2001). Crystal structure of the SMC head domain: an ABC ATPase with 900 residues antiparallel coiled-coil inserted. *Journal of Molecular Biology*, *306*(1), 25–35. https://doi.org/10.1006/jmbi.2000.4379

Maere, S., Heymans, K., & Kuiper, M. (2005). BiNGO: a Cytoscape plugin to assess

overrepresentation of gene ontology categories in biological networks. *Bioinformatics* , *21*(16), 3448–3449. https://doi.org/10.1093/bioinformatics/bti551

Mak, C. K. M., Hung, V. K. L., & Wong, J. T. Y. (2005). Type II topoisomerase activities in both the G1 and G2/M phases of the dinoflagellate cell cycle. *Chromosoma*, *114*(6), 420–431. https://doi.org/10.1007/s00412-005-0027-3

Mansfield, K. M., Carter, N. M., Nguyen, L., Cleves, P. A., Alshanbayeva, A., Williams, L. M., Crowder, C., Penvose, A. R., Finnerty, J. R., Weis, V. M., Siggers, T. W., & Gilmore, T. D. (2017). Transcription factor NF-κB is modulated by symbiotic status in a sea anemone model of cnidarian bleaching. *Scientific Reports*, *7*(1), 16025. https://doi.org/10.1038/s41598-017-16168-w

Maor-Landaw, K., van Oppen, M. J. H., & McFadden, G. I. (2020). Symbiotic lifestyle triggers drastic changes in the gene expression of the algal endosymbiont Breviolum minutum (Symbiodiniaceae). *Ecology and Evolution*, *10*(1), 451–466. https://doi.org/10.1002/ece3.5910

Marinov, G. K., & Lynch, M. (2015). Diversity and Divergence of Dinoflagellate Histone Proteins. *G3* , *6*(2), 397–422. https://doi.org/10.1534/g3.115.023275

Marinov, G. K., Trevino, A. E., Xiang, T., Kundaje, A., Grossman, A. R., & Greenleaf, W. J. (2020). Transcription-dependent domain-scale 3D genome organization in dinoflagellates. In *bioRxiv*. bioRxiv. https://doi.org/10.1101/2020.07.01.181685

Maruyama, S., Unsworth, J. R., Sawiccy, V., Students of Oregon State University's Z362 Spring 2021, & Weis, V. M. (2022). Algae from Aiptasia egesta are robust representations of Symbiodiniaceae in the free-living state. *PeerJ*, *10*, e13796. https://doi.org/10.7717/peerj.13796

Marx, A., Hoenger, A., & Mandelkow, E. (2009). Structures of kinesin motor proteins. *Cell Motility and the Cytoskeleton*, *66*(11), 958–966. https://doi.org/10.1002/cm.20392

Matthews, J. L., Sproles, A. E., Oakley, C. A., Grossman, A. R., Weis, V. M., & Davy, S. K. (2016). Menthol-induced bleaching rapidly and effectively provides experimental aposymbiotic sea anemones (Aiptasia sp.) for symbiosis investigations. *The Journal of Experimental Biology*, *219*(Pt 3), 306–310. https://doi.org/10.1242/jeb.128934

McIlroy, S. E., Cunning, R., Baker, A. C., & Coffroth, M. A. (2019). Competition and succession among coral endosymbionts. *Ecology and Evolution*, *9*(22), 12767–12778. https://doi.org/10.1002/ece3.5749

McIlroy, S. E., terHorst, C. P., Teece, M., & Coffroth, M. A. (2022). Nutrient dynamics in coral symbiosis depend on both the relative and absolute abundance of Symbiodiniaceae species. *Microbiome*, *10*(1), 192. https://doi.org/10.1186/s40168-022-01382-0

McKinley, K. L., & Cheeseman, I. M. (2016). The molecular basis for centromere identity and function. *Nature Reviews. Molecular Cell Biology*, *17*(1), 16–29. https://doi.org/10.1038/nrm.2015.5

McNulty, R., Sritharan, D., Pahng, S. H., Meisch, J. P., Liu, S., Brennan, M. A., Saxer, G., Hormoz, S., & Rosenthal, A. Z. (2023). Probe-based bacterial single-cell RNA sequencing predicts toxin regulation. *Nature Microbiology*, *8*(5), 934–945. https://doi.org/10.1038/s41564-023-01348-4

Mínguez, A., Franca, S., & Moreno Díaz de la Espina, S. (1994). Dinoflagellates have a eukaryotic nuclear matrix with lamin-like proteins and topoisomerase II. *Journal of Cell Science*, *107 (Pt 10)*, 2861–2873. https://doi.org/10.1242/jcs.107.10.2861

Morris, L. A., Voolstra, C. R., Quigley, K. M., Bourne, D. G., & Bay, L. K. (2019). Nutrient

Availability and Metabolism Affect the Stability of Coral-Symbiodiniaceae Symbioses. *Trends in Microbiology*, *27*(8), 678–689. https://doi.org/10.1016/j.tim.2019.03.004

Muscatine, L., Falkowski, P. G., Porter, J. W., Dubinsky, Z., & Smith, D. C. (1984). Fate of photosynthetic fixed carbon in light- and shade-adapted colonies of the symbiotic coral Stylophora pistillata. *Proceedings of the Royal Society of London. Series B. Biological Sciences*, *222*(1227), 181–202. https://doi.org/10.1098/rspb.1984.0058

Muscatine, L., Ferrier-Pagès, C., Blackburn, A., Gates, R. D., Baghdasarian, G., & Allemand, D. (1998). Cell-specific density of symbiotic dinoflagellates in tropical anthozoans. *Coral Reefs* , *17*(4), 329–337. https://doi.org/10.1007/s003380050133

Muscatine, L., Pool, R. R., Richmond, M. H., & Smith, D. C. (1997). Regulation of numbers of intracellular algae. *Proceedings of the Royal Society of London. Series B. Biological Sciences*, *204*(1155), 131–139. https://doi.org/10.1098/rspb.1979.0018

Muscatine, L., & Porter, J. W. (1977). Reef Corals: Mutualistic Symbioses Adapted to Nutrient-Poor Environments. *Bioscience*, *27*(7), 454–460. https://doi.org/10.2307/1297526

Newkirk, C. R., Frazer, T. K., & Martindale, M. Q. (2018). Acquisition and proliferation of algal symbionts in bleached polyps of the upside-down jellyfish, Cassiopea xamachana. *Journal of Experimental Marine Biology and Ecology*, *508*, 44–51. https://doi.org/10.1016/j.jembe.2018.08.010

Newkirk, C., Vadlapudi, S., Sadula, M., Arbello, C., & Xiang, T. (2022). Reproducible propagation technique for the symbiotic cnidarian model system Cassiopea xamachana. *Biology Open*, *11*(9). https://doi.org/10.1242/bio.059413

Oliveira, C. Y. B., Abreu, J. L., Santos, E. P., Matos, Â. P., Tribuzi, G., Oliveira, C. D. L., Veras, B. O., Bezerra, R. S., Müller, M. N., & Gálvez, A. O. (2022). Light induces peridinin and

docosahexaenoic acid accumulation in the dinoflagellate Durusdinium glynnii. *Applied Microbiology and Biotechnology*, *106*(18), 6263–6276. https://doi.org/10.1007/s00253-022-12131-6

Parkinson, J. E., Baumgarten, S., Michell, C. T., Baums, I. B., LaJeunesse, T. C., & Voolstra, C. R. (2016). Gene Expression Variation Resolves Species and Individual Strains among Coral-Associated Dinoflagellates within the Genus Symbiodinium. *Genome Biology and Evolution*, *8*(3), 665–680. https://doi.org/10.1093/gbe/evw019

Parkinson, J. E., Coffroth, M. A., & LaJeunesse, T. C. (2015). New species of Clade B Symbiodinium (Dinophyceae) from the greater Caribbean belong to different functional guilds: S. aenigmaticum sp. nov., S. antillogorgium sp. nov., S. endomadracis sp. nov., and S. pseudominutum sp. nov. *Journal of Phycology*, *51*(5), 850–858. https://doi.org/10.1111/jpy.12340

Park, Y.-J., & Luger, K. (2006). The structure of nucleosome assembly protein 1. *Proceedings of the National Academy of Sciences of the United States of America*, *103*(5), 1248–1253. https://doi.org/10.1073/pnas.0508002103

Pearse, V. B., & Muscatine, L. (1971). ROLE OF SYMBIOTIC ALGAE (ZOOXANTHELLAE) IN CORAL CALCIFICATION. *The Biological Bulletin*, *141*(2), 350–363. https://doi.org/10.2307/1540123

Pootakham, W., Mhuantong, W., Yoocha, T., Sangsrakru, D., Kongkachana, W., Sonthirod, C., Naktang, C., Jomchai, N., U-Thoomporn, S., Yeemin, T., Pengsakun, S., Sutthacheep, M., & Tangphatsornruang, S. (2021). Taxonomic profiling of Symbiodiniaceae and bacterial communities associated with Indo-Pacific corals in the Gulf of Thailand using PacBio sequencing of full-length ITS and 16S rRNA genes. *Genomics*, *113*(4), 2717–2729.

https://doi.org/10.1016/j.ygeno.2021.06.001

Potter, L. R. (2011). Guanylyl cyclase structure, function and regulation. *Cellular Signalling*, *23*(12), 1921–1926. https://doi.org/10.1016/j.cellsig.2011.09.001

Presnell, J. S., Wirsching, E., & Weis, V. M. (2022). Tentacle patterning during Exaiptasia diaphana pedal lacerate development differs between symbiotic and aposymbiotic animals. *PeerJ*, *10*, e12770. https://doi.org/10.7717/peerj.12770

Qin, Z., Yu, K., Chen, B., Wang, Y., Liang, J., Luo, W., Xu, L., & Huang, X. (2019). Diversity of Symbiodiniaceae in 15 Coral Species From the Southern South China Sea: Potential Relationship With Coral Thermal Adaptability. *Frontiers in Microbiology*, *10*, 2343. https://doi.org/10.3389/fmicb.2019.02343

Rädecker, N., Escrig, S., Spangenberg, J. E., Voolstra, C. R., & Meibom, A. (2023). Coupled carbon and nitrogen cycling regulates the cnidarian–algal symbiosis. *Nature Communications*, *14*(1), 1–10. https://doi.org/10.1038/s41467-023-42579-7

Rädecker, N., Pogoreutz, C., Gegner, H. M., Cárdenas, A., Roth, F., Bougoure, J., Guagliardo, P., Wild, C., Pernice, M., Raina, J.-B., Meibom, A., & Voolstra, C. R. (2021). Heat stress destabilizes symbiotic nutrient cycling in corals. *Proceedings of the National Academy of Sciences of the United States of America*, *118*(5). https://doi.org/10.1073/pnas.2022653118

Rädecker, N., Raina, J.-B., Pernice, M., Perna, G., Guagliardo, P., Kilburn, M. R., Aranda, M., & Voolstra, C. R. (2018). Using Aiptasia as a Model to Study Metabolic Interactions in Cnidarian-Symbiodinium Symbioses. *Frontiers in Physiology*, *9*, 214. https://doi.org/10.3389/fphys.2018.00214

R Core Team (2021). R: A language and environment for statistical computing. R Foundation for Statistical Computing, Vienna, Austria. URL https://www.R-project.org/.

Rodnina, M. V., Gromadski, K. B., Kothe, U., & Wieden, H.-J. (2005). Recognition and selection of tRNA in translation. *FEBS Letters*, *579*(4), 938–942. https://doi.org/10.1016/j.febslet.2004.11.048

Rodriguez de la Fuente, L., Law, A. M. K., Gallego-Ortega, D., & Valdes-Mora, F. (2021). Tumor dissociation of highly viable cell suspensions for single-cell omic analyses in mouse models of breast cancer. *STAR Protocols*, *2*(4), 100841. https://doi.org/10.1016/j.xpro.2021.100841

Rosic, N., Ling, E. Y. S., Chan, C.-K. K., Lee, H. C., Kaniewska, P., Edwards, D., Dove, S., & Hoegh-Guldberg, O. (2015). Unfolding the secrets of coral-algal symbiosis. *The ISME Journal*, *9*(4), 844–856. https://doi.org/10.1038/ismej.2014.182

Rosset, S. L., Oakley, C. A., Ferrier-Pagès, C., Suggett, D. J., Weis, V. M., & Davy, S. K. (2021). The Molecular Language of the Cnidarian-Dinoflagellate Symbiosis. *Trends in Microbiology*, *29*(4), 320–333. https://doi.org/10.1016/j.tim.2020.08.005

Roulland, Y., Ouararhni, K., Naidenov, M., Ramos, L., Shuaib, M., Syed, S. H., Lone, I. N., Boopathi, R., Fontaine, E., Papai, G., Tachiwana, H., Gautier, T., Skoufias, D., Padmanabhan, K., Bednar, J., Kurumizaka, H., Schultz, P., Angelov, D., Hamiche, A., & Dimitrov, S. (2016). The Flexible Ends of CENP-A Nucleosome Are Required for Mitotic Fidelity. *Molecular Cell*, *63*(4), 674–685. https://doi.org/10.1016/j.molcel.2016.06.023

Russo, J. A., Xiang, T., & Jinkerson, R. E. (2023). Protocol for the generation of Symbiodiniaceae mutants using UV mutagenesis. *STAR Protocols*, *4*(4), 102627. https://doi.org/10.1016/j.xpro.2023.102627

Saini, P., Eyler, D. E., Green, R., & Dever, T. E. (2009). Hypusine-containing protein eIF5A promotes translation elongation. *Nature*, *459*(7243), 118–121. https://doi.org/10.1038/nature08034

Santos, S. R., Taylor, D. J., & Coffroth, M. A. (2001). Genetic comparisons of freshly isolated versus cultured symbiotic dinoflagellates: Implications for extrapolating to the intact symbiosis. *Journal of Phycology*, *37*(5), 900–912. https://doi.org/10.1046/j.1529-8817.2001.00194.x

Scheib, U., Broser, M., Constantin, O. M., Yang, S., Gao, S., Mukherjee, S., Stehfest, K., Nagel, G., Gee, C. E., & Hegemann, P. (2018). Rhodopsin-cyclases for photocontrol of cGMP/cAMP and 2.3 Å structure of the adenylyl cyclase domain. *Nature Communications*, *9*(1), 2046. https://doi.org/10.1038/s41467-018-04428-w

Segeritz, C.-P., & Vallier, L. (2017). Chapter 9 - Cell Culture: Growing Cells as Model Systems In Vitro. In M. Jalali, F. Y. L. Saldanha, & M. Jalali (Eds.), *Basic Science Methods for Clinical Researchers* (pp. 151–172). Academic Press. https://doi.org/10.1016/B978-0-12-803077-6.00009-6

Shoguchi, E., Shinzato, C., Kawashima, T., Gyoja, F., Mungpakdee, S., Koyanagi, R., Takeuchi, T., Hisata, K., Tanaka, M., Fujiwara, M., Hamada, M., Seidi, A., Fujie, M., Usami, T., Goto, H., Yamasaki, S., Arakaki, N., Suzuki, Y., Sugano, S., … Satoh, N. (2013). Draft assembly of the Symbiodinium minutum nuclear genome reveals dinoflagellate gene structure. *Current Biology: CB*, *23*(15), 1399–1408. https://doi.org/10.1016/j.cub.2013.05.062

Silverstein, R. N., Correa, A. M. S., & Baker, A. C. (2012). Specificity is rarely absolute in coral-algal symbiosis: implications for coral response to climate change. *Proceedings. Biological Sciences / The Royal Society*, *279*(1738), 2609–2618. https://doi.org/10.1098/rspb.2012.0055

Silverstein, R. N., Cunning, R., & Baker, A. C. (2015). Change in algal symbiont communities after

bleaching, not prior heat exposure, increases heat tolerance of reef corals. *Global Change Biology*, *21*(1), 236–249. https://doi.org/10.1111/gcb.12706

Steen, R. G. (1986). Evidence For Heterotrophy By Zooxanthellae In Symbiosis With Aiptasia Pulchella. *The Biological Bulletin*, *170*(2), 267–278. https://doi.org/10.2307/1541808

Steer, M. L. (1975). Adenyl cyclase. *Annals of Surgery*, *182*(5), 603–609. https://doi.org/10.1097/00000658-197511000-00012

Steinke, M., Brading, P., Kerrison, P., Warner, M. E., & Suggett, D. J. (2011). Concentrations Of Dimethylsulfoniopropionate And Dimethyl Sulfide Are Strain-Specific In Symbiotic Dinoflagellates (Symbiodinium Sp., Dinophyceae). *Journal of Phycology*, *47*(4), 775–783. https://doi.org/10.1111/j.1529-8817.2011.01011.x

Tang, F., Barbacioru, C., Wang, Y., Nordman, E., Lee, C., Xu, N., Wang, X., Bodeau, J., Tuch, B. B., Siddiqui, A., Lao, K., & Surani, M. A. (2009). mRNA-Seq whole-transcriptome analysis of a single cell. *Nature Methods*, *6*(5), 377–382. https://doi.org/10.1038/nmeth.1315

Thornhill, D. J., Daniel, M. W., LaJeunesse, T. C., Schmidt, G. W., & Fitt, W. K. (2006). Natural infections of aposymbiotic Cassiopea xamachana scyphistomae from environmental pools of Symbiodinium. *Journal of Experimental Marine Biology and Ecology*, *338*(1), 50–56. https://doi.org/10.1016/j.jembe.2006.06.032

Thornhill, D. J., Xiang, Y., Pettay, D. T., Zhong, M., & Santos, S. R. (2013). Population genetic data of a model symbiotic cnidarian system reveal remarkable symbiotic specificity and vectored introductions across ocean basins. *Molecular Ecology*, *22*(17), 4499–4515. https://doi.org/10.1111/mec.12416

Tivey, T. R., Coleman, T. J., & Weis, V. M. (2022). Spatial and temporal patterns of symbiont colonization and loss during bleaching in the model sea anemone Aiptasia. *Frontiers in*

Marine Science, *9*. https://doi.org/10.3389/fmars.2022.808696

Tivey, T. R., Parkinson, J. E., & Weis, V. M. (2020). Host and Symbiont Cell Cycle Coordination Is Mediated by Symbiotic State, Nutrition, and Partner Identity in a Model Cnidarian-Dinoflagellate Symbiosis. *mBio*, *11*(2). https://doi.org/10.1128/mBio.02626-19

Toller, W. W., Rowan, R., & Knowlton, N. (2001). Repopulation of Zooxanthellae in the Caribbean corals Montastraea annularis and M. faveolata following experimental and disease-associated bleaching. *The Biological Bulletin*, *201*(3), 360–373. https://doi.org/10.2307/1543614

Tortorelli, G., Oakley, C. A., Davy, S. K., van Oppen, M. J. H., & McFadden, G. I. (2022). Cell wall proteomic analysis of the cnidarian photosymbionts Breviolum minutum and Cladocopium goreaui. *The Journal of Eukaryotic Microbiology*, *69*(1), e12870. https://doi.org/10.1111/jeu.12870

Tortorelli, G., Rautengarten, C., Bacic, A., Segal, G., Ebert, B., Davy, S. K., van Oppen, M. J. H., & McFadden, G. I. (2022). Cell surface carbohydrates of symbiotic dinoflagellates and their role in the establishment of cnidarian-dinoflagellate symbiosis. *The ISME Journal*, *16*(1), 190–199. https://doi.org/10.1038/s41396-021-01059-w

Venn, A. A., Loram, J. E., & Douglas, A. E. (2008). Photosynthetic symbioses in animals. *Journal of Experimental Botany*, *59*(5), 1069–1080. https://doi.org/10.1093/jxb/erm328

Wagner, G. P., Kin, K., & Lynch, V. J. (2012). Measurement of mRNA abundance using RNA-seq data: RPKM measure is inconsistent among samples. *Theory in Biosciences = Theorie in Den Biowissenschaften*, *131*(4), 281–285. https://doi.org/10.1007/s12064-012-0162-3

Wang, J. T., & Douglas, A. E. (1999). Essential amino acid synthesis and nitrogen recycling in an alga–invertebrate symbiosis. *Marine Biology*, *135*(2), 219–222.

https://doi.org/10.1007/s002270050619

Ward, J. M., Mäser, P., & Schroeder, J. I. (2009). Plant ion channels: gene families, physiology, and functional genomics analyses. *Annual Review of Physiology*, *71*, 59–82. https://doi.org/10.1146/annurev.physiol.010908.163204

Weis, V. M. (2008). Cellular mechanisms of Cnidarian bleaching: stress causes the collapse of symbiosis. *The Journal of Experimental Biology*, *211*(Pt 19), 3059–3066. https://doi.org/10.1242/jeb.009597

Weis, V. M. (2019). Cell Biology of Coral Symbiosis: Foundational Study Can Inform Solutions to the Coral Reef Crisis. *Integrative and Comparative Biology*, *59*(4), 845–855. https://doi.org/10.1093/icb/icz067

Weis, V. M., & Allemand, D. (2009). Physiology. What determines coral health? *Science*, *324*(5931), 1153–1155. https://doi.org/10.1126/science.1172540

Weis, V. M., Davy, S. K., Hoegh-Guldberg, O., Rodriguez-Lanetty, M., & Pringle, J. R. (2008). Cell biology in model systems as the key to understanding corals. *Trends in Ecology & Evolution*, *23*(7), 369–376. https://doi.org/10.1016/j.tree.2008.03.004

Wilkerson, F. P., Kobayashi, D., & Muscatine, L. (1988). Mitotic index and size of symbiotic algae in Caribbean Reef corals. *Coral Reefs* , *7*(1), 29–36. https://doi.org/10.1007/BF00301979

Wisecaver, J. H., & Hackett, J. D. (2011). Dinoflagellate genome evolution. *Annual Review of Microbiology*, *65*, 369–387. https://doi.org/10.1146/annurev-micro-090110-102841

Wolfowicz, I., Baumgarten, S., Voss, P. A., Hambleton, E. A., Voolstra, C. R., Hatta, M., & Guse, A. (2016). Aiptasia sp. larvae as a model to reveal mechanisms of symbiont selection in cnidarians. In *Scientific Reports* (Vol. 6, Issue 1). https://doi.org/10.1038/srep32366

Wood-Charlson, E. M., Hollingsworth, L. L., Krupp, D. A., & Weis, V. M. (2006). Lectin/glycan

interactions play a role in recognition in a coral/dinoflagellate symbiosis. *Cellular Microbiology*, *8*(12), 1985–1993. https://doi.org/10.1111/j.1462-5822.2006.00765.x

Xiang, T., Hambleton, E. A., DeNofrio, J. C., Pringle, J. R., & Grossman, A. R. (2013). Isolation of clonal axenic strains of the symbiotic dinoflagellate Symbiodinium and their growth and host specificity1. *Journal of Phycology*, *49*(3), 447–458. https://onlinelibrary.wiley.com/doi/abs/10.1111/jpy.12055

Xiang, T., Jinkerson, R. E., Clowez, S., Tran, C., Krediet, C. J., Onishi, M., Cleves, P. A., Pringle, J. R., & Grossman, A. R. (2018). Glucose-Induced Trophic Shift in an Endosymbiont Dinoflagellate with Physiological and Molecular Consequences. *Plant Physiology*, *176*(2), 1793–1807. https://doi.org/10.1104/pp.17.01572

Xiang, T., Lehnert, E., Jinkerson, R. E., Clowez, S., Kim, R. G., DeNofrio, J. C., Pringle, J. R., & Grossman, A. R. (2020). Symbiont population control by host-symbiont metabolic interaction in Symbiodiniaceae-cnidarian associations. *Nature Communications*, *11*(1), 108. https://doi.org/10.1038/s41467-019-13963-z

Xiang, T., Nelson, W., Rodriguez, J., Tolleter, D., & Grossman, A. R. (2015). Symbiodinium transcriptome and global responses of cells to immediate changes in light intensity when grown under autotrophic or mixotrophic conditions. *The Plant Journal: For Cell and Molecular Biology*, *82*(1), 67–80. https://doi.org/10.1111/tpj.12789

Zamora-Jordán, N., Hernández, M., & López, C. (2022). Biogeography of endosymbionts (Symbiodiniaceae) associated with zoantharian species (Hexacorallia: Anthozoa) from the Macaronesia and Cape Verde ecoregions. *Coral Reefs* , *41*(3), 511–522. https://doi.org/10.1007/s00338-022-02260-9

Zaquin, T., Zaslansky, P., Pinkas, I., & Mass, T. (2019). Simulating Bleaching: Long-Term

Adaptation to the Dark Reveals Phenotypic Plasticity of the Mediterranean Sea Coral Oculina patagonica. *Frontiers in Marine Science*, *6*. https://doi.org/10.3389/fmars.2019.00662

Zawada, K. J. A., Dornelas, M., & Madin, J. S. (2019). Quantifying coral morphology. *Coral Reefs* , *38*(6), 1281–1292. https://doi.org/10.1007/s00338-019-01842-4